Andreia Sofia Ladeira dos Santos Gouveia

Licenciatura em Ciências da Engenharia Química e Bioquímica

FACILITATED CO_2 SEPARATION MEMBRANES: MIXING CYANO AND AMINO ACID-BASED IONIC LIQUIDS

Dissertação para obtenção do Grau de Mestre em
Engenharia Química e Bioquímica

Orientador: Dra. Isabel Maria Delgado Jana Marrucho Ferreira,
Investigadora Coordenadora, Laboratório de Termodinâmica
Molecular, ITQB-UNL

Presidente: Dra. Susana Filipe Barreiros
Arguente: Dra. Luísa Alexandra Graça Neves
Vogal: Dra. Isabel Maria Delgado Jana Marrucho Ferreira

FACULDADE DE CIÊNCIAS E TECNOLOGIA
UNIVERSIDADE NOVA DE LISBOA

Outubro 2014

Universidade Nova de Lisboa

Faculdade de Ciências e Tecnologia

FACILITATED CO_2 SEPARATION MEMBRANES: MIXING CYANO AND AMINO ACID-BASED IONIC LIQUIDS

Andreia Sofia Ladeira dos Santos Gouveia

Licenciatura em Ciências da Engenharia Química e Bioquímica

Dissertação para obtenção do Grau de Mestre em Engenharia Química e Bioquímica

Orientador: Dra. Isabel Maria Delgado Jana Marrucho Ferreira, Investigadora Coordenadora, Laboratório de Termodinâmica Molecular, ITQB-UNL

Outubro 2014

FACILITATED CO_2 SEPARATION MEMBRANES: MIXING CYANO AND AMINO ACID-BASED IONIC LIQUIDS

COPYRIGHT

Andreia Sofia Ladeira dos Santos Gouveia

Faculdade de Ciências e Tecnologia
Universidade Nova de Lisboa

Agradecimentos

Ao longo deste desafiante percurso, que foi o Mestrado Integrado em Engenharia Química e Bioquímica, foram muitas as pessoas que me ajudaram a realizar esta etapa tão importante da minha formação académica, às quais quero deixar aqui o meu profundo agradecimento.

À minha orientadora, Dra. Isabel Marrucho, por me ter proporcionado as condições necessárias para a elaboração da minha dissertação e por me ter orientado e acompanhado ao longo de todo o trabalho. Agradeço também toda a simpatia e disponibilidade.

À Liliana Tomé, por ter sido muito importante e fundamental durante toda a dissertação, não só pelos conhecimentos transmitidos, que de certeza que irão ser indispensáveis no meu futuro, mas também pelo apoio e motivação, pelos conselhos, pela paciência, e por ter estado sempre presente e disponível para me ajudar em todas as ocasiões. Não tenho palavras que sejam suficientes para agradecer e transmitir toda a minha admiração. Obrigada por tudo!

À Catarina Florindo, por ter sido igualmente um apoio muito importante ao longo de toda a dissertação, por ter estado sempre disponível para me ajudar sempre que precisei, por todos os conselhos, pelos momentos de risadas e descontração, pelos desabafos, por tudo, um enorme obrigada.

À Karen João, ao Mateusz Marchel, ao David Patinha e ao Filipe Oliveira, por se terem demonstrado sempre disponíveis para me ajudar e por também terem proporcionado momentos de alegria durante estes últimos meses, que contribuíram, sem dúvida, para que esta fase final fosse muito menos stressante.

A todas as minhas colegas de curso, que para além de colegas, se tornaram amigas para a vida. À Sónia Branco, por ter sido um apoio muito importante principalmente ao longo destes últimos meses. Agradeço em especial, à Sofia Pires, por ter sido fundamental ao longo de todo este percurso académico, por me ter ajudado em todas as circunstâncias, por ter comemorado comigo os momentos bons e por ter estado ao meu lado em todos os momentos menos bons. Agradeço também à Bruna Pereira e à Carina Constantino, por terem sido excelentes amigas e companheiras de projeto. Obrigada pelos laços fortes de amizade criados e por terem estado sempre presentes em todos os momentos. Por fim, e não menos importante, quero agradecer à Sara Cândido, por ter sido também uma excelente amiga e companheira de trabalho ao longo destes cinco anos.

Ao Gonçalo, pelo amor e apoio incondicional, por estar sempre presente em todos os momentos, pela compreensão e paciência nos momentos mais stressantes, por me ter ajudado a ultrapassar momentos menos bons e por me apoiar e incentivar sempre a alcançar os meus objetivos. Obrigada por tudo!

À minha Família, em especial aos Meus Pais e ao Meu Irmão por acreditarem sempre em mim e naquilo que faço, por todos os ensinamentos de vida, por estarem sempre presentes e nunca me deixarem cair. Espero que esta etapa, que agora termino, possa, de alguma forma, retribuir e compensar todo o carinho, apoio e dedicação que, constantemente, me oferecem.

A eles, dedico todo este trabalho.

Our greatest weakness lies in giving up. The most certain way to succeed is always to try just one more time.

Thomas A. Edison

Palavras-chave

Separação de Gases, Líquidos Iónicos, Membranas Líquidas Suportadas, Aminoácidos, Transporte Facilitado

Resumo

Nos últimos anos, tem sido feito um grande esforço no desenvolvimento de processos de separação de CO_2 mais eficientes e sustentáveis. De entre as várias tecnologias utilizadas, as tecnologias baseadas em membranas, em particular, membranas de líquidos iónicos suportados (SILMs), têm atraído bastante atenção essencialmente devido às propriedades únicas dos líquidos iónicos.

Neste trabalho, foi explorado o uso de misturas de líquidos iónicos como novas fases líquidas para SILMs, tendo em conta que os líquidos iónicos baseados em aminoácidos apresentam grupos amina "reativos" que podem atuar como transportadores de CO_2, e que os aniões que contêm grupos ciano que apresentam geralmente viscosidades baixas. Deste modo, foram preparadas misturas de seis líquidos iónicos com um catião em comum ($[C_2mim]^+$) e diferentes aniões, tais como tricyanomethane ($[C(CN)_3]^-$), glycinate ($[Gly]^-$), L-alaninate ($[L\text{-}Ala]^-$), taurinate ($[Tau]^-$), L-serinate ($[L\text{-}Ser]^-$), L-prolinate ($[L\text{-}Pro]^-$). Estas misturas foram usadas como fases líquidas na preparação de membranas de líquidos iónicos suportados. Posteriormente, foram determinadas as propriedades de transporte (permeabilidade, difusão e solubilidade) ao CO_2 e N_2, a uma temperatura fixa e a vários diferenciais de pressão trans-membranar, utilizando o método de time-lag. Uma vez que tanto a viscosidade do liquido iónico como o volume molar são parâmetros importantes que têm impacto sobre as propriedades de transporte dos gases nas SILMs, as propriedades termofísicas dos líquidos iónicos puros e das misturas preparadas, tais como, a viscosidade, a densidade e o índice de refração, foram também medidas para que as suas tendências pudessem ser avaliadas.

Os resultados obtidos neste trabalho evidenciam permseletividades de CO_2/N_2 acima da Robeson upper bond, para duas das SILMs estudadas, o que permite afirmar que as misturas de líquidos iónicos podem ser uma estratégia promissora, como novas fases líquidas, para processos de separação de CO_2/N_2.

Keywords

CO_2 Separation, Ionic Liquids, Mixtures, Supported Ionic Liquid Membranes, Amino acids, Facilitated Transport

Abstract

A great deal of effort has been put on the development of efficient and sustainable CO_2 separation processes. Among them, membrane-based technologies, in particular, supported ionic liquid membranes (SILMs) have recently attracted considerable attention owing to the unique properties of ionic liquids (ILs).

In this work, different IL + IL mixtures were explored as new liquid phases for SILMs. Taking into account that ILs with amino acids present "reactive" amino groups that can work as CO_2 carriers and that ILs combining cyano-functionalized anions present remarkably low viscosities, mixtures of these ILs were studied. Thus, six ILs based on a common cation ($[C_2mim]^+$) and anions such as tricyanomethane ($[C(CN)_3]^-$), glycinate ($[Gly]^-$), L-alaninate ($[L\text{-}Ala]^-$), taurinate ($[Tau]^-$), L-prolinate ($[L\text{-}Pro]^-$) and L-serinate ($[L\text{-}Ser]^-$) were mixed and SILMs were prepared. The gas permeation properties (permeability, diffusivity and solubility) of CO_2 and N_2 were determined at a fixed temperature and different trans-membrane pressure differentials, using a time-lag apparatus. Since the IL viscosity and molar volume are significant parameters that impact the gas permeation properties of SILMs, the thermophysical properties of the pure ILs and their mixtures, namely viscosity, density and refractive index, were also measured so that trends could be evaluated.

The results obtained in this work showed CO_2/N_2 permselectivities above the upper bond for two facilitated SILMs, which clearly claim that mixing ionic liquids can be a promising strategy to design new liquid phases for CO_2/N_2 separation processes, since ILs offer clear pathway to fine-tune their gas permeation properties as well as their CO_2 separation performances.

Contents

List of Figures

List of Tables

List of Abbreviations

CCS	Carbon Capture and Storage
[C_2mim][$C(CN)_3$]	1-Ethyl-3-methylimidazolium tricyanomethane
[C_2mim][Gly]	1-Ethyl-3-methylimidazolium 2-aminoacetate
[C_2mim][L-Ala]	1-Ethyl-3-methylimidazolium (S)-2-aminopropanoate
[C_2mim][Tau]	1-Ethyl-3-methylimidazolium 2-aminoethanesulfonate
[C_2mim][L-Ser]	1-Ethyl-3-methylimidazolium (S)-2-amino-3-hydroxypropanoate
[C_2mim][L-Pro]	1-Ethyl-3-methylimidazolium (S)-pyrrolidine-2-carboxylate
ILs	Ionic Liquids
RTILs	Room Temperature Ionic Liquids
BLMs	Bulk Liquid Membranes
ELMs	Emulsion Liquid Membranes
MMMs	Mixed Matrix Membranes
SLMs	Supported Liquid Membranes
SILMs	Supported Ionic Liquid Membranes
FSILMs	Facilitated Supported Ionic Liquid Membranes
AAILs	Amino Acid-based Ionic Liquids
AA	Amino acid
EPDM	Ethylene Propylene Rubber
PTFE	Poly(tetrafluoroethylene)
TGA	Thermogravimetric Analysis

List of Symbols

M	Molecular Weight
T	Temperature
ρ	Density
η	Dynamic Viscosity
V_M	Molar Volume
V^E	Excess Molar Volume
α_P	Thermal Expansion Coefficient
x	Molar Fraction
E_a	Activation Energy
R	Ideal Gas Constant
n_D	Refractive Index
R_m	Molar Refraction
f_m	Free Molar Volume
P	Permeability
D	Diffusivity
S	Solubility
J	Flux
ℓ	Thickness
ΔP	Pressure Difference
θ	Time-lag
$\alpha_{i/j}$	Permeability Selectivity

1

Introduction

1.1 Motivation

One of the most important environmental challenges that our world faces today is related to the global warming largely associated with the rising concentration of anthropogenic carbon dioxide (CO_2), mainly as a result of fossil fuel power plant emissions. The escalating level of atmospheric CO_2 and the urgent need to take action to prevent irreversible climate change have hugely increased efforts in the development of new efficient and economic technologies for carbon capture and storage (CCS).[1]

Carbon capture and storage is a technology that can capture more than 90% of the CO_2 emissions produced from the use of fossil fuels in electricity generation and industrial processes, preventing the carbon dioxide from entering the atmosphere. The CCS chain consists of three parts: the CO_2 capture, the CO_2 transport and the CO_2 safe storage underground in depleted oil fields and gas formation or deep saline aquifer. Foremost, CO_2 capture technologies allow the separation of carbon dioxide from gases produced in electricity generation and industrial processes by three main techniques, namely pre-combustion capture, post-combustion capture and oxy-fuel combustion. Carbon dioxide is afterward transported by pipeline or by ship for safe storage and then stored in carefully selected geological rock formation that is typically located several kilometers below the Earth's surface.

Different industrial processes emit CO_2 streams with distinct compositions and consequently the development of processes for CO_2 removal from light gases such as CH_4, N_2, and H_2 is a key technical, economical and environmental challenge in several applications. As previously referred, there are three main different CO_2 capture systems such post-combustion, pre-combustion and oxy-fuel combustion.[2]

Pre-Combustion Process

Pre-combustion processes (Figure 1.1) involve a reaction between a fuel and oxygen or air and/or steam to give mainly a ‘synthesis gas’ (syngas) composed of carbon monoxide (CO) and hydrogen (H_2). The CO is reacted with steam in a catalytic reactor, called a shift converter, to give CO_2 and more H_2. CO_2 is then separated, usually by a physical or chemical absorption process, resulting in a hydrogen-rich fuel which can be used in several applications, such as boilers, furnaces, gas turbines, engines and fuel cells.[3]

In this technology, the CO_2 concentration of the flue stream is high, which requires smaller equipment and different solvents with lower regeneration energy requirements. However, the fuel conversion steps required for pre-combustion are more complex than the

processes involved in post-combustion, so the technology is more difficult to apply to existing power plants.[4]

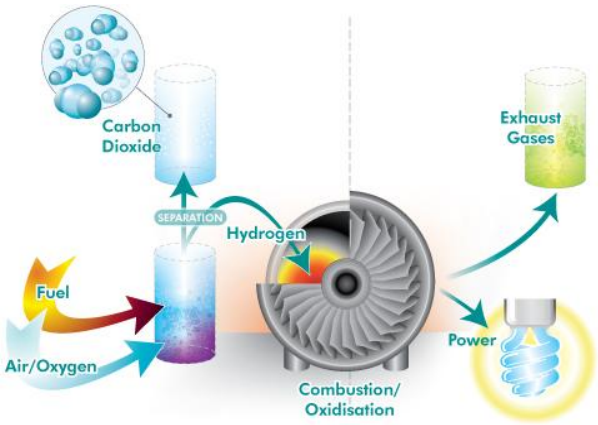

Figure 1.1 - Schematic representation of pre-combustion CO_2 capture.[4]

Post-Combustion Process

Post-combustion processes (Figure 1.2) capture CO_2 from flue gases generated as the combustion byproduct of fossil fuels or other carbonaceous materials (such as biomass) by absorbing it in a suitable solvent. The absorbed CO_2 is liberated from the solvent and is compressed for transportation and storage.[4]

Almost half of CO_2 emissions worldwide are related to the fossil fuel based stationary plants, namely power stations, oil refineries, petrochemical and gas plants, steel and cement plants.[5] In post-combustion CO_2 capture processes, the CO_2 concentration in flue gas is low (<20%), and its capture requires a high volume stream of flue gas containing other gases, predominantly N_2, Although this technology is suitable for retrofitting the existing plants, there is a high energy requirement associated with post-combustion CO_2 capture, due to solvent regeneration and loss during absorption, which needs improved solvents for cost savings.

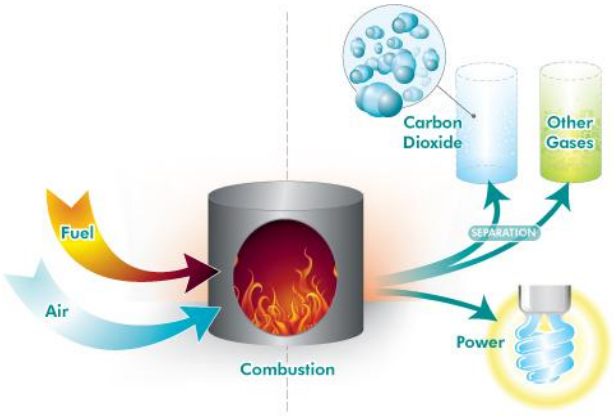

Figure 1.2 - Schematic representation of post-combustion CO_2 capture.[4]

Oxi-fuel Combustion Process

In oxy-fuel combustion processes (Figure 1.3), the fuel is combusted in a mixture of nearly pure O_2 (typically greater than 95% purity) and CO_2, the latter being recycled from the exhaust of the process.[6] The concentration of CO_2 in flue gas can be increased by using pure or enriched oxygen instead of air for combustion, either in a boiler or gas turbine. The oxygen is produced by cryogenic air separation (already industrially used on a large scale), and the CO_2-rich flue gas is recycled to avoid the excessively high-flame temperature associated with combustion in pure oxygen. The main attraction of this technology is that it produces a flue gas predominantly composed of CO_2 and H_2O. The H_2O content is easily removed by condensation, leaving a pure CO_2 stream, which is suitable for compression, transport and storage.[6]

The advantage of oxy-fuel combustion is that, because the flue gas contains a high concentration of CO_2, the CO_2 separation stage is simplified. The main disadvantage is that cryogenic oxygen is an expensive technique.

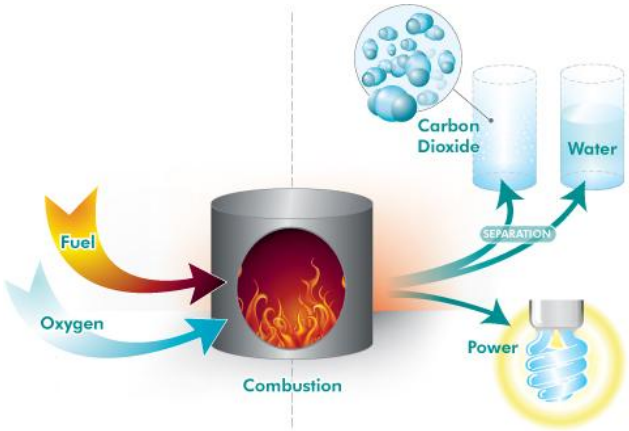

Figure 1.3 - Schematic representation of CO_2 capture by oxy-fuel combustion.[4]

Since post-combustion process captures CO_2 from flue gases produced by the combustion of fossil fuels and taking into account that a typical coal-fired flue gas contains predominantly CO_2 and N_2, the CO_2/N_2 separation will be the focus of this work.

As CO_2 separation is the first and most energy intensive step, new cost-effective and high performance technologies for carbon capture need to be researched and consequently the design of materials with the ability to efficiently separate CO_2 from other gases is of vital importance.

1.2 CO_2 Separation

1.2.1 Main Separation Technologies

It is necessary to develop efficient and suitable technologies for CO_2 separation with low operating cost and energy consumption. Separation technologies such as absorption with amines, adsorption with porous solids, membrane and cryogenic separation have been developed as potential candidates for CO_2 capture in post-combustion processes.

Amine-based absorption is undoubtedly the most common and efficient technology. Even though it has some advantages such as high reactivity and good absorption capacity, the use of amines involves several concerns related to their corrosive nature, volatility and high energy demand for regeneration.[7]

CO_2 adsorption with porous solids with high adsorbing properties such as zeolite or active carbon has some advantages including easy operation, rapid rate, low corrosion and low energy demand when regenerated. However, the selective separation of gases by these solid materials is less than ideal. Although some great progress has been achieved in solid adsorbents, additional research into how to improve their stability, recycling, cost and other parameters is needed for their application in industrial processes.[8]

Cryogenic distillation is a technique based on cooling and condensation. This process has good advantages such as no chemical absorbents are required and the process can be operated at atmospheric pressures. The main disadvantage of cryogenic technology is the high amounts of energy required to provide cooling for the process, which is especially prominent in low-concentration gas streams. This technique is suitable to high-concentration and high-pressure gases, namely in oxyfuel combustion and pre-combustion.[1, 9]

Alternatively, membrane separation technology (Figure 1.4) exhibits engineering and economical advantages over the other classical separation processes, namely the small scale of the equipment, relative environmental safety, ease of incorporation into existing processes, low energy consumption and operating costs.[10] The two parameters usually used to describe the performance of membranes are the permeability (measure of the membrane's ability to permeate gas) and selectivity (obtained dividing the permeability of the more permeable specie by the permeability of the less permeable specie).

Depending on the material, membranes are usually classified as polymeric, inorganic, and, more recently, mixed matrix membranes (MMMs). Polymeric membranes provide a range of characteristics desirable for membrane separations, such as mechanical properties, reproducibility and relative economical processing capability, making them one of the most common types of membrane. Rubbery polymers generally have higher CO_2 permeability than glassy polymers; however, their gas selectivity is low. Glassy polymers such as cellulose

acetate, polyacetylene, polyamide, polycarbonates, polyimides, poly(phylene oxide) and polysulfones have dominated industrial CO_2 separation applications due to their high gas selectivity and good mechanical properties. Despite glassy polymer membranes progress, large improvements in CO_2 separation efficiency require novel materials with enhanced separation performances. Their greatest application has been found for CO_2/CH_4 and CO_2/N_2 separations. On the other hand, rubbery polymeric membranes have attracted greater interest for CO_2/H_2 separation due to higher flux rates and high selectivity.[11]

Inorganic membranes, such as zeolite, silica, carbon molecular sieve and ceramic have the significant advantage of greater thermal and mechanical stability compared to organic polymers. However, some of the drawbacks of inorganic membranes are their high expected cost (including fabrication), high brittleness, low selectivity and permeability of highly selective dense membranes, particularly metal oxides at temperatures below 400 °C.[11]

Mixed-matrix membranes consist on the incorporation of inorganic particles into a continuous organic polymer matrix. These membranes attempt to combine the advantages of polymeric and inorganic materials, namely the desirable mechanical properties and economical processing capabilities of polymers with the high separation performance of molecular sieving materials.[12] Although mixed-matrix membranes have proven an enhancement of selectivity, it was observed that most of these membranes were endured with poor adhesion between the organic matrix and inorganic particles.[13]

Despite the large array of polymeric membranes for CO_2 separation developed during the last decades, there are still drawbacks to be overcome, such as the low CO_2 permeability and selectivity of solid membranes.[7] In order to circumvent these problems, supported liquid membranes have also been approached due to the high diffusion of gases in liquids when compared to solid membranes, leading to higher gas permeabilities.[14]

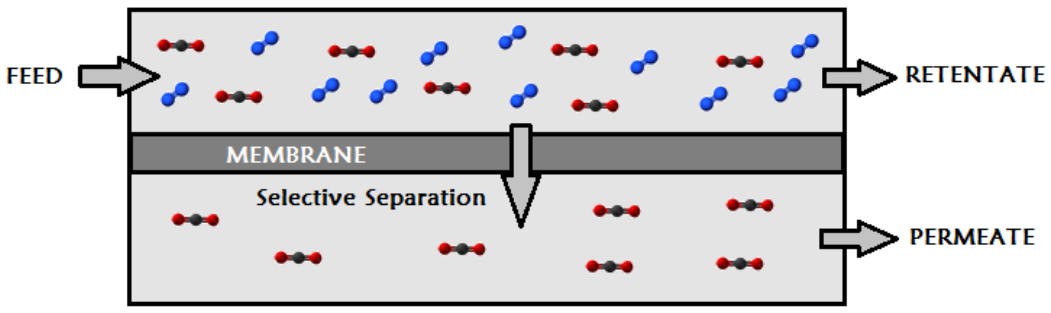

Figure 1.4 - Schematic of membrane gas separation.

1.3 Supported Liquid Membranes (SLMs)

Liquid membranes, based on configuration, can be broadly classified into three types: bulk, emulsion and supported liquid membranes. Bulk liquid membranes (BLMs) usually consist of an aqueous feed and stripping phase, separated by a water-immiscible liquid membrane phase in a U-tube. A small membrane surface area of BLMs makes them technologically not very attractive.[15]

On the other hand, emulsion liquid membranes (ELMs) have a very high surface area by unit of volume and low thickness which means that the separation process is fast**.** The disadvantages of ELMs concern the formation of the emulsion: the parameters that affect emulsion stability must be controlled and if, for any reason, the membrane does not remain intact during operation, the separation achieved up to that point is lost.[16]

Supported (or Immobilized) Liquid Membranes (SLMs) consist of two phases, a supporting porous membrane and a liquid solvent phase that resides inside the pores by capillary forces. In this case, the separation takes place in the liquid phase according to the solution-diffusion model, where the solute molecules dissolve into the liquid, diffuse through it and finally desorb at the opposite side of the membrane (Figure 1.5).[17, 18] The diffusion coefficient in liquids is at least three or four orders of magnitude higher than in polymer membranes.[15] Consequently, the permeability is expected to be much higher in the supported liquid membranes than in conventional polymeric membranes.

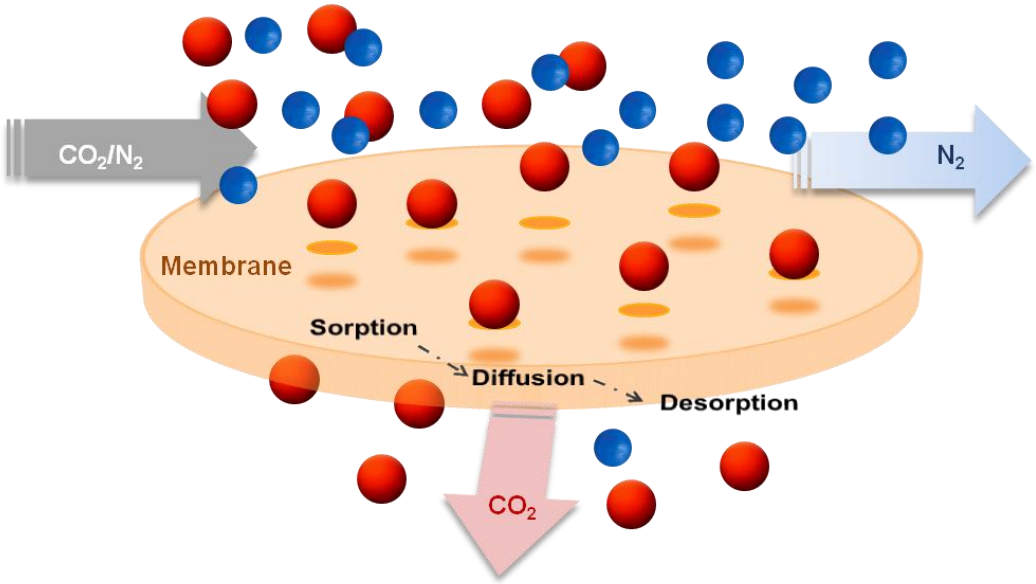

Figure 1.5 - Scheme of the gas transport mechanism through supported liquid membranes.

A significant parameter in the design of SLMs is the liquid viscosity. Several studies with different solvents have been performed showing that the effect of viscosity is not negligible.[19] In general, liquids with low viscosity result in higher CO_2 permeability due to the easy diffusion of CO_2 through the SLM.[20]

Despite the high gas diffusion and consequently the high gas permeabilities in supported liquid membranes, the main technical challenge of SLMs is the membrane stability since the solvent that is in the pores can evaporate at specific operating conditions, such as high temperature and pressure differentials.[7] In order to overcome this disadvantage, the most interesting strategy is the use of ionic liquids (ILs) due to their remarkable intrinsic properties, in particular, almost null volatility. In fact, ionic liquids have been introduced to replace volatile organic solvents, which have created barriers in the applications of SLMs.

1.4 Ionic Liquids

Ionic liquids (ILs) are salts entirely composed of ions that have melting points below 100 °C or even at room temperature due to the poor coordination of their ions.[21] This new class of compounds have been called Room-Temperature Ionic Liquids (RTILs) in order to differentiate them from traditional salts, which melt at much higher temperatures and are classified as "molten salts".[22]

As long as ILs have being designed as greener solvents to replace conventional volatile solvents, they are showing increasingly promising perspectives in diverse fields of synthesis, catalysis/biocatalysis, materials science, electrochemistry, and separation technology at both the laboratory level and on the industrial scale.[23] Although the first room temperature ionic liquids were first observed in the middle of the 19th Century, only since the 1980s they have attracted a significant and growing interest.[24] In recent years, ILs have been studied extensively due to their exceptional combination of properties, namely their negligible vapor pressure,[25] which means that ILs emit no volatile compounds, their high thermal stability,[26] low flammability and the fact that ILs are good solvents for a whole range of inorganic and organic materials. Moreover, another mentioned characteristic of ILs is the possibility of obtaining desired physicochemical properties by selecting proper combinations of cations and anions or by adding functional groups ("tunability"), which makes them "designer solvents". For example, ILs can be produced to be water-miscible, partially miscible or totally immiscible, and can also be synthesized with different viscosities.[22] These attractive properties make them absolutely unique and incomparable to other solvents.

Due to their unique properties, ILs are important candidates for several applications. Throughout the 1990s, it seemed that most of attention in the area of ionic liquids applications was directed toward their use as solvents for organic and transition-metal-catalyzed reactions. Definitely, this interest continues on to the present date, but the most innovative uses of ionic liquids span a much more diverse field than just synthesis. Some of the main topics of coverage include the application of ILs in various electronic applications (batteries, capacitors, and light-emitting materials), polymers (synthesis and functionalization), nanomaterials (synthesis and stabilization), and gas separations.[27]

Cation–anion combinations that exhibit low volatility coupled with high electrochemical and thermal stability, as well as ionic conductivity, create the possibility of designing ideal electrolytes for batteries. On the other hand, the low vapor pressure of these liquids, along with their ability to offer tuneable functionality, also makes them ideal as CO_2 absorbent materials.[28]

1.5 Supported Ionic Liquid Membranes (SILMs)

Supported ionic liquid membranes (SILMs) have been studied due to the intrinsic properties of ILs, namely negligible vapor pressure, high thermal stability and low flammability, as described in the previous section, that make them ideal liquid phases for supported liquid membrane applications. As referred, since ILs have negligible vapor pressure, an important advantage of using SILMs is that minimal membrane liquid loss through solvent evaporation is guaranteed, which allow more stable membranes due to the higher viscosity of ILs and greater capillary forces between the desired ionic liquid and the polymer membrane support.[7, 29]

On top of that, ionic liquids present good levels of solubility and selectivity of CO_2 over other light gases, such as N_2. Since gas solubility in ionic liquids is an important parameter in gas separation processes, a great deal of effort has been putted on the experimental determination and theoretical understanding of gas solubilities in ILs.[30-33] For example, Brennecke and co-authors carefully studied the CO_2 solubility in several commonly used ILs and concluded that the anion of the IL has a larger influence on CO_2 solubility than the cation.[34-37] Additionally, the influence of different functional groups, such as alkyl, ether, hydroxyl, amine, nitrile and fluorine, on the gas solubility properties of ILs has also been intensively investigated by different authors.[38]

Supported ionic liquid membranes (SILMs), in which the desired IL is immobilized into the pores of a solid membrane by capillary forces, are considered a very attractive approach compared to bulk-fluid ILs since much smaller amounts of IL are needed.[39] Moreover,

membranes constitute an attractive alternative gas separation technology, due to their inherent fundamental engineering and economic advantages.

A broad diversity of ILs has already been tested for developing SILM systems. Taking into account the good levels of solubility and selectivity of CO_2 in ILs as well as their highly tuneable nature, several studies on the permeation properties of gases through SILMs have explored the effect of the IL structure.[40] Concerning the influence of the cation, a number of research groups have investigated the gas permeation properties of different families of ionic liquids such as imidazolium,[18, 19, 41-45] pyrrolidinium,[46-48] piperidinium and morpholinium,[46] pyridinium,[49] ammonium,[50] phosphonium,[51, 52] or cholinium,[53] and improved results were obtained for imidazolium-based SILMs in terms of permeability and selectivity. Other studies, also focused on imidazolium ILs, explored different structural variations of the cation in order to improve CO_2 solubility and selectivity.[54, 55] In what concerns the anion variation, the performance of imidazolium-based ILs containing several different anions such as bis(trifluoromethylsulfonyl)imide ($[NTf_2]^-$),[18, 19] hexafluorophosphate ($[PF_6]^-$),[19, 51] dicyanamide ($[DCA]^-$),[18, 56] tricyanomethane ($[C(CN)_3]^-$),[56, 57] tetracyanoborate ($[B(CN)_4]^-$),[47, 56] among others, has been evaluated, and the results indicate that nitrile-containing anions promote an increase in both CO_2 permeability and CO_2/N_2 selectivity when compared to the $[NTf_2]^-$.

In this context, it is important to highlight that the ability to tailor the CO_2 affinity of the ionic liquid by combining different cations and anions is perhaps the most important feature of ILs for gas separation applications.

1.6 Facilitated Supported Ionic Liquid Membranes

Facilitated transport membranes have been intensively investigated, since their CO_2 permeability and selectivity can be simultaneously improved through reversible complexation reactions between CO_2 and carriers (such as carbonate, amine group and carboxylate) in the membrane by which its solubility is greatly enhanced.[58] The facilitated transport membrane originated from liquid membranes, in which the carriers can move freely and actively transport CO_2, leading to excellent performances.

Amino acid-based ionic liquids (AAILs) have been studied due to their high performance for effective and selective CO_2 capture.[59-64] AAILs have been shown to have a range of useful properties, which allow the facilitated transport membranes design, due to the fact that present both carboxyl and amine functional groups and can be used as either anions or cations.[65] AAILs were first introduced by Fukumoto *et al.*, wherein the AAIL was composed of imidazolium cations and amino acid anions,[61] and by Tao *et al.*, who reported ILs, in which the cations involved were derived directly from natural amino acids.[66]

A variety of cations (imidazolium, pyridinium, ammonium and phosphonium) have been be functionalized with amines for CO_2 capture. For example, Bates *et al*. studied the CO_2 fixation with amine-functionalized ILs by incorporating an amine group into the alkyl chain of the imidazolium cation, showing a significantly higher uptake of CO_2 than that of traditional ILs.[60] Besides ILs having amine groups on the cation, a number of amino acid-based ionic liquids bearing amine functionality in the anion have also been reported and used as absorbents to CO_2 capture.[61-64, 67] Additionally, Hanioka *et al*. showed that SILMs of amine functionalized imidazolium ILs are highly selective in CO_2/CH_4 separation due to facilitated CO_2 transport.[68] Myers *et al*. also reported high CO_2/H_2 separation performances at high temperatures of supported amine-functionalized ionic liquid membranes.[69] Moreover, Kasahara *et al.* investigated the CO_2 permeability and CO_2/N_2 selectivity of amino acid-based ionic liquids, as CO_2 carrier and diffusion medium in supported ionic liquid membranes, under low moisture. In that work, SILMs of $[P(C_4)_4][Gly]$ and $[C_2mim][Gly]$ were prepared. It was observed that the CO_2 permeabilities for $[P(C_4)_4][Gly]$ and $[C_2mim][Gly]$ drastically increased up to 5000 and 8300 Barrer, respectively, with increasing temperature. On the other hand, the permeabilities of N_2 for both the facilitated supported ionic liquid membranes (FSILMs) slightly increased. As a result, the CO_2/N_2 selectivity also increased significantly. Kasahara *et al.* concluded that the unusual dependence of CO_2 permeability on temperature suggests that SILMs with amino acid-based ionic liquids definitely reacted with CO_2 and facilitated the CO_2 transport even under dry conditions.[70] In conclusion, since AAILs present an amino–functionalized group, they can react with CO_2, form CO_2 complexes and, therefore, act as CO_2 carriers in facilitated SILMs[70].

Although the CO_2 absorption in AAILs is substantially improved, the relatively high viscosity of AAILs results in low sorption and desorption rates and might limit their eventual use in large-scale CO_2 gas separation.[62, 71]In order to overcome this disadvantage, ionic liquid mixtures were explored in this work, so that one IL component provides the desired chemical characteristics for the active transport while the other maintains the low viscosity.

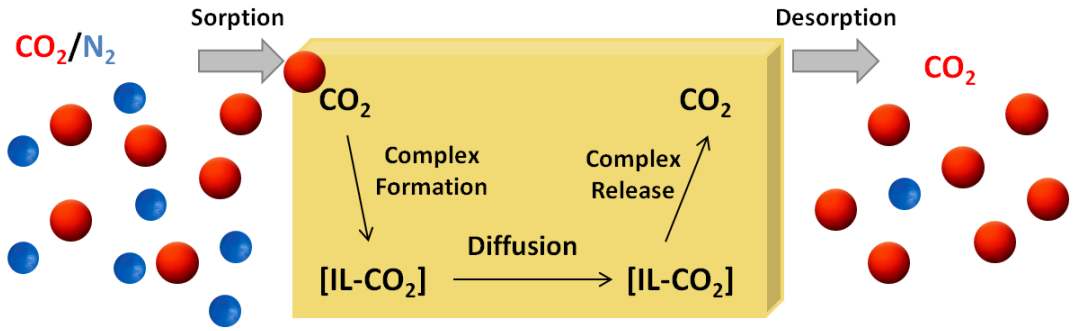

Figure 1.6 – Schematic illustration of facilitated transport of CO_2 in SILMs.

1.7 Ionic Liquid Mixtures

The concept of an ideal mixture comes from the observations of François Raoult that at a given temperature the ratio of partial vapour pressure of a component *A* above a liquid mixture (p_A) to its vapour pressure as a pure liquid (p^*_A) is approximately equal to its mole fraction in the liquid mixture (X_A):

$$\boldsymbol{p_A = X_A \times p_A^*} \quad \textbf{(1.1)}$$

Liquid mixtures that obey Raoult's Law (Equation 1.1) precisely are ideal solutions. When linear behaviour would be expected for ideal behaviour, deviation from the expected value is described as the difference between the observed volume of mixing and the ideal volume of mixing is the excess volume of mixing, V^E, which can take both positive and negative values. The definition of ideal mixing from Equation 1.1., also leads to the V^E=0.[72]

Mixing ILs with other ILs (IL + IL mixtures) is seen as a possible method to improve target properties of ILs while maintaining their favorable characteristics.[73]

Even though ionic liquid mixtures have been proposed as a mean to further increase flexibility and the fine-tune capacity of the physical and chemical properties of ILs, providing an extra degree of freedom for the design of new solvents,[72] only a few works have explored gas solubilities in binary IL + IL mixtures. Finotello *et al.*[74] measured the CO_2, CH_4 and N_2 solubilities of $[C_2mim][NTf_2]$ and $[C_2mim][BF_4]$ mixtures and the results showed that this approach can be used to enhance CO_2 solubility selectivity due to control over IL molar volume.

Recently, Tomé *et al.*[7] studied the gas permeation properties of CO_2, CH_4 and N_2 in several binary ionic liquid mixtures based on a common cation ($[C_2mim]^+$) and different anions such as bis(trifluoromethylsulfonyl) imide ($[NTf_2]^-$), acetate ($[Ac]^-$), lactate ($[Lac]^-$), dicyanamide ($[DCA]^-$) and thiocyanate ($[SCN]^-$) and showed that IL mixtures is an easy and promising strategy to perform CO_2 separation using SILMs, since the IL properties can be tuned by mixing anions with completely different chemical character. In addition, the highest CO_2 separation performances were found for the less viscous IL mixtures, meaning that a proper balance combining both the most selective and the less viscous anions is crucial to achieve improved CO_2 separation performances.[7] Furthermore, Tomé *et al.*[38] recently investigated new IL mixtures containing sulfate and/or cyano-functionalized anions proposed as liquid phases in SILM configurations for CO_2 separation and it was concluded that gas permeabilities through SILMs are not entirely controlled by their gas diffusivities and their respective IL viscosities. In fact, they are also linked to the CO_2 solubilities.[38]

Taking into account that the anions of ILs have a stronger influence on CO_2 solubility than the cations,[75] and that the CO_2 molecules have a larger affinity for anion *versus* cation associations,[17, 30] in this work IL + IL mixture systems with a common cation and different anions were studied. Since ILs containing amino acids-based anions, with "reactive" amine groups which work as a CO_2 carriers,[70] and taking into account that ILs combining cyano-functionalized anions present remarkably low viscosities,[76] mixtures of these ILs based on a common imidazolium cation ($[C_2mim]^+$) were considered. The $[C(CN)_3]^-$ anion was selected since it has a extraordinarily low viscosity as previously referred. On the other hand, glycinate anion ($[Gly]^-$) was chosen because it is the simplest available amino acid. Additionally, L-alaninate ($[L\text{-}Ala]^-$) was selected due to its similar chemical structure compared to glycinate. L-serinate ($[L\text{-}Ser]^-$) was chosen because it not only has a similar chemical structure to glycinate and L-serinate but also comprise an additional hydroxyl group. In order to evaluate the effects of a cyclic structure and the sulfonic group, both L-prolinate ($[L\text{-}Pro]^-$) and taurinate ($[Tau]^-$) were also selected, respectively. The chemical structures of the ionic liquids studied in this work are present in Figure 1.7.

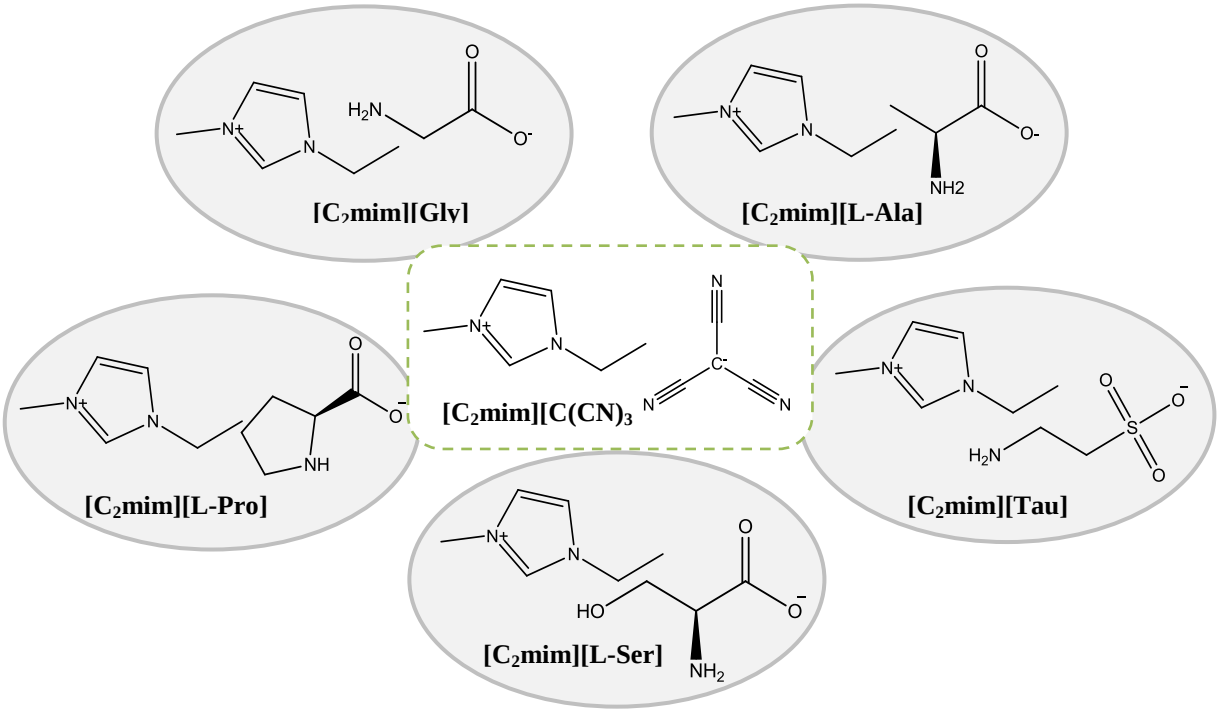

Figure 1.7 - Chemical structures of ionic liquids used in this work.

1.8 Objectives

The main purpose of this work is to evaluate the performance of IL + IL mixtures as new liquid phases to prepare facilitated supported ionic liquid membranes for flue gas separation (CO_2/N_2). For this purpose, AAILs were selected, so that CO_2 facilitated transport could be attained, and mixed with $[C_2mim][C(CN)_3]$, a very low viscous IL. In order to increase the flexibility in tailoring both the permeability and selectivity of these membranes for flue gas separation (CO_2/N_2), mixtures of varying concentrations were prepared.

Five ionic liquids based on a common cation ($[C_2mim]^+$) and anions such as tricyanomethane ($[C(CN)_3]^-$), glycinate ($[Gly]^-$), L-alaninate ($[L\text{-}Ala]^-$), taurinate ($[Tau]^-$), L-serinate ($[L\text{-}Ser]^-$) and L-prolinate ($[L\text{-}Pro]^-$) were mixed and SILMs were prepared.

The gas permeation properties (permeability, diffusivity and solubility) of CO_2 and N_2 were determined using a time-lag apparatus.

Since viscosity and molar volume, are parameters that impact the gas permeation properties of SILMs, the thermophysical properties of the pure ILs and their mixtures, namely viscosity, density and refractive index, were also measured so that trends could be evaluated.

2

Synthesis and Characterization of AAILs

The amino acid-based ionic liquids used in this study, namely 1-ethyl-3-methylimidazolium 2-aminoacetate ([C_2mim][Gly]), 1-ethyl-3-methylimidazolium (S)-2-aminopropanoate ([C_2mim][L-Ala]), 1-ethyl-3-methylimidazolium 2-aminoethanesulfonate ([C_2mim][Tau]), 1-ethyl-3-methylimidazolium (S)-2-amino-3-hydroxypropanoate ([C_2mim][L-Ser]) and 1-Ethyl-3-methylimidazolium (S)-pyrrolidine-2-carboxylate ([C_2mim][L-Pro]), were synthesized via a two-step anion exchange reaction and were characterized by ^{1}H and ^{13}C NMR.

The thermogravimetric analysis (TGA) of the pure ionic liquids and their mixtures was also performed in order to establish the degradation temperature of these liquid phases and thus their upper working temperature limit. This step was especially important in this work since high temperatures are necessary to overcome the energy barrier required for the active gas transport complex formation.

2.1 Materials and Synthesis of AAILs

2.1.1 Materials

Glycine (≥ 98.5 %), L-alanine (≥ 99.5 %), taurine (≥ 99 %), L-serine (≥ 99.5 %) and L-proline (≥ 99 %), acetonitrile (99.8 %) and methanol (99.8 %) were provided by Sigma Aldrich. The 1-ethyl-3-methylimidazolium tricyanomethane ([C_2mim][$C(CN)_3$]), > 98 wt% pure, and the 1-ethyl-3-methylimidazolium chloride [C_2mim][Cl], > 98 wt% pure, were supplied by IoLiTec GmbH.

2.1.2 Synthesis of amino acid ionic liquids (AAILs)

The ionic liquids used in this study were synthesized via a two-step anion exchange reaction, following an established procedure developed by Ohno *et al.*[61] First, an aqueous solution of 1-ethyl-3-methylimidazolium hydroxide ([C_2mim][OH]) was prepared by passing an aqueous solution of [C_2mim][Cl] through a column filled with anion exchange resin (SUPELCO AMBERLITE IRN-78) (Figure 2.1) in the hydroxide form. Afterwards, the [C_2mim][OH] was neutralized by the dropwise addition of a slight excess of the corresponding equimolar amino acid aqueous solution with cooling. The mixtures were stirred at ambient temperature and pressure for 12 h. Excess of water was then removed by rotary evaporation under reduced pressure. A mixture of acetonitrile and methanol (9:1 v/v) was added to precipitate the unreacted amino acid. After filtration, the solvents were removed by rotary evaporation and the obtained crude products were dried under vacuum (10^{-3} kPa) and subjected to vigorous stirring at moderate temperature (≃318 K) for at least 4 days immediately prior to use. The water

contents of the pure ILs and their mixtures were determined by Karl Fischer titration (831 KF Coulometer, Metrohm).

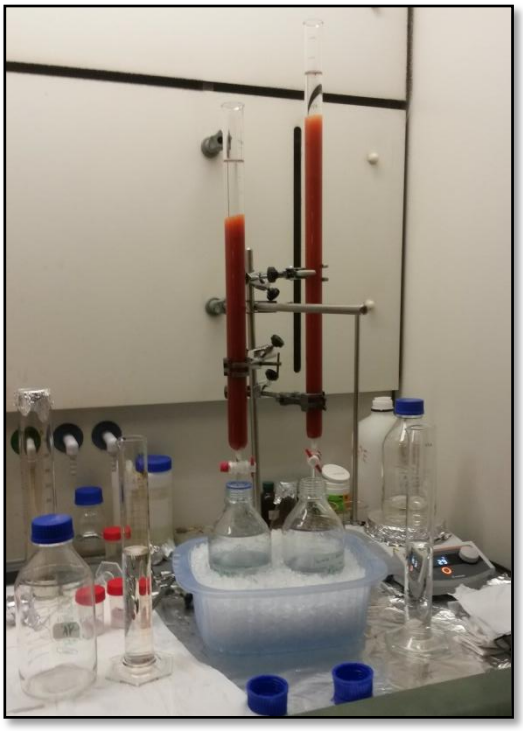

Figure 2.1 - AAILs synthesis method.

Figure 2.2 shows the neat imidazolium-based AAILs at room temperature after the drying procedure. Their purities were confirmed by ^{1}H and ^{13}C NMR analysis (see Appendix 1 for further details).

Figure 2.2 - Pure imidazolium-based AAILs at room temperature after the drying procedure.

2.2 Thermogravimetric Analysis (TGA)

The onset and decomposition temperatures of the pure ionic liquids and the prepared ionic liquid mixtures with 0.5 of molar fraction were measured using a thermal gravimetric analyzer (TA instrument Model TGA Q50). The samples were placed inside aluminium pans and heated up to 500 °C at a heating rate of 10 °C·min^{-1} until complete thermal degradation was achieved. All samples were recorded under a nitrogen atmosphere. Universal Analysis, version 4.4A software, was used to determine the onset and the decomposition temperatures, as the temperatures at which the baseline slope changes 5% during the heating, and at which the point of greatest rate of change on the weight loss curve (first derivative peak) is observed, respectively.

Figure 2.3 - TGA 2950/Q500 analyzer.

Considering that temperature is also a crucial parameter on the performance of the prepared SILMs, it was necessary to determine the degradation temperature of the pure ILs and their mixtures considered in the gas transport measurements (*Chapter 4*).

The obtained onset, $T_{5\%}$ and decomposition, $T_{deg\ 1}$ and $T_{deg\ 2}$, temperatures are presented in Table 2.1. Two different decomposition temperatures were considered since two different peaks were obtained in the first derivative weight loss curve, for the five IL mixtures studied.

From Table 2.1, it can be observed that the decomposition temperature for all samples with the exception of the pure [C_2mim][$C(CN)_3$] is near to 500 K.

Table 2.1 – Onset ($T_{5\%}$) and decomposition ($T_{deg\ 1}$ and $T_{deg\ 2}$) temperatures of the pure ILs and their mixtures.

Ionic Liquids	$T_{5\%}$ (K)	$T_{deg\ 1}$ (K)	$T_{deg\ 2}$ (K)
$[C_2mim][C(CN)_3]$	606	634	—
$[C_2mim][C(CN)_3]_{0.5}$ $[Gly]_{0.5}$	484	518	624
$[C_2mim][C(CN)_3]_{0.5}$ $[L\text{-}Ala]_{0.5}$	484	512	628
$[C_2mim][C(CN)_3]_{0.5}$ $[Tau]_{0.5}$	530	540	597
$[C_2mim][C(CN)_3]_{0.5}$ $[L\text{-}Ser]_{0.5}$	488	524	631
$[C_2mim][C(CN)_3]_{0.5}$ $[L\text{-}Pro]_{0.5}$	476	517	551
$[C_2mim][Gly]$	430	500	—
$[C_2mim][L\text{-}Ala]$	455	509	—
$[C_2mim][Tau]$	500	574	—
$[C_2mim][L\text{-}Ser]$	476	514	—
$[C_2mim][L\text{-}Pro]$	416	536	—

The two decomposition temperatures obtained, through the first derivative weight loss curve, are illustrated in Figure 2.7, as an example, for the $[C_2mim][C(CN)_3]_{0.5}[L\text{-}Ala]_{0.5}$ mixture.

Additionally, Figures 2.4, 2.5, 2.8 and 2.9 present the TGA thermogram and derivative weight loss curve, respectively, of the pure $[C_2mim][C(CN)_3]$ and $[C_2mim][L\text{-}Ala]$, as examples. Comparing these results with those of pure ILs it can be concluded that the first decomposition temperature, $T_{deg\ 1}$, belongs to the AA anion while the second decomposition temperature, $T_{deg\ 2}$, is related to $[C(CN)_3]^-$ anion. The remaining TGA thermograms and derivative weight loss curves are displayed in Figures 7.11-7.26 (Appendix 2).

From Figure 2.4, it can also be observed that the pure $[C_2mim][C(CN)_3]$ did not achieve entirely degradation until ≃ 873 K, which means that higher temperatures would be required for its complete degradation. This is entirely in agreement to what has been observed in the literature for ILs containing the $[C(CN)_3]^-$ anion,[77] Furthermore, the decomposition temperatures of the pure amino acid-based ILs can be ordered as: $[C_2mim][Gly] < [C_2mim][L\text{-}Ala] < [C_2mim][L\text{-}Ser] < [C_2mim][L\text{-}Pro] < [C_2mim][Tau]$.

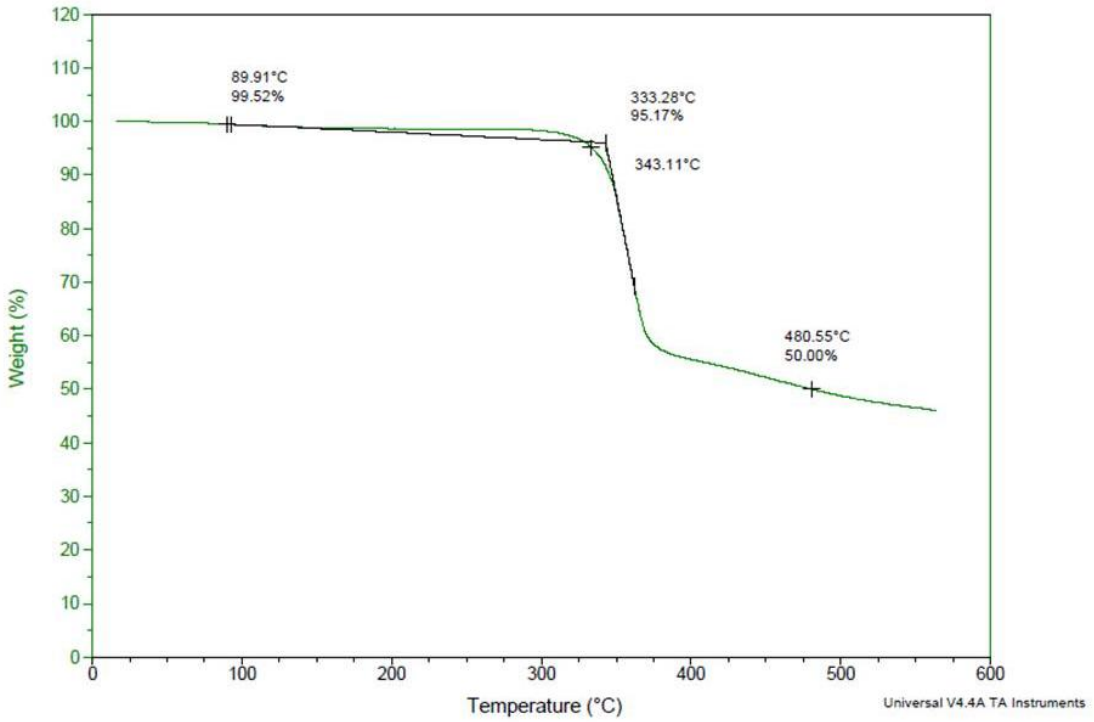

Figure 2.4 - TGA thermogram of the pure $[C_2mim][C(CN)_3]$.

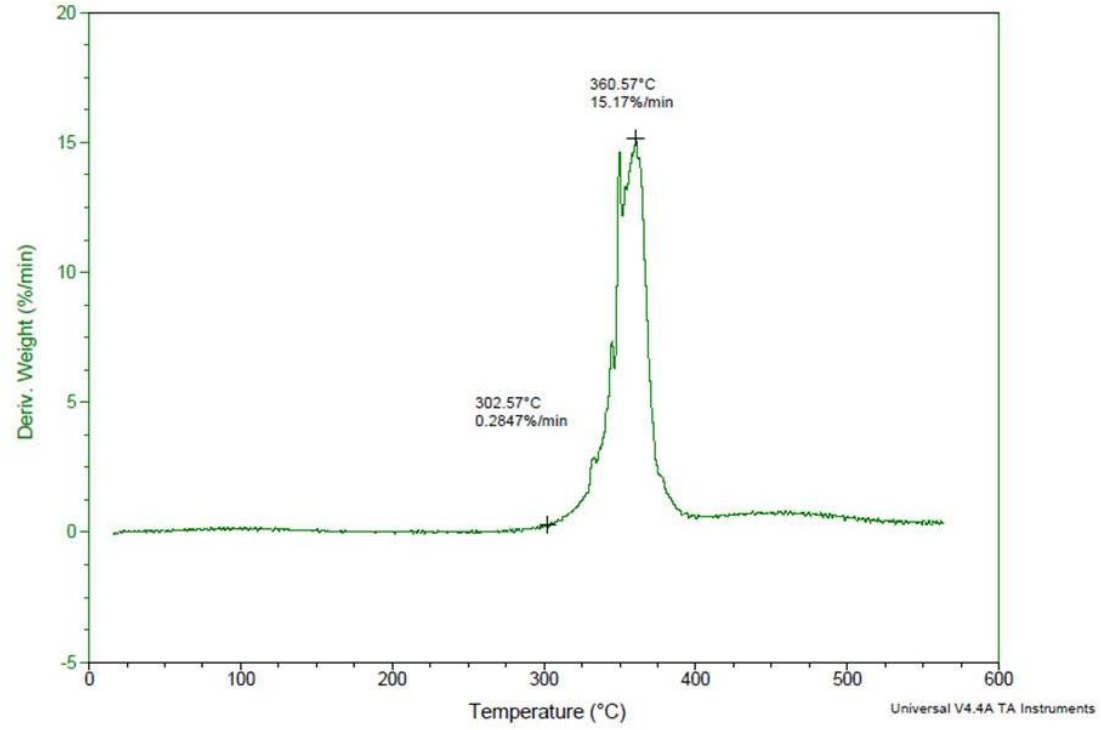

Figure 2.5 - Derivative weight (%/min) of the pure $[C_2mim][C(CN)_3]$ as a function of temperature (*T*).

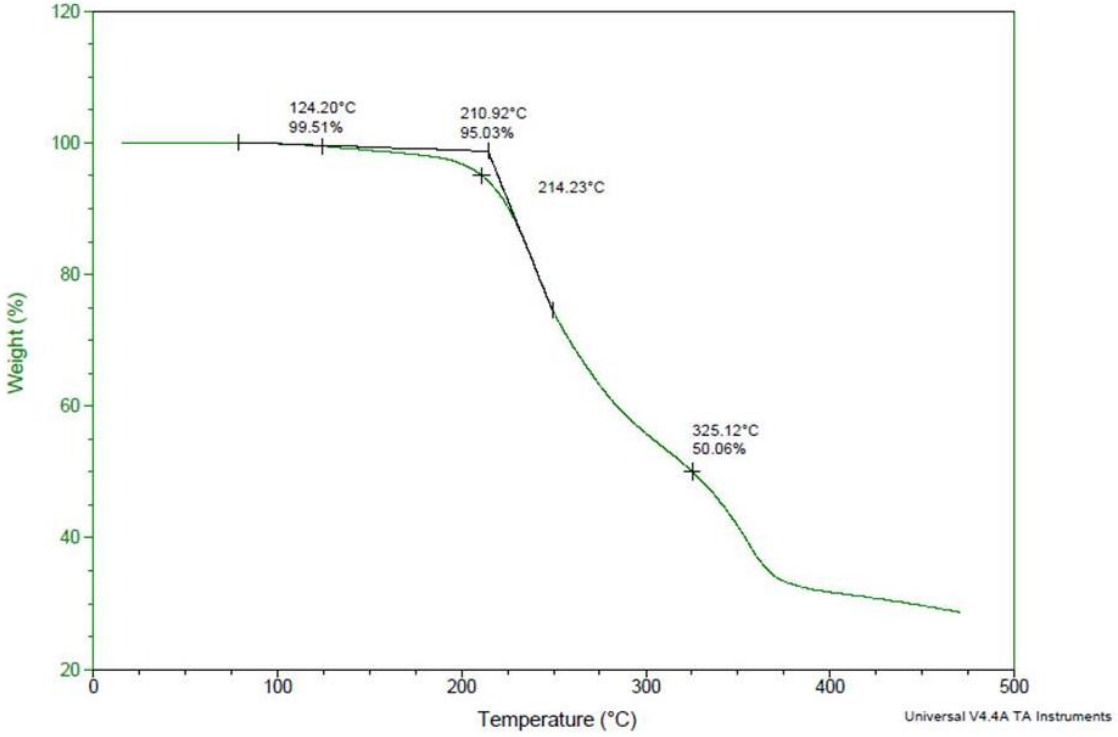

Figure 2.6 – TGA thermogram of $[C_2mim][C(CN)_3]_{0.5}[L\text{-}Ala]_{0.5}$ mixture.

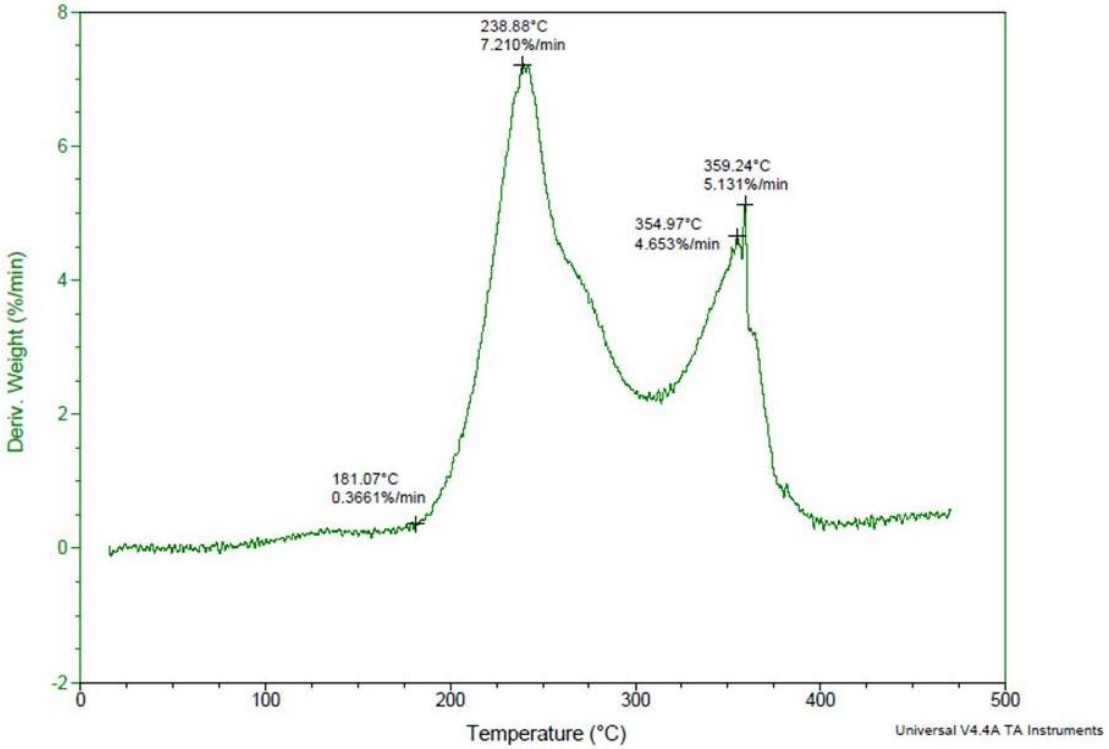

Figure 2.7- Derivative weight (%/min) of $[C_2mim][C(CN)_3]_{0.5}[L\text{-}Ala]_{0.5}$ mixture as a function of temperature (*T*).

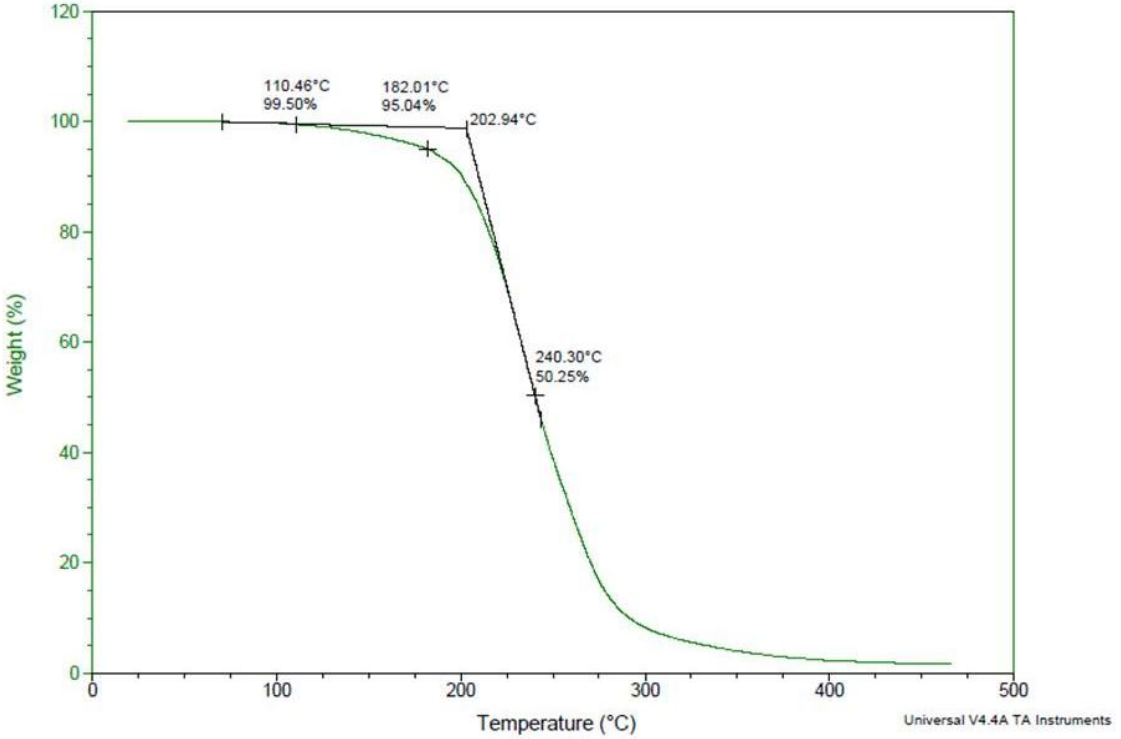

Figure 2.8 - TGA thermogram of the pure [C_2mim][L-Ala].

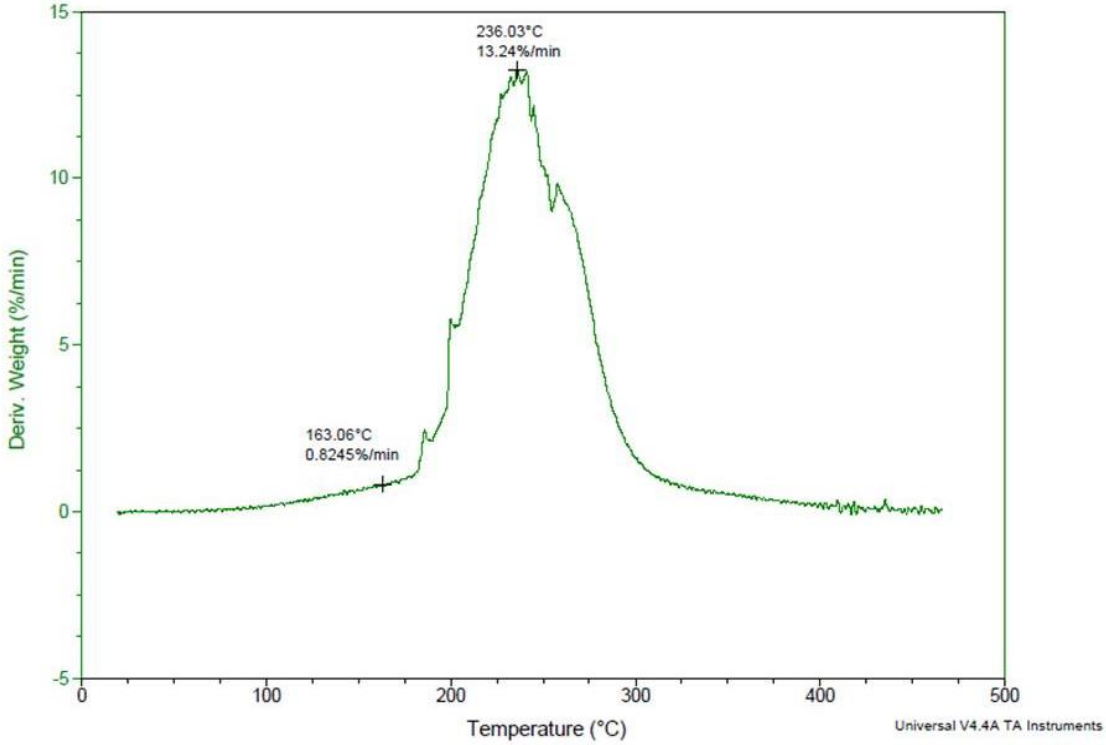

Figure 2.9 - Derivative weight (%/min) of the pure [C_2mim][L-Ala] as a function of temperature (*T*).

3

Thermophysical Characterization

The study of the thermophysical properties of ionic liquids is crucial to design and synthesize them with suitable properties for a desired application.[78]

The focus of this work is to study new binary IL + IL mixtures as liquid phases in FSILMs. The use of mixtures instead of pure ionic liquids can be viewed as another step towards the increase in their flexibility in tailoring permeability and selectivity for flue gas separation (CO_2/N_2), as referred in C*hapter 1*.

Amino acid based-ionic liquids can work as CO_2 carriers but their high viscosities limit their application as liquid phases in SILMs due the large decrease in mass transfer properties, namely gas permeabilities and diffusivities.[70] In order to overcome this limitation and prepare low viscous liquid phases for CO_2 facilitated SILMs, amino acid based-ionic liquids were mixed with the $[C_2mim][C(CN)_3]$ IL, which is well known for its remarkable low viscosity.[76]

The IL viscosity is a significant thermophysical property that impacts the gas permeation properties of SILMs. Another important parameter is the molar volume that is associated to the solubility. Despite extensive research on ionic liquids, the correlation between structure and transport properties is still far from being fully understood.[79] Stokes–Einstein relation estimates the self-diffusion that can be expected for a given viscosity:

$$\boldsymbol{D = \frac{kT}{6\pi\eta R}} \qquad \textbf{(3.1)}$$

where the diffusion coefficient (D) for a particle in a free volume depends on the Boltzmann constant (k), the absolute temperature (T), the viscosity of the solution (η), and the hydrodynamic radius (R) of the particle.[79]

Due to the limited amount of data available on ion self diffusion constants for ionic liquids, owing to the intricate interactions pattern displayed by these fluids, it is difficult to provide a precise assessment of their behaviour. For the relative order of diffusion constants at a given mixture ratio, a similar depiction emerges as for the pure liquids, with cations diffusing faster than anions and the relative order within each group consistent with the corresponding simple ionic liquids.[72]

In order to evaluate trends between the transport properties and thermophysical properties, the viscosity, density and refractive index of the pure ionic liquids ($[C_2mim][C(CN)_3]$, $[C_2mim][Gly]$, $[C_2mim][L\text{-}Ala]$, $[C_2mim][Tau]$, $[C_2mim][L\text{-}Ser]$ and $[C_2mim][L\text{-}Pro]$) and their mixtures were measured in the temperature range between 293.15 and 353.15K at atmospheric pressure. It should be noted that since was considered a common cation ($[C_2mim]^+$), it only appears once in the IL mixtures nomenclature throughout this work.

Refractive indexes were also measured in order to enable the calculation of the free molar volume. This parameter can be especially important in the interpretation of gas solubility

results. In a very simple analysis, the solubility of a gas in a solvent can be divided in two different contributions, physical and chemical. The physical contribution is related to the volume of the cavity needed to insert a gas molecule inside of the solvent and the intermolecular interactions established between the two molecules. The chemical contribution, when it exists, is related to the formation of new species between the solute and the solvent, such as the formation complexes. Indeed, the free molar volume can be related to the interpretation of the physical solubility where no "reaction" between gas and solute is considered.

3.1 Preparation of the ionic liquid mixtures

The IL + IL mixtures (Figure 3.1) were prepared using an analytical high-precision balance with an uncertainty of ± 10^{-5} g by syringing known masses of the IL components into glass vials. Good mixing was assured by magnetic stirring for at least 30 minutes. Then, the prepared IL mixtures were dried under vacuum (10^{-3} kPa) at a moderate temperature (≈318 K) for another 4 days. The samples were prepared immediately prior to the measurements to avoid variations in composition. The measured thermophysical properties, viscosity, η, and density, ρ, and the calculated molar volume, V_m, of the pure ionic liquids and their mixtures at 293.15K as well as their water contents are presented in Table 3.1.

Common cation $[C_2mim]^+$ 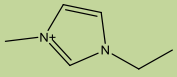	% of $[C(CN)_3]^-$ 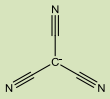		
	25	**50**	**75**
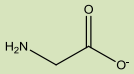 **$[Gly]^-$**	**X**	**X**	**X**
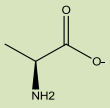 **$[L\text{-}Ala]^-$**	**X**	**X**	**X**
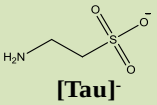 **$[Tau]^-$**	**X**	**X**	**X**
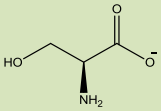 **$[L\text{-}Ser]^-$**	**X**	**X**	**X**
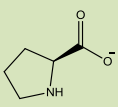 **$[L\text{-}Pro]^-$**	**X**	**X**	**X**

Figure 3.1 – Chemical structures of ions used and composition matrix of the prepared IL + IL mixtures.

Table 3.1 - Thermophysical properties, viscosity (η), density (ρ), and calculated molar volume (V_m), at 293.15 K as well as water contents of the pure ionic liquids and their mixtures studied in this work.

Ionic liquid sample	wt % of water	M ($g \cdot mol^{-1}$)	η (mPa·s)	ρ ($g \cdot cm^{-3}$)	V_m ($cm^3 \cdot mol^{-1}$)
$[C_2mim][Gly]$	1.44	185.22	240.183	1.164	159.08
$[C_2mim][L\text{-}Ala]$	1.23	199.25	382.060	1.126	176.91
$[C_2mim][Tau]$	0.20	235.30	760.887	1.255	187.49
$[C_2mim][L\text{-}Ser]$	0.67	215.25	3630.267	1.207	178.36
$[C_2mim][L\text{-}Pro]$	0.70	225.29	2134.400	1.144	196.89
$[C_2mim][C(CN)_3]_{0.25}[Gly]_{0.75}$	2.22	189.22	94.033	1.140	165.96
$[C_2mim][C(CN)_3]_{0.25}[L\text{-}Ala]_{0.75}$	0.43	199.75	146.567	1.114	179.35
$[C_2mim][C(CN)_3]_{0.25}[Tau]_{0.75}$	0.14	226.78	242.413	1.208	187.78
$[C_2mim][C(CN)_3]_{0.25}[L\text{-}Ser]_{0.75}$	1.68	211.75	586.840	1.177	179.87
$[C_2mim][C(CN)_3]_{0.25}[L\text{-}Pro]_{0.75}$	1.96	219.28	551.760	1.138	192.75
$[C_2mim][C(CN)_3]_{0.5}[Gly]_{0.5}$	0.65	193.23	55.692	1.118	172.77
$[C_2mim][C(CN)_3]_{0.5}[L\text{-}Ala]_{0.5}$	0.10	200.24	78.604	1.102	181.68
$[C_2mim][C(CN)_3]_{0.5}[Tau]_{0.5}$	0.05	218.27	84.495	1.165	187.38
$[C_2mim][C(CN)_3]_{0.5}[L\text{-}Ser]_{0.5}$	0.29	208.24	168.520	1.142	182.37
$[C_2mim][C(CN)_3]_{0.5}[L\text{-}Pro]_{0.5}$	0.28	213.26	224.150	1.120	190.46
$[C_2mim][C(CN)_3]_{0.75}[Gly]_{0.25}$	0.54	197.23	29.045	1.101	179.10
$[C_2mim][C(CN)_3]_{0.75}[L\text{-}Ala]_{0.25}$	0.10	200.74	31.551	1.093	183.67
$[C_2mim][C(CN)_3]_{0.75}[Tau]_{0.25}$	0.07	205.49	35.420	1.124	186.60
$[C_2mim][C(CN)_3]_{0.75}[L\text{-}Ser]_{0.25}$	0.55	204.74	42.012	1.113	183.97
$[C_2mim][C(CN)_3]_{0.75}[L\text{-}Pro]_{0.25}$	0.02	207.25	57.468	1.103	187.86
$[C_2mim][C(CN_3)]$	0.01	201.23	16.624	1.085	185.54

3.2 Experimental Procedure

3.2.1 Viscosity and density measurements

Measurements of viscosity and density of the pure ILs and their mixtures were performed in the temperature range between 293.15 and 353.15K at atmospheric pressure using an SVM 3000 Anton Paar rotational Stabinger viscometer-densimeter. The SVM 3000 uses Peltier elements for fast and efficient thermostability and the temperature uncertainty is ± 0.02 K. The precision of the dynamic viscosity measurements is ± 0.5 % and the absolute uncertainty of the density is ± 0.0005 $g \cdot cm^{-3}$. The overall uncertainty of the viscosity measurements (taking into account the purity and handling of the samples) was estimated to be 2 %. Triplicates of each sample were performed to ensure accuracy and the reported results are the average values.

Figure 3.2 - SVM 3000 Anton Paar rotational Stabinger viscometer-densimeter

3.2.2 Refractive Index measurements

The refractive indices were measured at atmospheric pressure in a temperature range between 293.15K and 353.15K through an automated Anton Paar Refractometer Abbemat 500 with a precision of ± $5 \cdot 10^{-5}$. Triplicates of each sample were measured and the results presented are average values. The absolute uncertainty of the refractive indices was ± 0.00005.

Figure 3.3 - Anton Paar Refractometer Abbemat 500

3.3 Results and Discussion

3.3.1 Thermophysical properties for pure ILs and their mixtures

Some of the obtained results are presented at T = 318.15K, since the gas permeation measurements were performed at this temperature (*Chapter 4*).

3.3.1.1 Density measurements

The density values, ρ (g·cm^{-3}), of the pure ILs and their mixtures were measured in the temperature range from 293.15K to 353.15K and are reported in Tables 7.1-7.4 (Appendix 3) and illustrated in Figures 3.4-3.7.

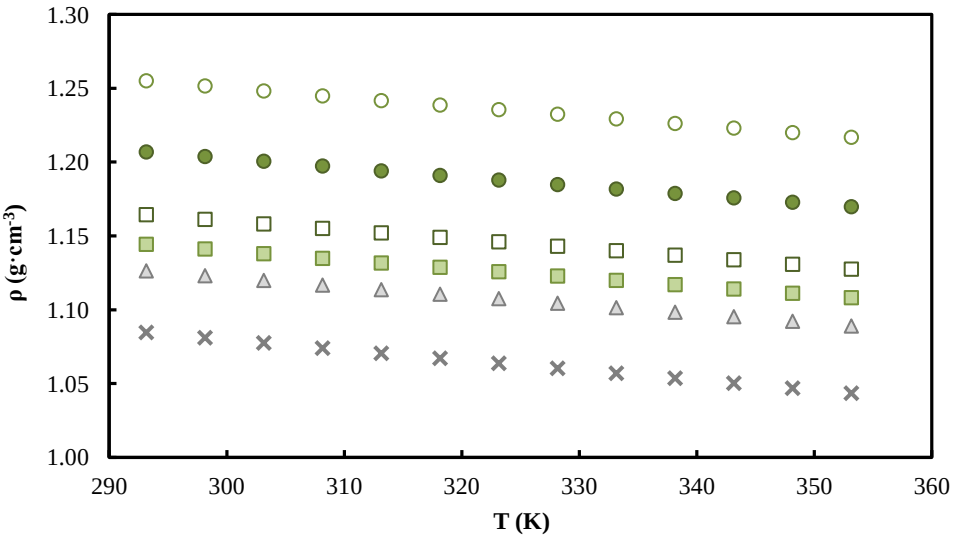

Figure 3.4 - Densities (ρ) of the pure ionic liquids measured in this work as a function of temperature (T): [C_2mim][C(CN)$_3$] (×), [C_2mim][Gly] (□), [C_2mim][L-Ala] (▲), [C_2mim][Tau] (○), [C_2mim][L-Ser] (●), [C_2mim][L-Pro] (■).

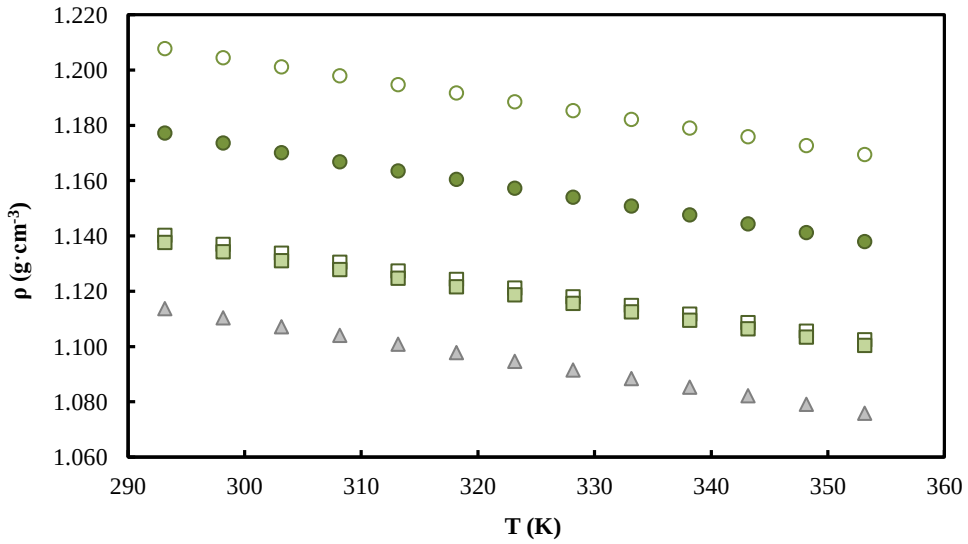

Figure 3.5 - Densities (ρ) of the ionic liquids mixtures measured in this work as a function of temperature (T): $[C_2mim][C(CN)_3]_{0.25}[Gly]_{0.75}$ (□), $[C_2mim][C(CN)_3]_{0.25}$[L-Ala]$_{0.75}$ (▲), $[C_2mim][C(CN)_3]_{0.25}[Tau]_{0.75}$ (○), $[C_2mim][C(CN)_3]_{0.25}$[L-Ser]$_{0.75}$ (●), $[C_2mim][C(CN)_3]_{0.25}$[L-Pro]$_{0.75}$ (■).

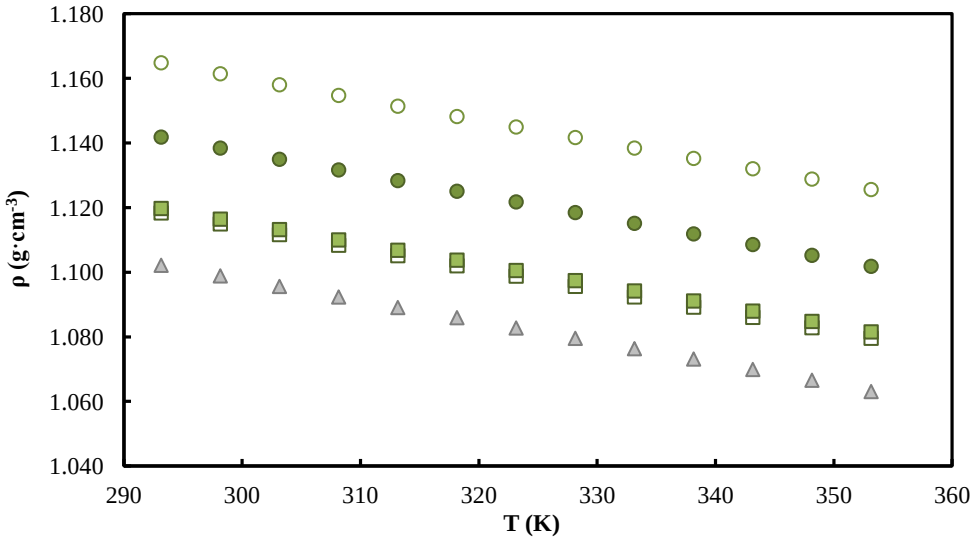

Figure 3.6 - Densities (ρ) of the ionic liquids mixtures measured in this work as a function of temperature (T): $C_2mim][C(CN)_3]_{0.5}[Gly]_{0.5}$ (□), $[C_2mim][C(CN)_3]_{0.5}$[L-Ala]$_{0.5}$ (▲), $[C_2mim][C(CN)_3]_{0.5}[Tau]_{0.5}$ (○), $[C_2mim][C(CN)_3]_{0.5}$[L-Ser]$_{0.5}$ (●), $[C_2mim][C(CN)_3]_{0.5}$[L-Pro]$_{0.5}$ (■).

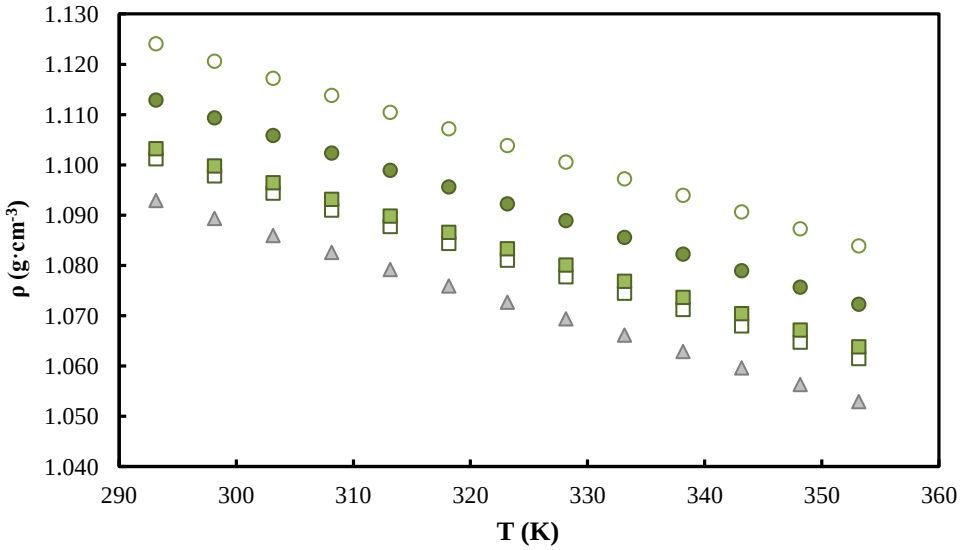

Figure 3.7 - Densities (ρ) of the ionic liquids mixtures measured in this work as a function of temperature (T): C_2mim][C(CN)$_3$]$_{0.75}$[Gly]$_{0.25}$ (□), [C_2mim][C(CN)$_3$]$_{0.75}$[L-Ala]$_{0.25}$ (▲), [C_2mim][C(CN)$_3$]$_{0.75}$[Tau]$_{0.25}$ (○), [C_2mim][C(CN)$_3$]$_{0.75}$[L-Ser]$_{0.25}$ (●), [C_2mim][C(CN)$_3$]$_{0.75}$[L-Pro]$_{0.25}$ (■).

From the analysis of Figures 3.4-3.7, it can be observed that the density decreases linearly with temperature for all pure ILs and their mixtures, in the whole temperature range studied in this work. Moreover, as expected, the density values of the IL mixtures are in between those of the pure ILs, for the five amino acid-based ionic liquids studied.

An overall comparison of the densities for the different ionic liquid mixtures, as a function of composition, as well as for the pure fluids at a fixed temperature of 318 K is presented in Figure 3.8.

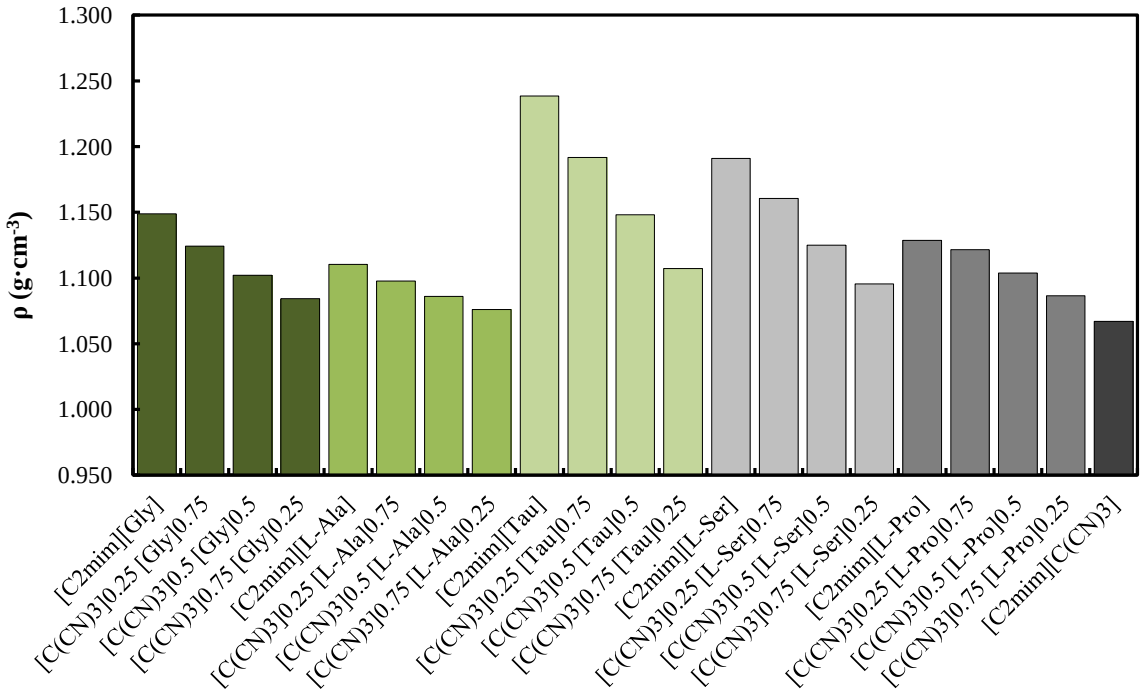

Figure 3.8 - Density values of the prepared IL mixtures with different compositions at T = 318.15 K.

The density values of the pure amino acid-based ionic liquids can be ordered as $[C_2mim][L\text{-}Ala] < [C_2mim][L\text{-}Pro] < [C_2mim][Gly] < [C_2mim][L\text{-}Ser] < [C_2mim][Tau]$. Additionally, within one mixture, the density decreases as the molar fraction of $[C_2mim][C(CN)_3]$ increases in the IL mixture. This behaviour is common to all five amino acid-based ionic liquids, leading to the conclusion that for a fixed composition, the AA-based ILs density order is maintained.

Another interesting conclusion from Figure 3.8 is that if a specific density is needed, several mixtures of different AA-based ILs with different compositions can be used. This fact illustrates the flexibility provided by the use of the IL mixtures.

The density values were fitted as a function of temperature, *T* (K), by the least squares method using the linear expression given by Equation 3.2:

$$\boldsymbol{\rho = a + b\,(T)} \qquad \textbf{(3.2)}$$

where *a* and *b* are adjustable parameters which are listed in Table 3.2. A good adjustment of the density values as a function of temperature was achieved, as can be evaluated by the correlation coefficient, R^2.

Table 3.2 - Fitted parameters of the linear expression given by Equation (3.2) and respective correlation coefficient, R^2.

Ionic Liquids	*a* (g·cm^{-3})	*b* x 10^{-4} (g·cm^{-3}K^{-1})	R^2
[C_2mim][Gly]	1.3431	-6.10	0.9999
[C_2mim][L-Ala]	1.3072	-6.18	0.9999
[C_2mim][Tau]	1.4398	-6.32	0.9997
[C_2mim][L-Ser]	1.3880	-6.19	0.9997
[C_2mim][L-Pro]	1.3196	-5.99	0.9997
[C_2mim][$C(CN)_3$]$_{0.25}$[Gly]$_{0.75}$	1.3241	-6.28	0.9999
[C_2mim][$C(CN)_3$]$_{0.25}$[L-Ala]$_{0.75}$	1.2972	-6.27	0.9999
[C_2mim][$C(CN)_3$]$_{0.25}$[Tau]$_{0.75}$	1.3937	-6.35	0.9999
[C_2mim][$C(CN)_3$]$_{0.25}$[L-Ser]$_{0.75}$	1.3668	-6.48	0.9998
[C_2mim][$C(CN)_3$]$_{0.25}$[L-Pro]$_{0.75}$	1.3182	-6.17	0.9998
[C_2mim][$C(CN)_3$]$_{0.5}$[Gly]$_{0.5}$	1.3067	-6.43	0.9999
[C_2mim][$C(CN)_3$]$_{0.5}$[L-Ala]$_{0.5}$	1.2916	-6.46	0.9999
[C_2mim][$C(CN)_3$]$_{0.5}$[Tau]$_{0.5}$	1.3557	-6.52	0.9999
[C_2mim][$C(CN)_3$]$_{0.5}$[L-Ser]$_{0.5}$	1.3363	-6.64	0.9999
[C_2mim][$C(CN)_3$]$_{0.5}$[L-Pro]$_{0.5}$	1.3054	-6.34	0.9999
[C_2mim][$C(CN)_3$]$_{0.75}$[Gly]$_{0.25}$	1.2949	-6.61	0.9999
[C_2mim][$C(CN)_3$]$_{0.75}$[L-Ala]$_{0.25}$	1.2866	-6.62	0.9999
[C_2mim][$C(CN)_3$]$_{0.75}$[Tau]$_{0.25}$	1.3194	-6.67	0.9999
[C_2mim][$C(CN)_3$]$_{0.75}$[L-Ser]$_{0.25}$	1.3101	-6.74	0.9999
[C_2mim][$C(CN)_3$]$_{0.75}$[L-Pro]$_{0.25}$	1.2946	-6.53	0.9999
[C_2mim][$C(CN)_3$]	1.2846	-6.83	0.9999

The thermal expansion coefficients (α_P), which considers the volumetric changes of a substance with increasing temperature at constant pressure, were calculated for the pure ILs using the following equation (3.3)[80, 81]:

$$\boldsymbol{\alpha_P = -\frac{1}{\rho}\left(\frac{\partial ln\rho}{\partial T}\right)_P = -\left(\frac{\partial ln\rho}{\partial T}\right)_P = -\frac{b}{a+bT}} \quad \textbf{(3.3)}$$

where ρ is the density in g·cm^{-3}, T is the temperature in K, P is the pressure in kPa and a and b are adjustable parameters obtained by Equation 3.3.

Table 3.3 – Thermal expansion coefficients (α_P) of the pure ionic liquids studied in this work, at atmospheric pressure.

	α_P x 10^4 (K^{-1})					
T(K)	**[C_2mim][Gly]**	**[C_2mim][L-Ala]**	**[C_2mim][Tau]**	**[C_2mim][L-Ser]**	**[C_2mim][L-Pro]**	**[C_2mim][$C(CN)_3$]**
293.15	5.239	5.488	5.038	5.130	5.236	6.299
298.15	5.253	5.503	5.050	5.144	5.250	6.318
303.15	5.267	5.519	5.063	5.157	5.264	6.338
308.15	5.281	5.534	5.076	5.170	5.277	6.359
313.15	5.295	5.549	5.089	5.184	5.291	6.379
318.15	5.309	5.565	5.102	5.197	5.305	6.399
323.15	5.323	5.580	5.115	5.211	5.320	6.420
328.15	5.337	5.596	5.128	5.224	5.334	6.441
333.15	5.351	5.611	5.141	5.238	5.348	6.461
338.15	5.366	5.627	5.155	5.252	5.362	6.482
343.15	5.380	5.643	5.168	5.265	5.377	6.503
348.15	5.395	5.659	5.181	5.279	5.391	6.525
353.15	5.409	5.675	5.195	5.293	5.406	6.546

From Table 3.3, it can be concluded that the thermal expansion coefficients of the pure ionic liquids do not change considerably with temperature, in accordance to what has been observed for other ILs[82, 83]. Additionally, the thermal expansion coefficients for the pure amino acid-based ionic liquids can be ordered as: [C_2mim][Tau] < [C_2mim][L-Ser] < [C_2mim][L-Pro] < [C_2mim][Gly] < [C_2mim][L-Ala]. The same trend for the pure amino acid based-ionic liquids, excepting [C_2mim][Tau], was reported by Muhammad *et al*[81].

The molar volumes (V_m) of the pure ILs and their mixtures were calculated through the density values, by Equation 2.2 and are presented in Tables 7.5-7.8 (Appendix 4) and illustrated in Figures 3.9-3.12

$$\boldsymbol{V_m = \frac{x_1 M_1 + x_2 M_2}{\rho}} \qquad \textbf{(3.4)}$$

where ρ corresponds to the density ($g \cdot cm^{-3}$), x is the molar fraction and the M corresponds to the molar mass ($g \cdot mol^{-1}$). The subscript *1* and *2* refer to the pure ILs.

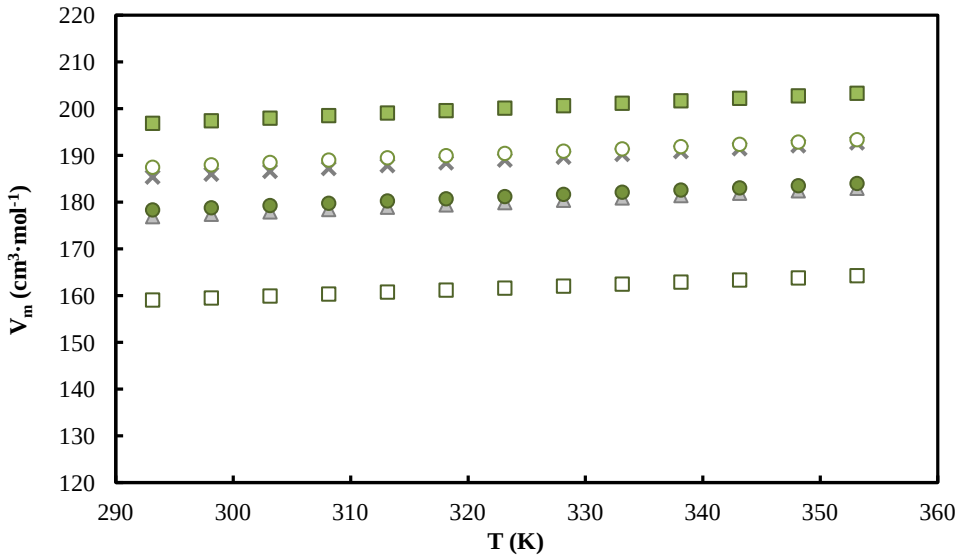

Figure 3.9 - Molar Volumes (V_m) of the pure ionic liquids measured in this work as a function of temperature (T): [C_2mim][C(CN)$_3$] (×), [C_2mim][Gly] (□), [C_2mim][L-Ala] (▲), [C_2mim][Tau] (○), [C_2mim][L-Ser] (●), [C_2mim][L-Pro] (■).

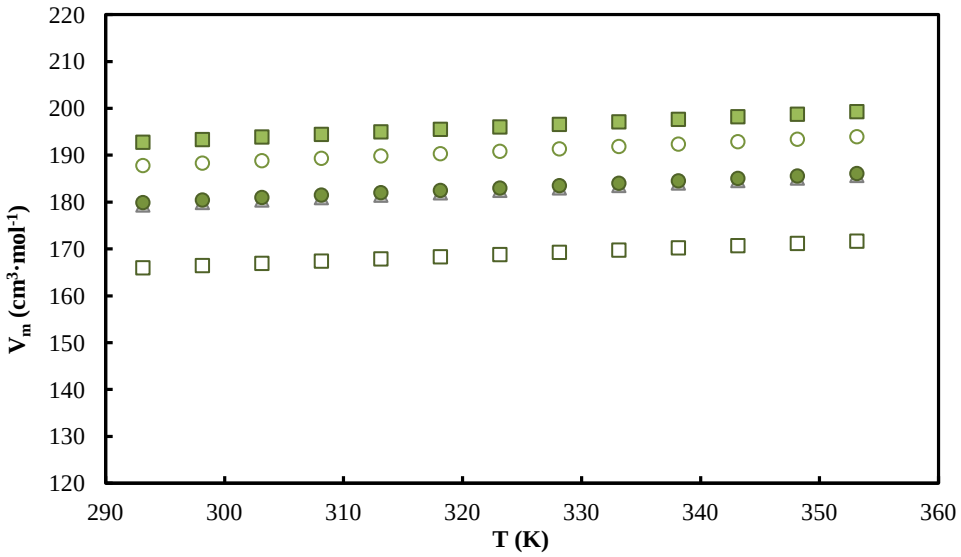

Figure 3.10 - Molar Volumes (V_m) of the ionic liquids mixtures measured in this work as a function of temperature (T): $[C_2mim][C(CN)_3]_{0.25}[Gly]_{0.75}$ (□), $[C_2mim][C(CN)_3]_{0.25}$[L-Ala]$_{0.75}$ (▲), $[C_2mim][C(CN)_3]_{0.25}[Tau]_{0.75}$ (○), $[C_2mim][C(CN)_3]_{0.25}$[L-Ser]$_{0.75}$ (●), $[C_2mim][C(CN)_3]_{0.25}$[L-Pro]$_{0.75}$ (■).

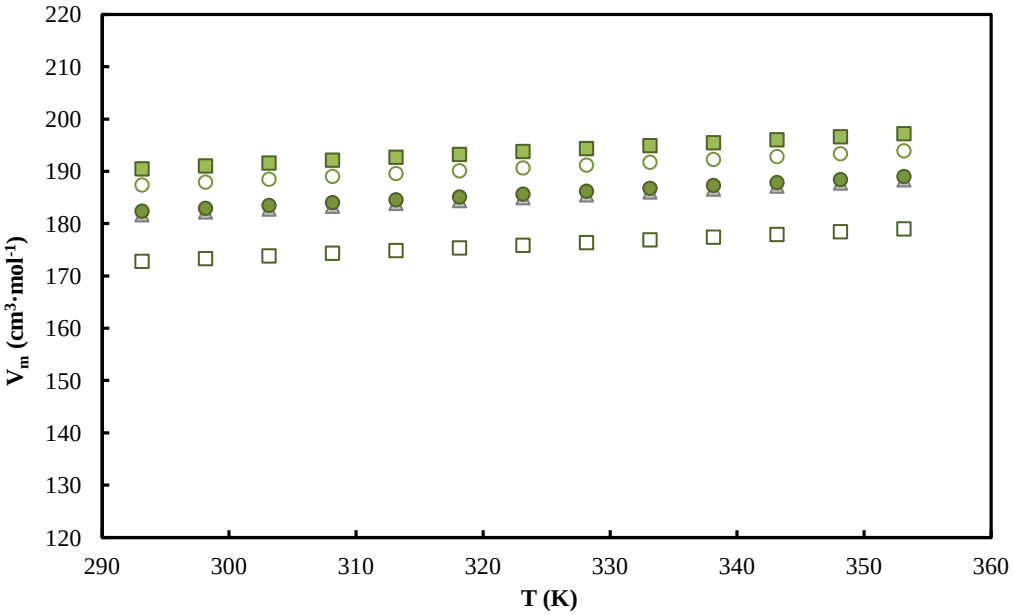

Figure 3.11 - Molar Volumes (V_m) of the ionic liquids mixtures measured in this work as a function of temperature (T): $C_2mim][C(CN)_3]_{0.5}[Gly]_{0.5}$ (□), [$C_2mim][C(CN)_3]_{0.5}$[L-Ala]$_{0.5}$ (▲), $[C_2mim][C(CN)_3]_{0.5}[Tau]_{0.5}$ (○), $[C_2mim][C(CN)_3]_{0.5}$[L-Ser]$_{0.5}$ (●), $[C_2mim][C(CN)_3]_{0.5}$[L-Pro]$_{0.5}$ (■).

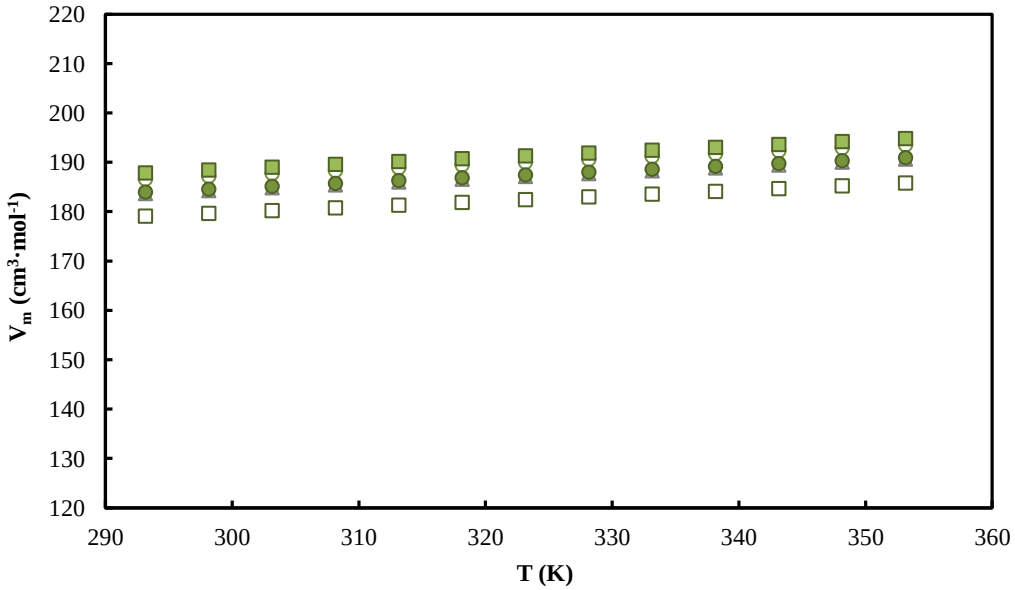

Figure 3.12 - Molar Volumes (V_m) of the ionic liquids mixtures measured in this work as a function of temperature (T): C_2mim][C(CN)$_3$]$_{0.75}$[Gly]$_{0.25}$ (□), [C_2mim][C(CN)$_3$]$_{0.75}$[L-Ala]$_{0.25}$ (▲), [C_2mim][C(CN)$_3$]$_{0.75}$[Tau]$_{0.25}$ (○), [C_2mim][C(CN)$_3$]$_{0.75}$[L-Ser]$_{0.25}$ (●), [C_2mim][C(CN)$_3$]$_{0.75}$[L-Pro]$_{0.25}$ (■).

The molar volume scale was kept constant throughout these figures to enable a clear comparison. The molar volumes of all samples increase with increasing temperature. Furthermore, the pure [C_2mim][L-Pro] presents the highest molar volume while the pure [C_2mim][Gly] shows the lowest, in the whole range of temperatures studied. Also to be mentioned that [C_2mim][C(CN)$_3$] and [C_2mim][Tau] present very similar molar volumes. The same behaviour is also found for [C_2mim][L-Ser] and [C_2mim][L-Ala].

The excess molar volume (V^E) of the IL mixtures was calculated by Equation 3.5[84]:

$$\boldsymbol{V^E = \frac{x_1 M_1 + x_2 M_2}{\rho_M} - \frac{x_1 M_1}{\rho_1} - \frac{x_2 M_2}{\rho_2}} \quad \textbf{(3.5)}$$

where ρ corresponds to the density ($g \cdot cm^{-3}$), x is the molar fraction and the M corresponds to the molar mass ($g \cdot mol^{-1}$). The subscript *1* and *2* refer to the pure ILs and the subscript *M* denotes the IL mixtures.

The calculated excess molar volumes values are listed in Tables 7.9-7.11 (Appendix 4) and are depicted in Figure 3.13 at T=318.15K. Note that the excess molar volumes are very small (tens of the unit) in comparison to the molar volumes (in order of hundredths of the unit) used in their calculations. Thus, the accuracy of the density measurements is very important in the discussion of the excess molar volumes.

The excess molar volumes are the result of contributions from several effects, namely: chemical, physical and structural modifications.[85] Physical contributions, which are non-specific interactions between the species present in the mixture, originate positive V^E values.[86] Negative V^E values are a result of chemical contributions (charge-transfer type forces, changes in hydrogen bonding equilibrium or electrostatic interactions) or structural contributions (geometrical fitting or changes of free volume).[87]

As can be seen in Figure 3.13, all the studied IL mixtures show positive V^E, except the $[C_2mim][C(CN)_3]$[L-Pro] mixture that presents negative V^E values. The $[C_2mim][C(CN)_3]$[L-Ser] mixture also shows a different behaviour compared to the other IL mixtures since it exhibits positive and negative V^E values at low and high $[C_2mim]$[AA] molar fractions, respectively. There are two mixtures with very similar excess volumes in the whole composition range $[C_2mim][C(CN)_3]$[Gly] and $[C_2mim][C(CN)_3]$[L-Ala]. In fact, $[C_2mim][C(CN)_3]$[L-Ser] also presents very similar V^E values at the 0.25 and 0.5 mole fractions, but the value at 0.75 mole fraction is substantially different from that observed for the other two mixtures. This indicates that at 0.75 mole fraction, the $[C_2mim][C(CN)_3]$[L-Ser] mixture is affected by chemical contributions, such as charge-transfer type forces or changes in hydrogen bonding equilibrium, or structural contributions, namely geometrical fitting or changes of free volume.

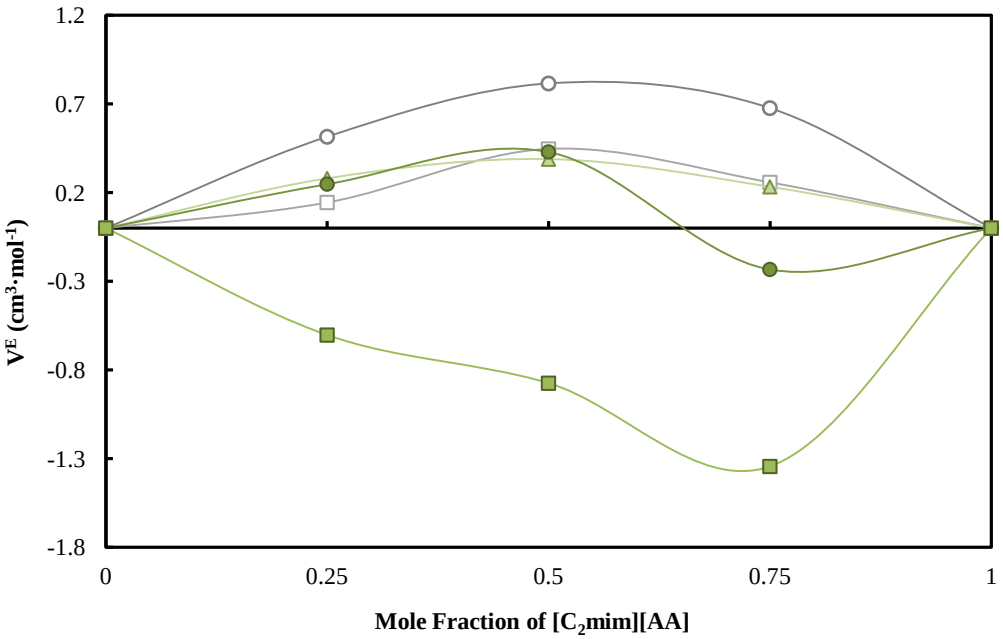

Figure 3.13 - Excess molar volumes of the ionic liquid mixtures at 318.15K: C_2mim][$C(CN)_3$][Gly] (□), [C_2mim][$C(CN)_3$][L-Ala] (▲), [C_2mim][$C(CN)_3$][Tau] (○), [C_2mim][$C(CN)_3$][L-Ser] (●), [C_2mim][$C(CN)_3$]L-Pro] (■).

3.3.1.2 Viscosity measurements

The viscosity values, η (mPa·s), of the pure ILs and their mixtures were measured in the temperature range from 293.15K to 353.15K and are reported in Tables 7.12, 7.13-7.15 (Appendix 5) and illustrated in Figures 3.14-3.17.

Viscosity also decreases linearly with temperature for all pure ILs and their mixtures, in the whole temperature range studied in this work. From Figure 3.14 it can be observed that the pure [C_2mim][L-Ser] exhibits higher viscosity compared to the other pure ionic liquids. In fact, the viscosity values for the five AA-based ILs can be ordered as: [C_2mim][Gly] < [C_2mim][L-Ala] < [C_2mim][Tau] < [C_2mim][L-Pro] < [C_2mim][L-Ser].

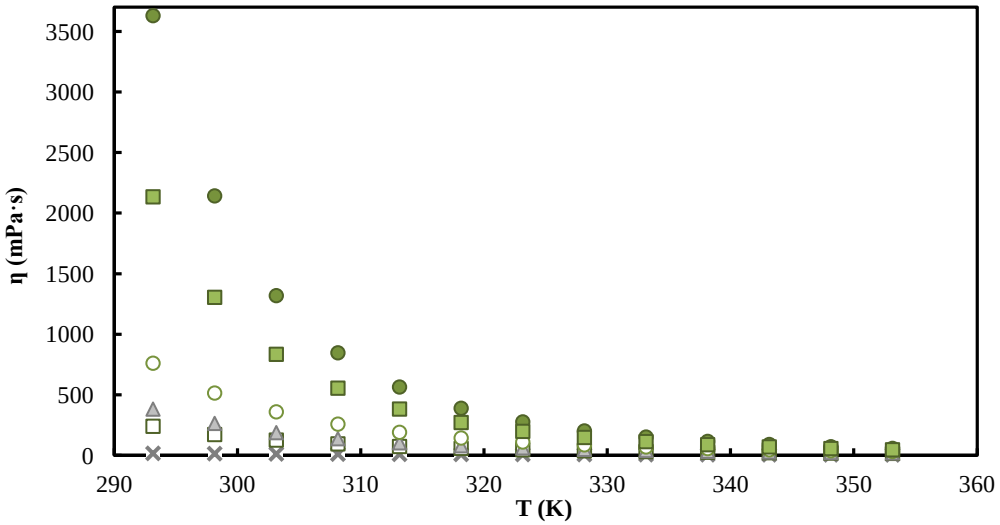

Figure 3.14 - Measured viscosities (η) of the pure ionic liquids studied in this work as a function of temperature (T): [C_2mim][$C(CN)_3$] (×), [C_2mim][Gly] (□), [C_2mim][L-Ala] (▲), [C_2mim][Tau] (○), [C_2mim][L-Ser] (●), [C_2mim][L-Pro] (■).

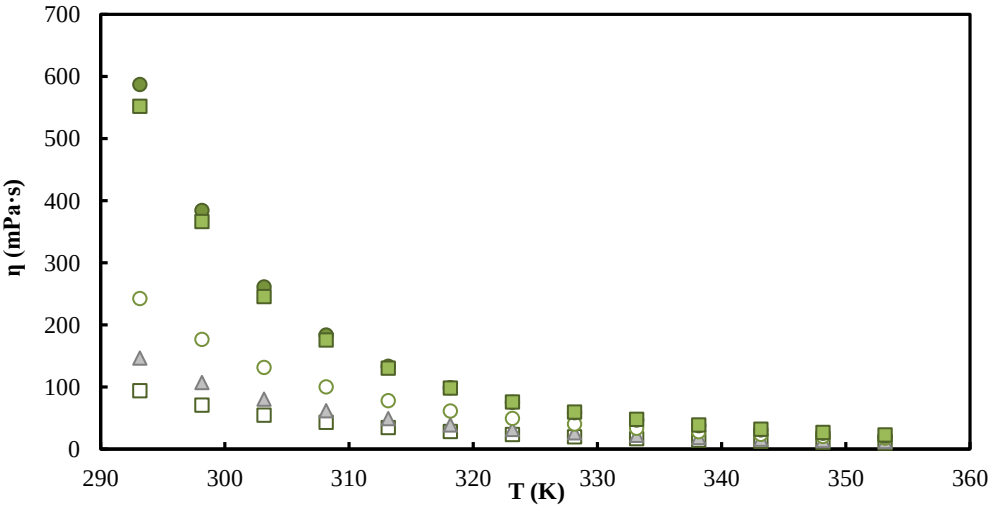

Figure 3.15 - Measured viscosities (η) of the ionic liquids mixtures studied in this work as a function of temperature (T): $[C_2mim][C(CN)_3]_{0.25}[Gly]_{0.75}$ (□), $[C_2mim][C(CN)_3]_{0.25}[L\text{-}Ala]_{0.75}$ (▲), $[C_2mim][C(CN)_3]_{0.25}[Tau]_{0.75}$ (○), $[C_2mim][C(CN)_3]_{0.25}[L\text{-}Ser]_{0.75}$ (●), $[C_2mim][C(CN)_3]_{0.25}[L\text{-}Pro]_{0.75}$ (■).

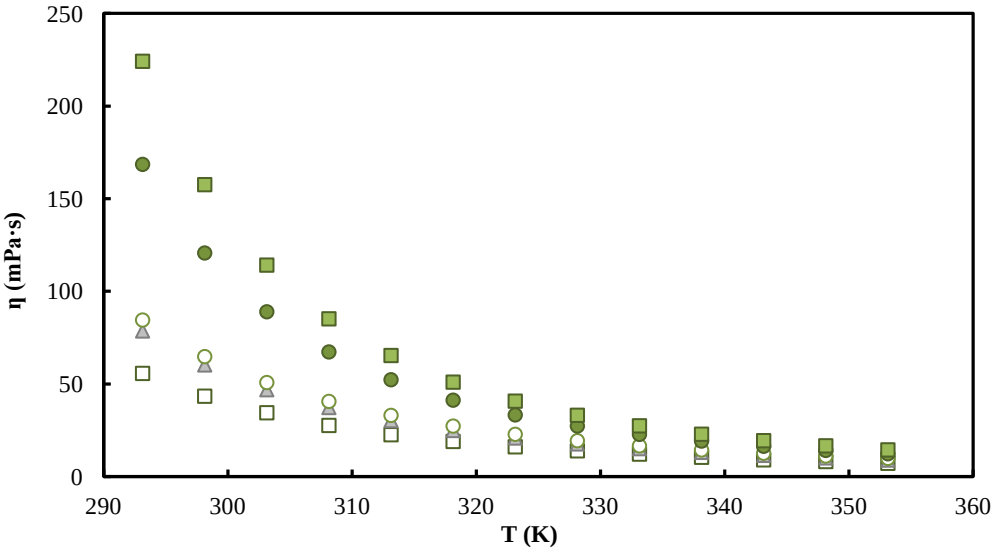

Figure 3.16 - Measured viscosities (η) of the ionic liquids mixtures studied in this work as a function of temperature (T): $C_2mim][C(CN)_3]_{0.5}[Gly]_{0.5}$ (□), $[C_2mim][C(CN)_3]_{0.5}[L\text{-}Ala]_{0.5}$ (▲), $[C_2mim][C(CN)_3]_{0.5}[Tau]_{0.5}$ (○), $[C_2mim][C(CN)_3]_{0.5}[L\text{-}Ser]_{0.5}$ (●), $[C_2mim][C(CN)_3]_{0.5}[L\text{-}Pro]_{0.5}$ (■).

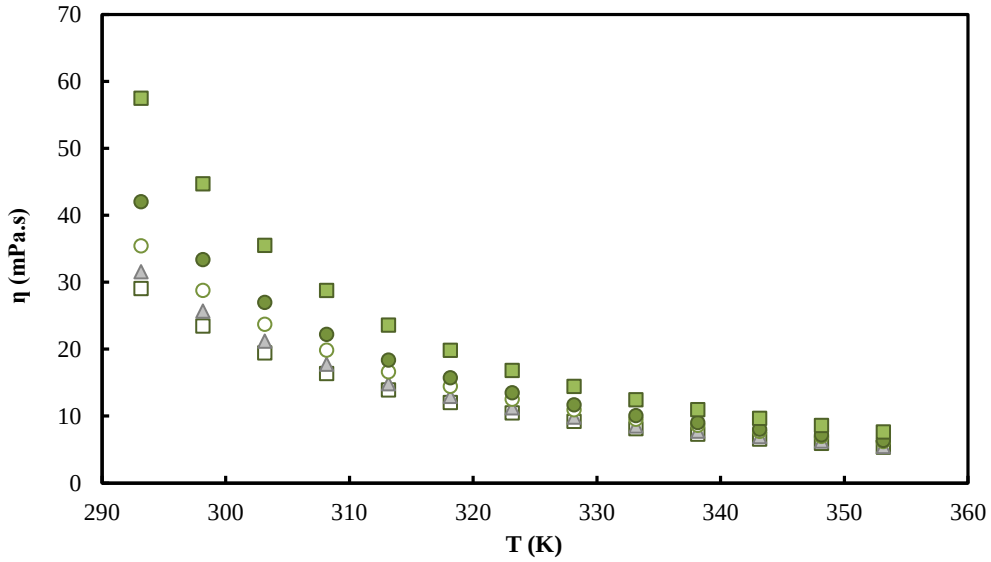

Figure 3.17 - Measured viscosities (η) of the ionic liquids mixtures studied in this work as a function of temperature (T): C_2mim][C(CN)$_3$]$_{0.75}$[Gly]$_{0.25}$ (□), [C_2mim][C(CN)$_3$]$_{0.75}$[L-Ala]$_{0.25}$ (▲), [C_2mim][C(CN)$_3$]$_{0.75}$[Tau]$_{0.25}$ (○), [C_2mim][C(CN)$_3$]$_{0.75}$[L-Ser]$_{0.25}$ (●), [C_2mim][C(CN)$_3$]$_{0.75}$[L-Pro]$_{0.25}$ (■).

The Figures 3.14-3.17 display some very interesting behaviours. For the two most viscous AA-based IL mixtures with [C_2mim][C(CN)$_3$], [C_2mim][C(CN)$_3$][L-Ser] and [C_2mim][C(CN)$_3$][L-Pro], their relative viscosity order changes as the relative concentrations of the two ILs change. To this end, it can be seen that for temperatures below 310 K, the η ([C_2mim][C(CN)$_3$]$_{0.25}$[L-Ser]$_{0.75}$) > η ([C_2mim][C(CN)$_3$]$_{0.25}$[L-Pro]$_{0.75}$). However, this order is reversed for the other compositions (0.50/0.50 and 0.75/0.25) of these mixtures. In fact, for the lowest composition of ([C_2mim][C(CN)$_3$], the viscosity order observed is the same as for pure AA-based ILs. Only for 0.50/0.50 mixtures the order is reversed meaning that [C_2mim][C(CN)$_3$] is more effective in disrupting the [C_2mim][L-Ser] liquid structure than that of [C_2mim][L-Pro].

The Figure 3.18 presents the viscosity values for all the IL series at T = 318.15 K. The viscosity values of IL mixtures are in between those of the pure ionic liquids, for the five AA-based ILs. This behaviour can be also observed in the whole temperature range studied in this work. A very marked decrease in viscosity can be observed for the two most viscous AA-based ILs, [C_2mim][L-Ser] and [C_2mim][L-Pro].

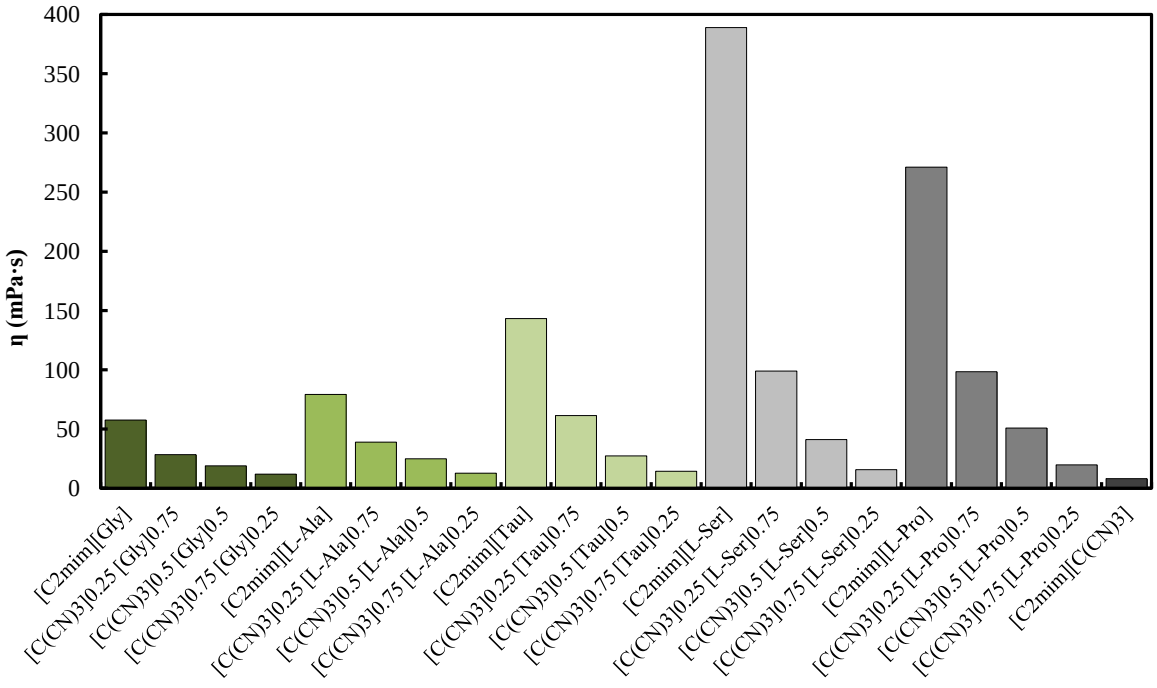

Figure 3.18 - Viscosity comparison for all the ionic liquid series at T = 318.15 K.

The experimental viscosity values were fitted as a function of temperature, using the Vogel−Fulcher−Tammann (VFT) model described in Equation 3.6:

$$\ln \eta = A_\eta + \frac{B_\eta}{(T - C_\eta)} \quad \textbf{(3.6)}$$

where η is the viscosity in mPa·s, T is the temperature in K, and A_η, B_η, and C_η are adjustable parameters. The adjustable parameters were determined from the fitting of the experimental values and are listed in Table 3.4 as well as the activation energy values, E_a, (kJ·mol^{-1}) at T = 318.15 K.

The activation energy was calculated based on the viscosity dependence with temperature using the following equation (3.7)[76]:

$$\boldsymbol{E_a = R.\frac{\partial(\ln \eta)}{\partial\left(\frac{1}{T}\right)} = R.\left(\frac{B_\eta}{\left(\frac{C_\eta^2}{T^2}-\frac{2C_\eta}{T}+1\right)}\right)} \quad \textbf{(3.7)}$$

where η is the viscosity, T is the temperature, B_η and C_η are the adjustable parameters obtained from equation 3.6, and R is the universal gas constant.

It should be noted that the experimental viscosity values were also correlated using a logarithmic equation based on Arrhenius model, described by the Equation 3.8:

$$\boldsymbol{\ln(\eta) = \ln(\eta_\infty) - \frac{E_a}{RT}} \quad \textbf{(3.8)}$$

where η is the viscosity (mPa·s), η_∞ is a pre-exponential constant (mPa·s), Ea is the activation energy (kJ·mol^{-1}), R is the ideal gas constant and T is the temperature (K).

However, the fitting of viscosity values as a function of temperature using this equation was not obtained, as can be evaluated by the correlation coefficients, R^2, listed in Table 7.16 (Appendix 6). Consequently, the VFT model was chosen, taking into account that it has a larger number of adjustable parameters than Arrhenius model, which allows a better adjustment of the experimental viscosity values as a function of temperature.

Table 3.4 - Fitted parameters of VFT expresson given by Equation 3.6 and activation energy values at T = 318.15 K.

Ionic Liquid Samples	Parameters			R^2	$Ea_{318.15K}$ (kJ·mol^{-1})
	A_η (mPa.s)	B_η (K)	C_η (K)		
[C_2mim][Gly]	-1.766	738.601	191.275	1.0	38.6
[C_2mim][L-Ala]	-1.971	798.653	192.303	1.0	42.4
[C_2mim][Tau]	-2.049	910.854	188.296	1.0	45.5
[C_2mim][L-Ser]	-2.461	1003.108	199.095	1.0	59.6
[C_2mim][L-Pro]	-2.297	953.392	197.476	1.0	55.1
[C_2mim][$C(CN)_3$]$_{0.25}$ [Gly]$_{0.75}$	-1.681	654.712	187.962	1.0	32.5
[C_2mim][$C(CN)_3$]$_{0.25}$ [L-Ala]$_{0.75}$	-1.702	678.486	191.746	1.0	35.7
[C_2mim][$C(CN)_3$]$_{0.25}$ [Tau]$_{0.75}$	-1.965	825.404	182.502	1.0	37.8
[C_2mim][$C(CN)_3$]$_{0.25}$ [L-Ser]$_{0.75}$	-2.261	833.326	196.652	1.0	47.5
[C_2mim][$C(CN)_3$]$_{0.25}$ [L-Pro]$_{0.75}$	-1.671	723.147	202.561	1.0	45.6
[C_2mim][$C(CN)_3$]$_{0.5}$ [Gly]$_{0.5}$	-1.748	632.609	183.439	0.9998	29.3
[C_2mim][$C(CN)_3$]$_{0.5}$ [L-Ala]$_{0.5}$	-1.606	625.181	188.483	1.0	31.3
[C_2mim][$C(CN)_3$]$_{0.5}$ [Tau]$_{0.5}$	-1.596	653.691	184.787	1.0	30.9
[C_2mim][$C(CN)_3$]$_{0.5}$ [L-Ser]$_{0.5}$	-1.681	653.298	197.224	1.0	37.6
[C_2mim][$C(CN)_3$]$_{0.5}$ [L-Pro]$_{0.5}$	-1.643	664.071	199.051	1.0	39.4
[C_2mim][$C(CN)_3$]$_{0.75}$ [Gly]$_{0.25}$	-1.478	546.202	180.340	1.0	24.2
[C_2mim][$C(CN)_3$]$_{0.75}$ [L-Ala]$_{0.25}$	-1.840	652.869	169.726	0.9996	24.9
[C_2mim][$C(CN)_3$]$_{0.75}$ [Tau]$_{0.25}$	-1.535	595.406	176.467	0.9999	25.0
[C_2mim][$C(CN)_3$]$_{0.75}$ [L-Ser]$_{0.25}$	-1.570	582.662	183.379	0.9999	27.0
[C_2mim][$C(CN)_3$]$_{0.75}$ [L-Pro]$_{0.25}$	-1.491	582.893	187.969	1.0	28.9
[C_2mim][$C(CN)_3$]	-1.898	663.573	152.177	1.0	20.3

Looking at Figure 3.19, where the activation energy (E_a) values for the five IL series at T = 318.15 K are represented, it can be observed that the E_a decreases as the molar fraction of [C_2mim][$C(CN)_3$] increases in the IL mixture. This behaviour is found for the five amino acid-based ionic liquids.

Furthermore, the [C_2mim][L-Ser] shows the highest E_a value while [C_2mim][Gly] displays the lowest E_a value, which means that the ions of [C_2mim][L-Ser] have more difficult to move past each other than the ions of [C_2mim][Gly]. This can be a direct consequence of the presence of stronger interactions within the fluid. The presence of the terminal OH group in [C_2mim][L-Ser], providing extra hydrogen bonding points, has a very strong influence in the

viscosity of this IL and its $[C_2mim][C(CN)_3]_{0.25}[L\text{-}Ser]_{0.75}$ mixture. Conversely, $[C_2mim][L\text{-}Pro]$ is the IL that has the largest molar volume, probably due to the cyclic amine present in its structure. This might be a possible explanation for its high viscosity, when compared to the other ILs $[C_2mim][Gly]$, $[C_2mim][Ala]$ and $[C_2mim][Tau]$. It is also important to note that, as it can be confirmed on Table 3.4, the *Ea* values for all the $[C_2mim][C(CN)_3]_{0.75}$ $[AA]_{0.25}$ are very similar to each other indicating similar viscosity values and thus a disruption of most the AA-based IL network.

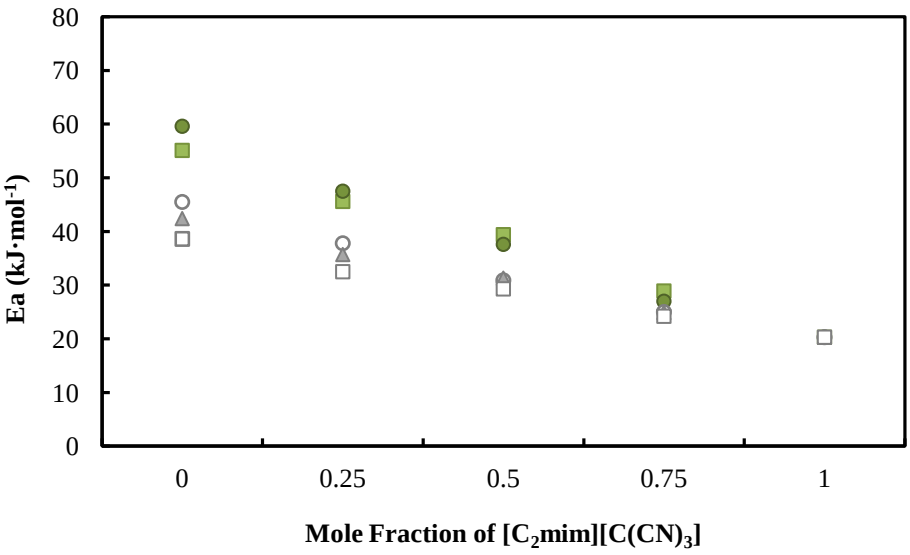

Figure 3.19 - Calculated activation energy (*Ea*) values of ionic liquid series studied in this work at 318.15K: $[C_2mim][C(CN)_3][Gly]$ (□), $[C_2mim][C(CN)_3][L\text{-}Ala]$ (▲), $[C_2mim][C(CN)_3][Tau]$ (○), $[C_2mim][C(CN)_3][L\text{-}Ser]$ (●), $[C_2mim][C(CN)_3][L\text{-}Pro]$ (■).

The viscosity deviations, $\Delta\, ln(\eta)$, for the ionic liquid mixtures were calculated using Equation 3.9:

$$\Delta \ln(\eta) = \ln(\eta_M) - [x_1 \ln(\eta_1) + (1 - x_1)\ln(\eta_2)] \quad \textbf{(3.9)}$$

where η corresponds to viscosity (mPa·s) and x is the mole fraction. The subscript *1* and *2* correspond to the two pure ILs and the subscript *M* denotes the IL mixture. The calculated viscosity deviations values are presented in Tables 7.17-7.19 (Appendix 7). The viscosity deviations for the studied IL mixtures are represented in Figure 3.20, at *T*=318.15K.

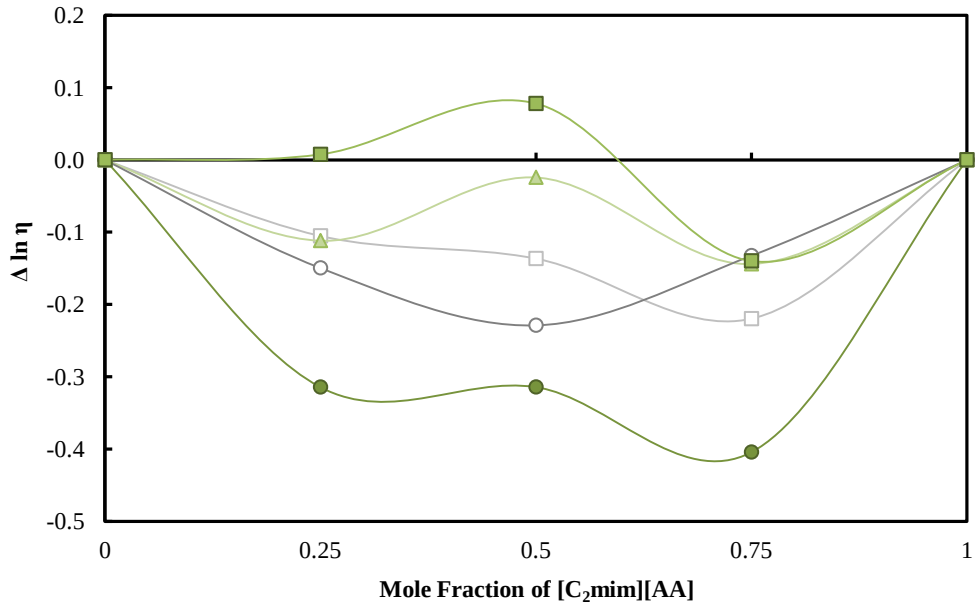

Figure 3.20 - Viscosity deviations of the ionic liquid mixtures at 318.15 K: C_2mim][C(CN)$_3$][Gly] (□), [C_2mim][C(CN)$_3$][L-Ala] (▲), [C_2mim][C(CN)$_3$][Tau] (○), [C_2mim][C(CN)$_3$][L-Ser] (●), [C_2mim][C(CN)$_3$][L-Pro] (■).

Regarding the viscosity deviations, positive $\Delta\, ln(\eta)$ values are related to the charge transfer and hydrogen bonding interactions while negative $\Delta\, ln(\eta)$ values are usually obtained for systems where molecular size and shapes of the components, dispersion and dipolar interactions, are considered.

It can be observed from Figure 3.20, that all the IL mixtures studied show negative viscosity deviations, in the entire range of temperatures, with the exception of [C_2mim][C(CN)$_3$]$_{0.5}$[L-Pro]$_{0.5}$ and [C_2mim][C(CN)$_3$]$_{0.75}$[L-Pro]$_{0.25}$ mixtures that present positive viscosity deviations, which are related to the charge transfer and hydrogen bonding interactions. The negative $\Delta\, ln(\eta)$ value for the [C_2mim][C(CN)$_3$]$_{0.25}$[L-Pro]$_{0.75}$ mixture can be associated to the molecular size and shape of [C_2mim][L-Pro].

3.3.1.3 Refractive Index measurements

The refractive index values (n_D) of the pure ionic liquids and their mixtures were measured in the temperature range from 293.15 K to 353.15 K and are reported in Tables 7.20-7.23 (Appendix 8) and illustrated in Figures 3.21-3.24.

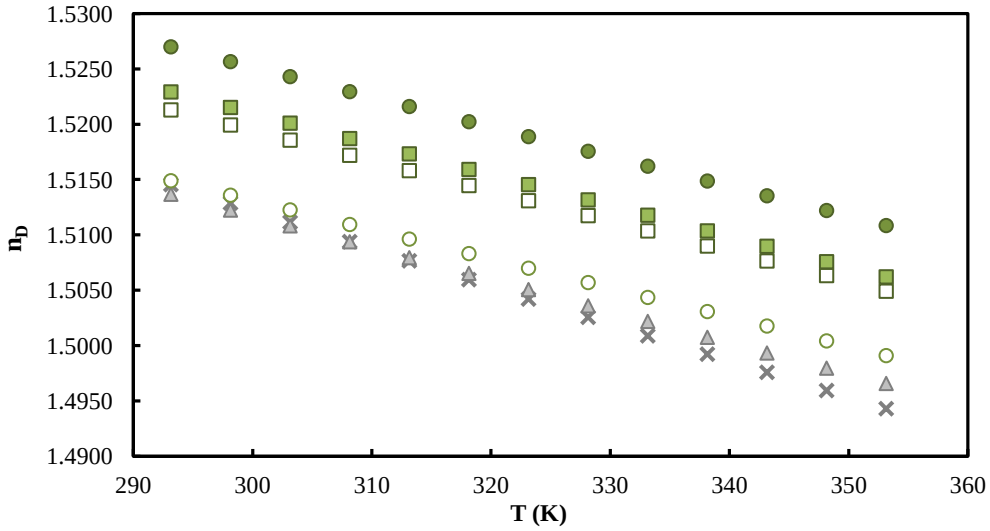

Figure 3.21 - Measured refractive indices (n_D) of the pure ionic liquids studied in this work as a function of temperature (T): $[C_2mim][C(CN)_3]$ (×), $[C_2mim][Gly]$ (□), $[C_2mim][L\text{-}Ala]$ (▲), $[C_2mim][Tau]$ (○), $[C_2mim][L\text{-}Ser]$ (●), $[C_2mim][L\text{-}Pro]$ (■).

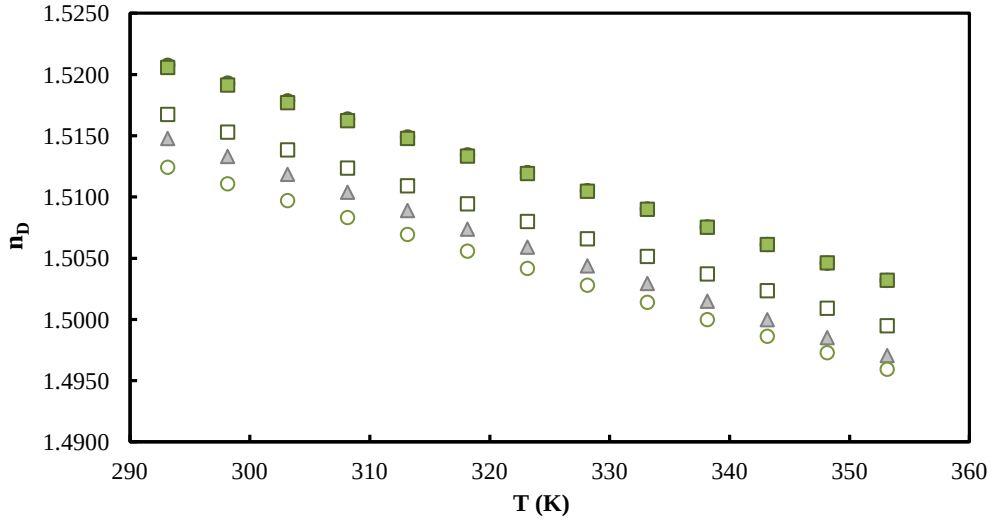

Figure 3.22 - Measured refractive indices (n_D) of the ionic liquids mixtures studied in this work as a function of temperature (T): $[C_2mim][C(CN)_3]_{0.25}[Gly]_{0.75}$ (□), $[C_2mim][C(CN)_3]_{0.25}[L\text{-}Ala]_{0.75}$ (▲), $[C_2mim][C(CN)_3]_{0.25}[Tau]_{0.75}$ (○), $[C_2mim][C(CN)_3]_{0.25}[L\text{-}Ser]_{0.75}$ (●), $[C_2mim][C(CN)_3]_{0.25}[L\text{-}Pro]_{0.75}$ (■).

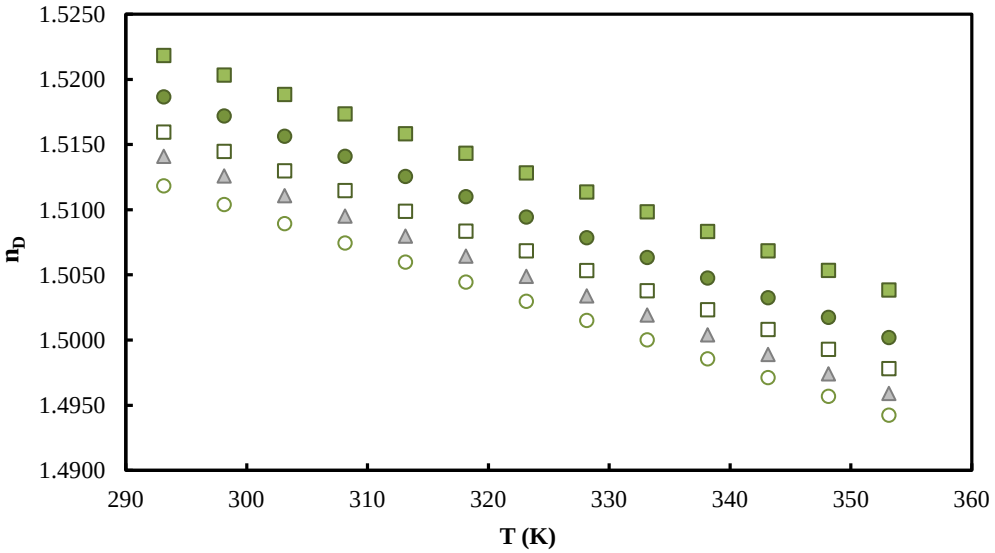

Figure 3.23 - Measured refractive indices (n_D) of the ionic liquids mixtures studied in this work as a function of temperature (T): $[C_2mim][C(CN)_3]_{0.5}[Gly]_{0.5}$ (□), $[C_2mim][C(CN)_3]_{0.5}[L\text{-}Ala]_{0.5}$ (▲), $[C_2mim][C(CN)_3]_{0.5}[Tau]_{0.5}$ (○), $[C_2mim][C(CN)_3]_{0.5}[L\text{-}Ser]_{0.5}$ (●), $[C_2mim][C(CN)_3]_{0.5}[L\text{-}Pro]_{0.5}$ (■).

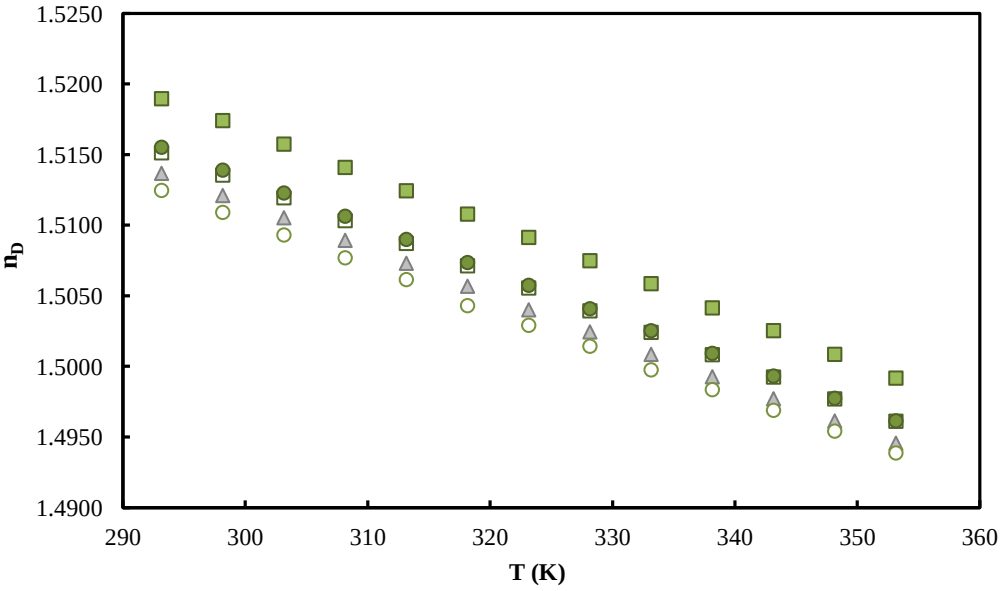

Figure 3.24 - Measured refractive indices (n_D) of the ionic liquids mixtures studied in this work as a function of temperature (T): $[C_2mim][C(CN)_3]_{0.75}[Gly]_{0.25}$ (□), $[C_2mim][C(CN)_3]_{0.75}[L\text{-}Ala]_{0.25}$ (▲), $[C_2mim][C(CN)_3]_{0.75}[Tau]_{0.25}$ (○), $[C_2mim][C(CN)_3]_{0.75}[L\text{-}Ser]_{0.25}$ (●), $[C_2mim][C(CN)_3]_{0.75}[L\text{-}Pro]_{0.25}$ (■).

The molar refraction or molar polarizability (R_m) was calculated from experimental data of both molar volume (V_m) and refractive index (n_D) at the studied range of temperatures using the Lorentz-Lorenz relation (Equation 3.10):

$$\boldsymbol{R_m = \left(\frac{n_D^2 - 1}{n_D^2 + 2}\right) V_m} \quad \textbf{(3.10)}$$

where V_m is the molar volume ($cm^3 \cdot mol^{-1}$) and n_D is the refractive index.

The unoccupied fraction of the molar volume of an ionic liquid is defined as molar free volume (f_m), which can be estimated by Equation 3.11:

$$\boldsymbol{f_m = (V_m - R_m)} \quad \textbf{(3.11)}$$

where V_m and R_m are the molar volume and the molar refraction of the IL, respectively.

The calculated molar refraction (R_m) values as well as the molar free volumes (f_m) of all the studied samples are listed in Tables 7.24-7.27 (Appendix 9).

The Figures 3.26-3.29 present the molar free volume (f_m) as a function of temperature (T) for all the pure ILs and their mixtures. It can be observed from Figure 3.26 that the pure [C_2mim][L-Pro] presents the highest free molar volume, while the pure [C_2mim][Gly] has the lowest free molar volume. This property can be directly associated to the gas solubility of SILMs since it is related to the space available to accommodate the gas. This behaviour can also be observed for all mixtures of different molar fractions studied containing [C_2mim][L-Pro].

Moreover, the pure [C_2mim][Gly], [C_2mim][L-Ala] and [C_2mim][L-Ser] display lower free molar volumes compared to the pure [C_2mim][$C(CN)_3$]. Additionally, the pure [C_2mim][Tau] presents similar free molar volume compared to [C_2mim][$C(CN)_3$].

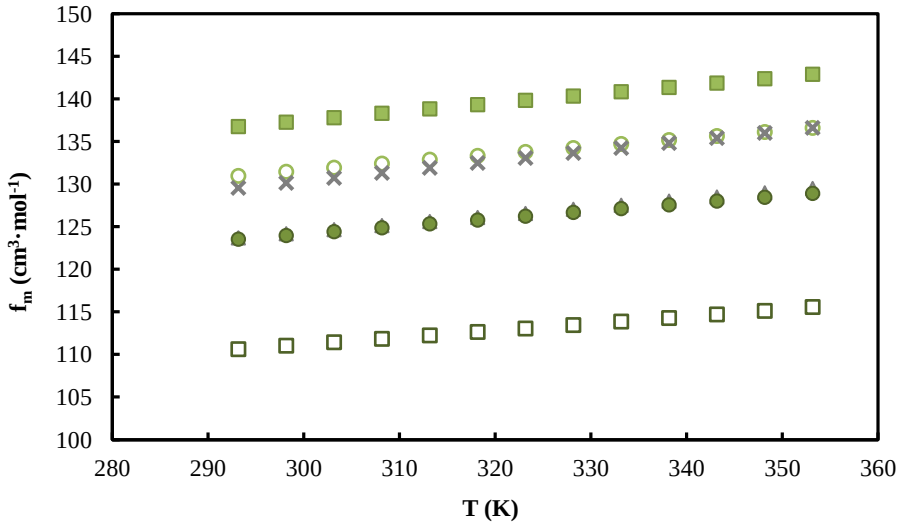

Figure 3.25 - Measured free molar volumes (f_m) of the pure ionic liquids studied in this work as a function of temperature (T): [C_2mim][C(CN)$_3$] (×), [C_2mim][Gly] (□), [C_2mim][L-Ala] (▲), [C_2mim][Tau] (○), [C_2mim][L-Ser] (●), [C_2mim][L-Pro] (■)

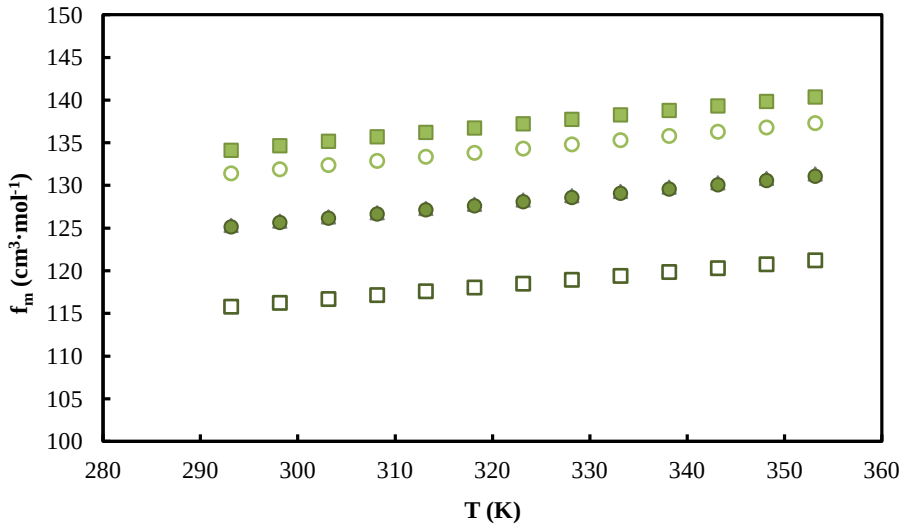

Figure 3.26 - Measured free molar volumes (f_m) of the ionic liquids mixtures studied in this work as a function of temperature (T): [C_2mim][C(CN)$_3$]$_{0.25}$[Gly]$_{0.75}$ (□), [C_2mim][C(CN)$_3$]$_{0.25}$[L-Ala]$_{0.75}$ (▲), [C_2mim][C(CN)$_3$]$_{0.25}$[Tau]$_{0.75}$ (○), [C_2mim][C(CN)$_3$]$_{0.25}$[L-Ser]$_{0.75}$ (●), [C_2mim][C(CN)$_3$]$_{0.25}$[L-Pro]$_{0.75}$ (■).

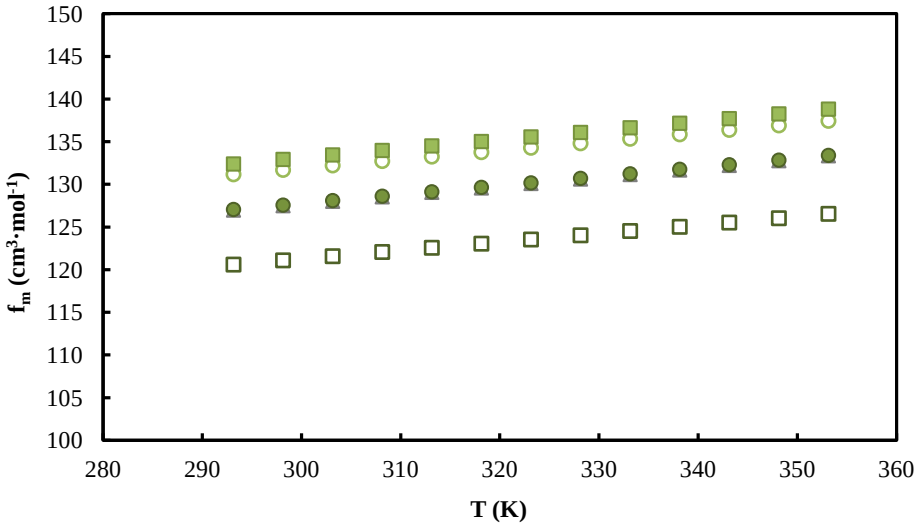

Figure 3.28 - Measured free molar volumes (f_m) of the ionic liquids mixtures studied in this work as a function of temperature (T): $[C_2mim][C(CN)_3]_{0.5}[Gly]_{0.5}$ (□), $[C_2mim][C(CN)_3]_{0.5}[L\text{-}Ala]_{0.5}$ (▲), $[C_2mim][C(CN)_3]_{0.5}[Tau]_{0.5}$ (○), $[C_2mim][C(CN)_3]_{0.5}[L\text{-}Ser]_{0.5}$ (●), $[C_2mim][C(CN)_3]_{0.5}[L\text{-}Pro]_{0.5}$ (■).

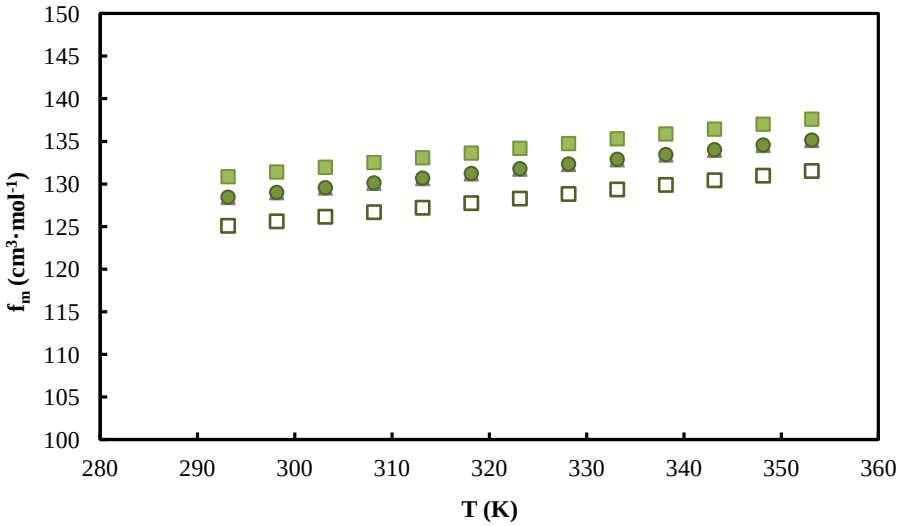

Figure 3.27 - Measured free molar volumes (f_m) of the ionic liquids mixtures studied in this work as a function of temperature (T): $[C_2mim][C(CN)_3]_{0.75}[Gly]_{0.25}$ (□), $[C_2mim][C(CN)_3]_{0.75}[L\text{-}Ala]_{0.25}$ (▲), $[C_2mim][C(CN)_3]_{0.75}[Tau]_{0.25}$ (○), $[C_2mim][C(CN)_3]_{0.75}[L\text{-}Ser]_{0.25}$ (●), $[C_2mim][C(CN)_3]_{0.75}[L\text{-}Pro]_{0.25}$ (■).

As can be seen in the Figures 3.25-3.28, the molar free volumes increase linearly with increasing temperature for all the pure ILs and their mixtures.

A comparison of density, viscosity and refractive index values at T = 318.15 K with literature[81] was made for the pure AA-based ILs, with the exception of the pure [C_2mim][Tau], that was not reported in the literature.

As it can be seen in Figure 3.29, the measured density values exhibit a similar behaviour compared to the literature values. On the other hand, from Figure 3.30, the experimental viscosity values show also a similar trend compared to the literature values. However, experimental viscosity values of [C_2mim][L-Ser] and [C_2mim][L-Pro] measured in this work are higher than those reported in literature. This can be related to the water content of the ILs. Although a direct comparison among the literature and the obtained water contents, was not possible, the large difference between the experimental and the literature viscosity values of [C_2mim][L-Ser] and [C_2mim][L-Pro] lead to suggest that the water contents obtained in this work were lower than those obtained by Muhammad *et al.*[81] Moreover, it was reported in the same work that before water measurement, each sample was dried in a vacuum oven for 4h at 80°C. This confirms the previous suggestion since, in this work, the pure ILs and their mixtures were all dried under vacuum (10^{-3} kPa) at a moderate temperature (≈ 318 K) for at least 4 days.

Additionally, from Figure 3.31, both experimental and literature refractive index values of the pure AA-based ILs can be ordered as: [C_2mim][L-Ala] < [C_2mim][Gly] < [C_2mim][L-Pro] < [C_2mim][L-Ser].

Table 3.5 - Comparison of density (ρ) [81], viscosity (η) [81] and refractive index (n_D) [81] values of the pure ionic liquids measured in this work with those from literature at T = 318.15 K.

T = 318.15 K						
AAIL	**ρ (g·cm^{-3})**		**η (mPa·s)**		**n_D**	
	This work	**Literature**	**This work**	**Literature**	**This work**	**Literature**
[C_2mim][Gly]	1.1490	1.1422	57.66	24.89	1.51445	1.49827
[C_2mim][L-Ala]	1.1105	1.1235	79.34	56.62	1.50651	1.49735
[C_2mim][L-Ser]	1.1909	1.1820	389.00	105.80	1.52022	1.50774
[C_2mim][L-Pro]	1.1287	1.1426	271.20	114.27	1.51591	1.50511

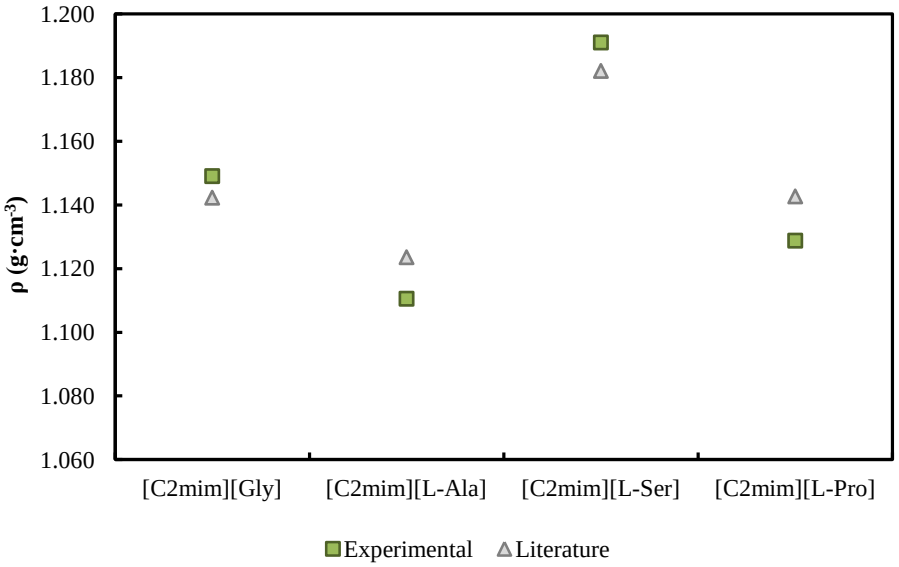

Figure 3.29 – Experimental and literature density values of the pure amino acid-based ionic liquids studied at T = 318.15 K.

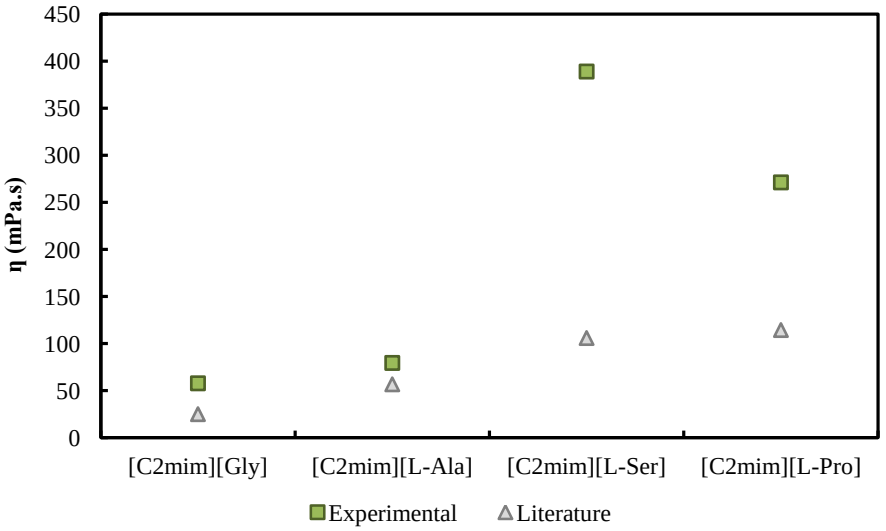

Figure 3.30 - Experimental and literature viscosity values of the pure amino acid-based ionic liquids studied at T = 318.15 K.

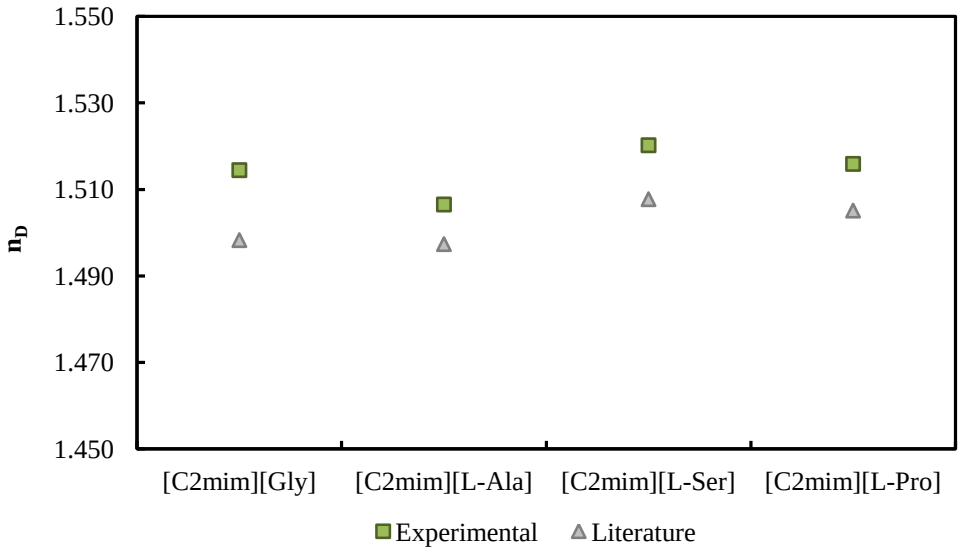

Figure 3.31 - Experimental and literature refractive index values of the pure amino acid-based ionic liquids studied at T = 318.15 K.

4

Gas Permeation Properties

As illustrated in Figure 1.5, the gas transport through a dense liquid membrane occurs according to a solution-diffusion mass transfer mechanism where the permeability (*P*) is related to solubility (*S*) and diffusivity (*D*) as follows[88]:

$$\boldsymbol{P = S \times D} \qquad \textbf{(4.1)}$$

The solution-diffusion mechanism is described by three steps: (1) gas absorption or adsorption on the upstream side of the membrane, (2) diffusion of the absorbed species through the membrane driven by a concentration gradient (partial pressure difference), and (3) gas desorption on the downstream side of the membrane. Thus, in order to better understand the mechanism behind gas permeation, it is important to evaluate not only gas permeability but also solubility and diffusivity, of the gas. In this study, the CO_2 and N_2 permeation properties of the prepared supported ionic liquid membranes were measured by using a time-lag apparatus, which allows for the simultaneous measurement of gas permeability and diffusivity, while the solubility was calculated from Equation (4.1). The gas permeation experiments were performed at a fixed temperature (318.15 K) and different trans-membrane pressure differentials (2.5, 5, 10, 25, 50 and 100 kPa).

4.1 Preparation of the facilitated supported ionic liquid membranes (FSILMs)

Omnipore porous hydrophilic poly(tetrafluoroethylene) (PTFE) membranes provided by MerckMillipore, with a pore size of 0.2 μm and an average thickness of 65 μm, were used to support the pure ILs and their mixtures. PTFE membrane filters were selected in order to improve the chemical resistance and the compatibility of the support.

To achieve stable SILMs, much care is needed to ensure that the IL sample completely fills the membranes pores. In this work, the SILM configuration process only used 1 mL of the pure ILs or their mixtures (previously dried). First, the membrane filter was introduced inside a vacuum chamber for 1h in order to remove the air within the pores and facilitate the membrane wetting. Then, drops of the IL sample were spread on the membrane surface using a syringe, while keeping the vacuum inside the chamber. As the liquid penetrated into the membrane pores, the membrane became transparent. The SILM was left inside the chamber under vacuum for another 1h. Finally, the SILM was taken out of the chamber and the excess of IL was wiped from the membrane surface with paper tissue. From gas permeation measurements, it was obvious if the liquid did not completely fill the membrane pores.

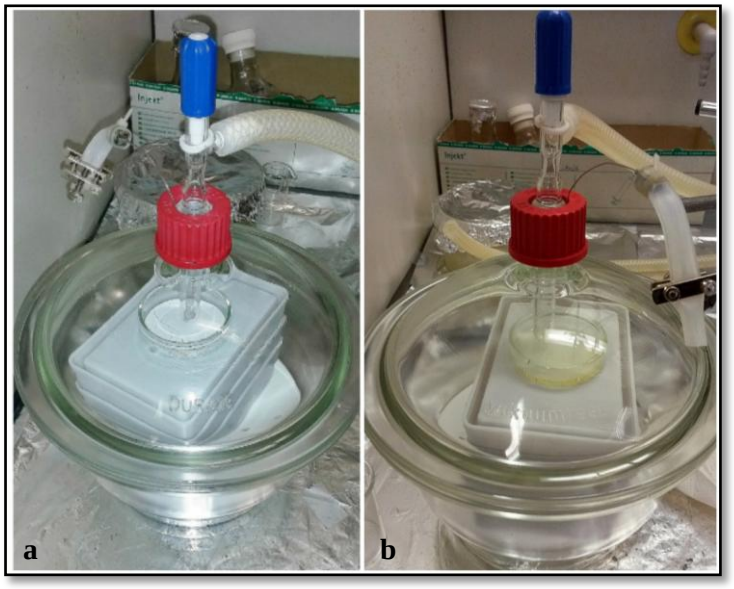

Figure 4.1 – Vacuum chamber a) before and b) after the IL sample impregnation.

Considering that the relatively high viscosity of amino acid-based ionic liquids promotes low sorption and desorption rates, and consequently results in low gas permeabilities, only SILMs of the pure $[C_2mim][C(CN)_3]$ and the following IL mixtures $[C_2mim][C(CN)_3]_{0.5}[Gly]_{0.5}$, $[C_2mim][C(CN)_3]_{0.5}[L\text{-}Ala]_{0.5}$, $[C_2mim][C(CN)_3]_{0.5}[Tau]_{0.5}$, $[C_2mim][C(CN)_3]_{0.5}[L\text{-}Ser]_{0.5}$ and $[C_2mim][C(CN)_3]_{0.5}[L\text{-}Pro]_{0.5}$ (Figure 4.2) were tested. In order to evaluate the influence of the amino groups in the gas transport properties of SILMs, the gas permeation results obtained for the IL mixtures were compared to those of the pure $[C_2mim][C(CN)_3]$.

Common cation $[C_2mim]^+$	% of $[C(CN)_3]^-$		
	25	50	75
$[Gly]^-$		x	
$[L\text{-}Ala]^-$		x	
$[Tau]^-$		x	
$[L\text{-}Ser]^-$		x	
$[L\text{-}Pro]^-$		x	

Figure 4.2 - Chemical structures of ions and composition matrix of the IL + IL mixtures tested as liquid phases in SILMs.

4.2 Gas permeation measurements

Experimental CO_2 and N_2 permeation measurements through the prepared facilitated SILMs were conducted for single gas feed using a time-lag apparatus, which is schematically represented in Figure 4.3.

The time-lag apparatus is composed of two stainless steel tanks, one of them with 5 dm^3 (feed) and the other with (34.2 ± 0.2) cm^3 (permeate). Both reservoirs are connected to the permeation cell, which has 13.9 cm^2 of effective area.

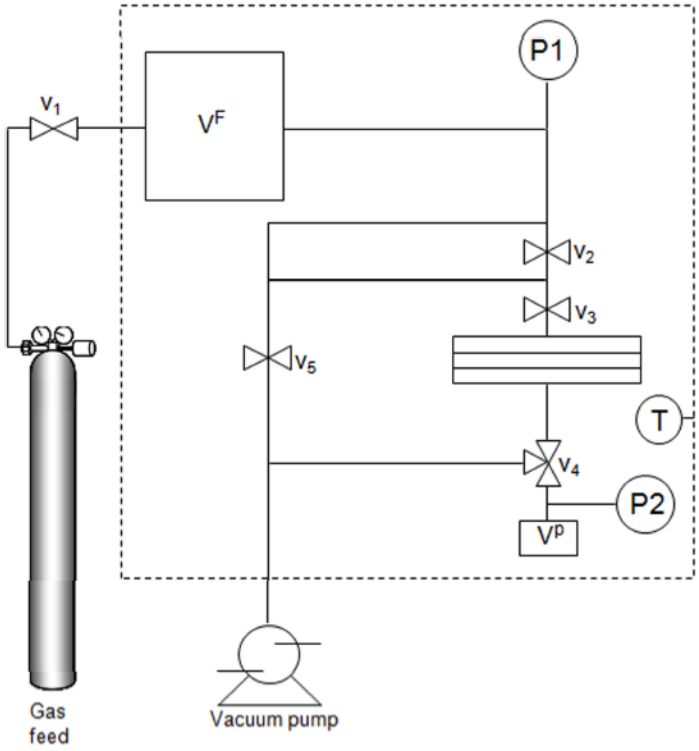

Figure 4.3 - Time-lag apparatus. *P* represents the pressure sensors, *V* the manual valves, V^F the feed tank, V^P the permeate tank and *T* a thermostatic air bath.

Each prepared membrane was positioned on the top of a highly porous sintered disk for providing mechanical stability and installed into the flat-type permeation cell (Figure 4.4), where it was degassed under vacuum during 12 hours before testing. An EPDM o-ring was used to seal the membrane inside de permeation cell.

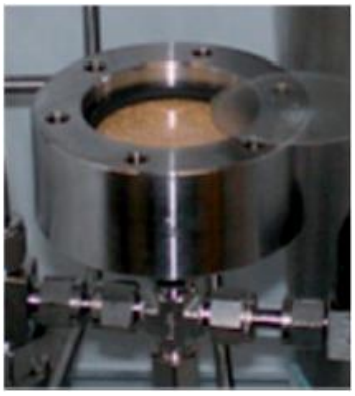

Figure 4.4 - Stainless steel flat-type permeation cell used in this work.

Two sensors controlled pressure, one at the feed tank (S-10 WIKA, 600 KPa ± 0.05% FS, P1) and in the permeate tank there was a high precision absolute pressure sensor (MKS e-Baratron, ref. 628C, 13.33 kPa, 0.001% FS, P2) for measuring pressure variations. The time-lag unit was placed inside a thermostatic cabinet with a precision of ± 0.05K. A rotatory high vacuum pump (BOC Edwards, RV3) guaranteed vacuum conditions.

The gas bottles (CO_2 and N_2) are placed on the system to allow the filling of the feed tank (V^F) for thermostating the gas through the valve v_1.The valves v_2, v_3, v_4 and v_5, are displayed in the installation in order to be manipulated outside of the thermostatic cabinet for preventing disturbs in temperature.

Initially, vacuum was applied to the system (valve v_2 closed; valves v_3 and v_4 opened) to ensure that is achieved a pressure as low as possible, i.e., that the concentration of the permeate side is practically null ($C_0 \backsimeq 0$). Then, the vacuum was isolated (valves v_4 and v_5 closed) and gas was introduced into the system (valves v_2 and v_3 opened), feeding the membrane at the desired pressure p_1.

The single gas permeation experiments using CO_2 and N_2 were performed at T = 318.15 K and trans-membrane pressure differentials between 2.5 and 100 kPa and vacuum (< 0.1 kPa) as the initial downstream pressure (permeate). At least three separate experiments of each gas on a single membrane sample were carried out. Between each run, the permeation cell and lines were evacuated on both upstream and downstream sides until the pressure was below 0.1 kPa. No residual IL sample was found inside the permeation cell at the end of the experiments which indicates that the membrane mass remained approximately constant throughout the experiment.

The thickness of the prepared SILMs was assumed to be equivalent to the membrane filter thickness (0.065 mm).

Carbon dioxide (CO_2) and nitrogen (N_2) were supplied by Air Liquid and were of at least 99.99% purity. Gases were used without further purification.

4.3 Results and Discussion

The CO_2 and N_2 permeation properties (permeability, diffusivity and solubility) were determined at T = 318.15 K and different trans-membrane pressure differentials (2.5, 5, 10, 25, 50 and 100 kPa).

In Table 4.1 are summarized the water contents as well as the thermophysical properties of the pure $[C_2mim][C(CN)_3]$ and the IL mixtures used to prepare the SILMs studied, namely $[C_2mim][C(CN)_3]_{0.5}[Gly]_{0.5}$, $[C_2mim][C(CN)_3]_{0.5}[L\text{-}Ala]_{0.5}$, $[C_2mim][C(CN)_3]_{0.5}[Tau]_{0.5}$, $[C_2mim][C(CN)_3]_{0.5}[L\text{-}Ser]_{0.5}$ and $[C_2mim][C(CN)_3]_{0.5}[L\text{-}Pro]_{0.5}$..

Table 4.1 – Thermophysical Properties (at T = 318.15 K) and water contents of pure $[C_2mim][C(CN)_3]$ and IL mixtures used to prepare the SILMs studied.

Ionic liquid sample	wt% of water	M ($g \cdot mol^{-1}$)	η (mPa·s)	ρ ($g \cdot cm^{-3}$)	V_m ($cm^3 \cdot mol^{-1}$)
$[C_2mim][C(CN)_3]_{0.5}$ $[Gly]_{0.5}$	0.65	193.23	18.972	1.102	175.340
$[C_2mim][C(CN)_3]_{0.5}$ $[L\text{-}Ala]_{0.5}$	0.10	200.24	24.899	1.086	184.394
$[C_2mim][C(CN)_3]_{0.5}$ $[Tau]_{0.5}$	0.05	218.27	27.272	1.148	190.093
$[C_2mim][C(CN)_3]_{0.5}$ $[L\text{-}Ser]_{0.5}$	0.29	208.24	41.254	1.125	185.091
$[C_2mim][C(CN)_3]_{0.5}$ $[L\text{-}Pro]_{0.5}$	0.28	213.26	50.983	1.104	193.217
$[C_2mim][C(CN_3)]$	0.01	201.23	8.202	1.067	188.461

4.3.2 Gas Permeability

The gas permeability values were determined from the steady-state flux through the membrane (J), the membrane thickness (ℓ) and the pressure difference across the membrane (Δp) according to:

$$\boldsymbol{P = J\frac{\ell}{\Delta p}} \quad \textbf{(4.2)}$$

Permeability is often expressed in Barrer, where:

$$\textbf{1 barrer} = \frac{\mathbf{10^{-10}}\boldsymbol{cm^3(STP)cm}}{\boldsymbol{cm^2 s\ cmHg}} \quad \textbf{(4.3)}$$

The gas permeabilities through the prepared SILMs measured at T=318.15 K and different trans-membrane pressure differentials (2.5, 5, 10, 25, 50 and 100 kPa) are presented in Table 4.2 and depicted in Figures 4.3-4.7.

It is important to note that it was not possible to perform gas permeation experiments under a feed pressure of 100 kPa for the $[C_2mim][C(CN)_3]_{0.5}[Gly]_{0.5}$ and $[C_2mim][C(CN)_3]_{0.5}[L\text{-}Ala]_{0.5}$-based SILMs since after two-three days of continue operating measurement conditions, the stability of these SILMs is compromised. In order words, it was not possible to reproduce gas experiments since the gas flux is much increased after each run and at a given time the pressure on the permeate side just instantaneously raised to its upper limit, meaning that the gas molecules are not diffusing through the membrane by a solution-diffusion mechanism.

Table 4.2 – Gas permeabilities at T = 318.15 K and different feed pressures.

Permeability (Barrer) at *T*=318.15K				
SILM sample	**Feed Pressure: 2.5 kPa**			
	CO_2	**STDEV**	**N_2**	**STDEV**
$[C_2mim][C(CN)_3]_{0.5}$ $[Gly]_{0.5}$	392	7.41	14.5	0.40
$[C_2mim][C(CN)_3]_{0.5}$ $[L\text{-}Ala]_{0.5}$	765	19.11	16.97	0.61
$[C_2mim][C(CN)_3]_{0.5}$ $[Tau]_{0.5}$	733	14.62	10.6	0.22
$[C_2mim][C(CN)_3]_{0.5}$ $[L\text{-}Ser]_{0.5}$	338	7.25	10.0	0.27
$[C_2mim][C(CN)_3]_{0.5}$ $[L\text{-}Pro]_{0.5}$	144	3.80	7.8	0.07
$[C_2mim][C(CN_3)]$	539	8.38	25.4	0.58

	Feed Pressure: 5 kPa			
$[C_2mim][C(CN)_3]_{0.5}$ $[Gly]_{0.5}$	262	1.06	9.6	0.04
$[C_2mim][C(CN)_3]_{0.5}$ $[L\text{-}Ala]_{0.5}$	517	17.84	13.5	0.04
$[C_2mim][C(CN)_3]_{0.5}$ $[Tau]_{0.5}$	460	16.35	8.7	0.03
$[C_2mim][C(CN)_3]_{0.5}$ $[L\text{-}Ser]_{0.5}$	231	7.11	8.6	0.08
$[C_2mim][C(CN)_3]_{0.5}$ $[L\text{-}Pro]_{0.5}$	105	2.15	6.6	0.10
$[C_2mim][C(CN_3)]$	570	3.94	21.6	0.12
	Feed Pressure: 10 kPa			
$[C_2mim][C(CN)_3]_{0.5}$ $[Gly]_{0.5}$	198	1.87	9.0	0.10
$[C_2mim][C(CN)_3]_{0.5}$ $[L\text{-}Ala]_{0.5}$	351	12.67	13.4	0.12
$[C_2mim][C(CN)_3]_{0.5}$ $[Tau]_{0.5}$	297	3.65	7.9	0.04
$[C_2mim][C(CN)_3]_{0.5}$ $[L\text{-}Ser]_{0.5}$	160	3.37	8.1	0.02
$[C_2mim][C(CN)_3]_{0.5}$ $[L\text{-}Pro]_{0.5}$	75	1.85	5.9	0.04
$[C_2mim][C(CN_3)]$	561	1.94	21.1	0.19
	Feed Pressure: 25 kPa			
$[C_2mim][C(CN)_3]_{0.5}$ $[Gly]_{0.5}$	148	3.49	8.6	0.05
$[C_2mim][C(CN)_3]_{0.5}$ $[L\text{-}Ala]_{0.5}$	351	12.67	12.5	0.03
$[C_2mim][C(CN)_3]_{0.5}$ $[Tau]_{0.5}$	175	1.25	7.4	0.05
$[C_2mim][C(CN)_3]_{0.5}$ $[L\text{-}Ser]_{0.5}$	127	2.59	7.3	0.03
$[C_2mim][C(CN)_3]_{0.5}$ $[L\text{-}Pro]_{0.5}$	64	1.29	5.6	0.35
$[C_2mim][C(CN_3)]$	564	4.18	19.4	0.03
	Feed Pressure: 50 kPa			
$[C_2mim][C(CN)_3]_{0.5}$ $[Gly]_{0.5}$	123	0.90	7.3	0.11
$[C_2mim][C(CN)_3]_{0.5}$ $[L\text{-}Ala]_{0.5}$	199	3.18	13.5	0.40
$[C_2mim][C(CN)_3]_{0.5}$ $[Tau]_{0.5}$	127	1.85	7.0	0.01
$[C_2mim][C(CN)_3]_{0.5}$ $[L\text{-}Ser]_{0.5}$	103	2.07	7.1	0.03
$[C_2mim][C(CN)_3]_{0.5}$ $[L\text{-}Pro]_{0.5}$	60	0.25	5.2	0.07
$[C_2mim][C(CN_3)]$	562	5.16	19.1	0.03
	Feed Pressure: 100 kPa			
$[C_2mim][C(CN)_3]_{0.5}$ $[Gly]_{0.5}$	-	-	-	-
$[C_2mim][C(CN)_3]_{0.5}$ $[L\text{-}Ala]_{0.5}$	-	-	-	-
$[C_2mim][C(CN)_3]_{0.5}$ $[Tau]_{0.5}$	109	0.53	6.9	0.03
$[C_2mim][C(CN)_3]_{0.5}$ $[L\text{-}Ser]_{0.5}$	118	3.26	7.3	0.01
$[C_2mim][C(CN)_3]_{0.5}$ $[L\text{-}Pro]_{0.5}$	59	1.04	5.03	0.12
$[C_2mim][C(CN_3)]$	556	5.99	18.1	0.02

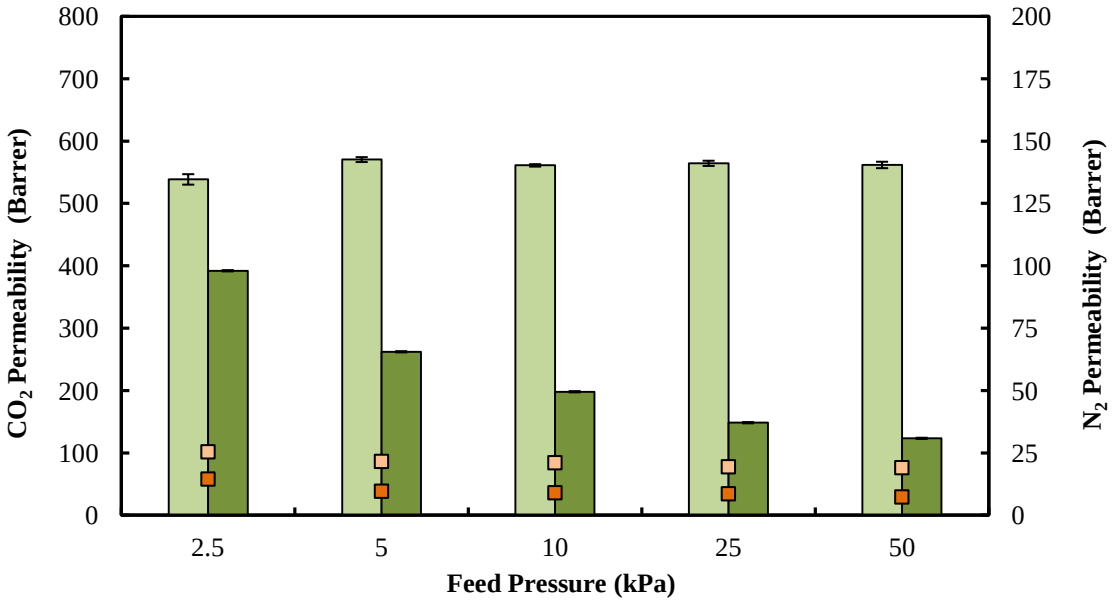

Figure 4.5 - Gas permeabilities at T = 318.15 K and different feed pressures: $[C_2mim][C(CN)_3]$ (CO_2) (■), $[C_2mim][C(CN)_3]$ (N_2) (■), $[C_2mim][C(CN)_3]_{0.5}[Gly]_{0.5}$ (CO_2) (■), **[**$C_2mim][C(CN)_3]_{0.5}$ $[Gly]_{0.5}$ (N_2) (■)

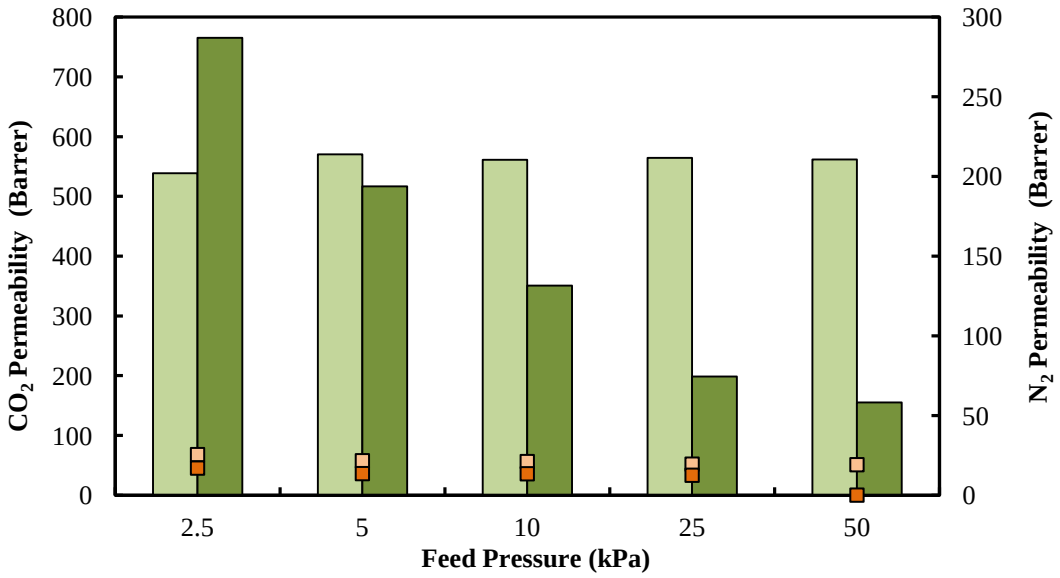

Figure 4.6 - Gas permeabilities at T = 318.15 K and different feed pressures: $[C_2mim][C(CN)_3]$ (CO_2) (■), $[C_2mim][C(CN)_3]$ (N_2) (■), $[C_2mim][C(CN)_3]_{0.5}[L\text{-}Ala]_{0.5}$ (CO_2) (■), **[**$C_2mim][C(CN)_3]_{0.5}$ $[L\text{-}Ala]_{0.5}$ (N_2) (■)

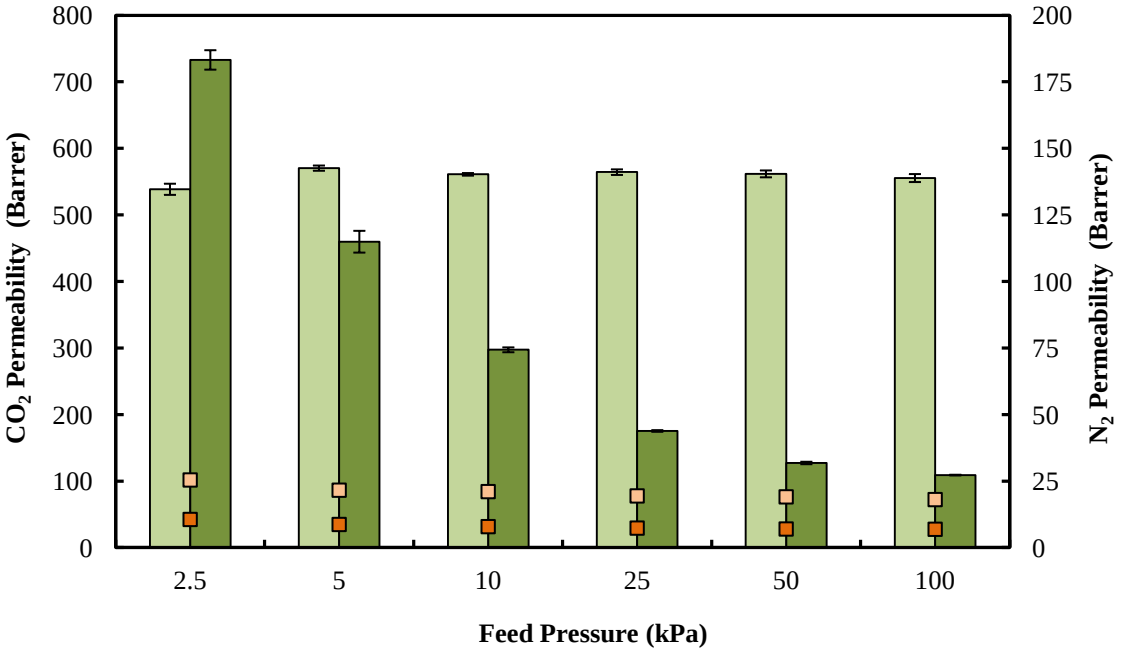

Figure 4.7 - Gas permeabilities at T = 318.15 K and different feed pressures: $[C_2mim][C(CN)_3]$ (CO_2) (■), $[C_2mim][C(CN)_3]$ (N_2) (■), $[C_2mim][C(CN)_3]_{0.5}[Tau]_{0.5}$ (CO_2) (■), $[C_2mim][C(CN)_3]_{0.5}[Tau]_{0.5}$ (N_2) (■)

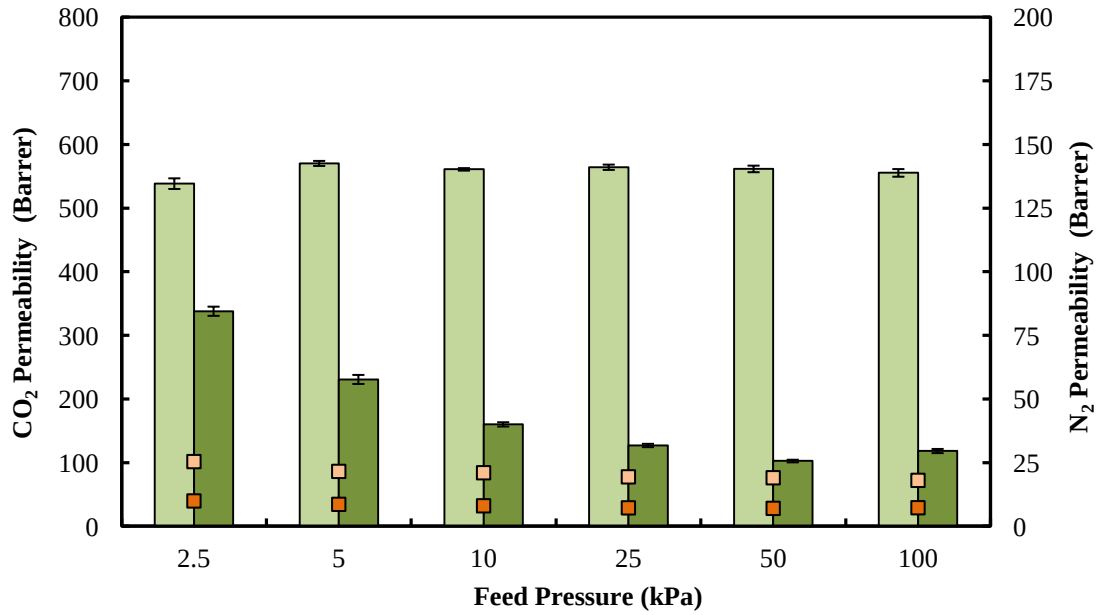

Figure 4.8 - Gas permeabilities at T = 318.15 K and different feed pressures: $[C_2mim][C(CN)_3]$ (CO_2) (■), $[C_2mim][C(CN)_3]$ (N_2) (■), $[C_2mim][C(CN)_3]_{0.5}[L\text{-}Ser]_{0.5}$ (CO_2) (■), $[C_2mim][C(CN)_3]_{0.5}[L\text{-}Ser]_{0.5}$ (N_2) (■)

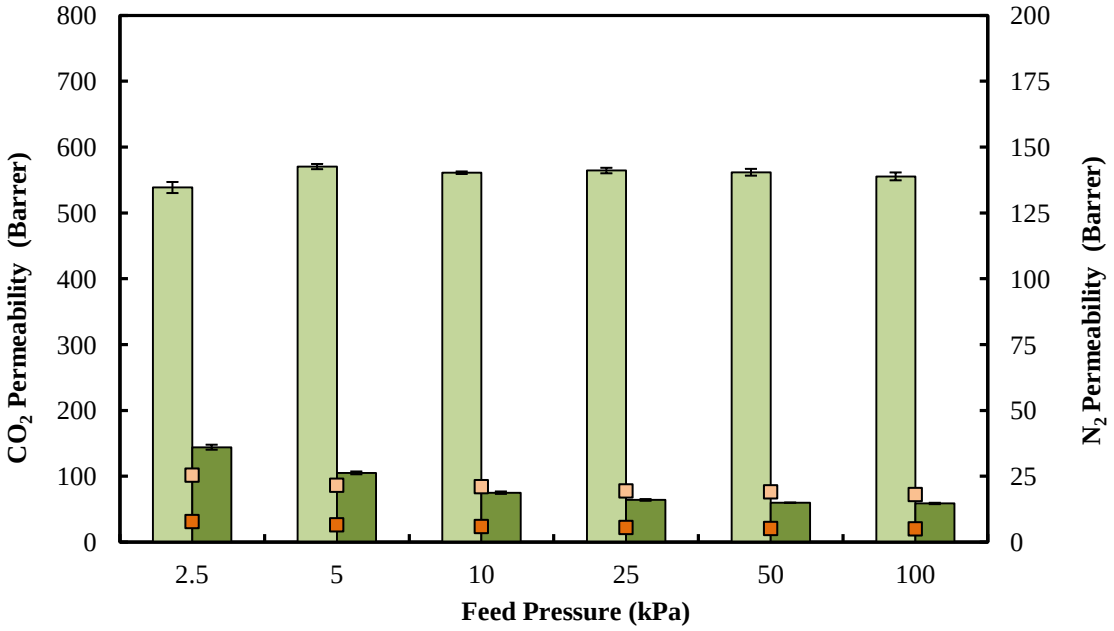

Figure 4.9 - Gas permeabilities at T = 318.15 K and different feed pressures: $[C_2mim][C(CN)_3]$ (CO_2) (■), $[C_2mim][C(CN)_3]$ (N_2) (■), $[C_2mim][C(CN)_3]_{0.5}[L\text{-}Pro]_{0.5}$ (CO_2) (■), **[**$C_2mim][C(CN)_3]_{0.5}$ $[L\text{-}Pro]_{0.5}$ (N_2) (■)

As it can be seen from Figures 4.5-4.9, the CO_2 permeability through the pure $[C_2mim][C(CN)_3]$ based SILMs does not significantly change under different feed pressure conditions. In contrast, the CO_2 permeability of all the supported IL mixture increases as the feed pressure decreases, while N_2 permeability remains unchanged, meaning that the prepared supported IL mixtures still have the ability to perform CO_2 facilitated transport. For instance, under 2.5 kPa of feed pressure, the CO_2 permeability values measured through the SILMs based on the $[C_2mim][C(CN)_3]_{0.5}[L\text{-}Ala]_{0.5}$ and $[C_2mim][C(CN)_3]_{0.5}[Tau]_{0.5}$ mixtures are, respectively, 42 % and 36 % higher than that of the pure $[C_2mim][C(CN)_3]$.

Figure 4.10 shows the CO_2 permeability values through the prepared SILMs at T=318.15 K and 2.5 kPa of feed pressure as a function of viscosity (η). With the exception of the pure $[C_2mim][C(CN)_3]$ and the $[C_2mim][C(CN)_3]_{0.5}[Gly]_{0.5}$ mixture, the CO_2 permeability decreases with increasing IL viscosity. This behaviour is in agreement to the general trend scaling gas permeability with IL viscosity that has been observed in SILMs by different authors.[39, 56, 89-91] However, the $[C_2mim][C(CN)_3]_{0.5}[Gly]_{0.5}$ mixture can be considered an exception to this general trend. Although it has the lowest viscosity, the $[C_2mim][C(CN)_3]_{0.5}[Gly]_{0.5}$ mixture does not present the highest CO_2 permeability values, as expected. It means that the description of gas permeability simply in terms of IL viscosity does not provide a full understanding of the gas transport through SILMs.

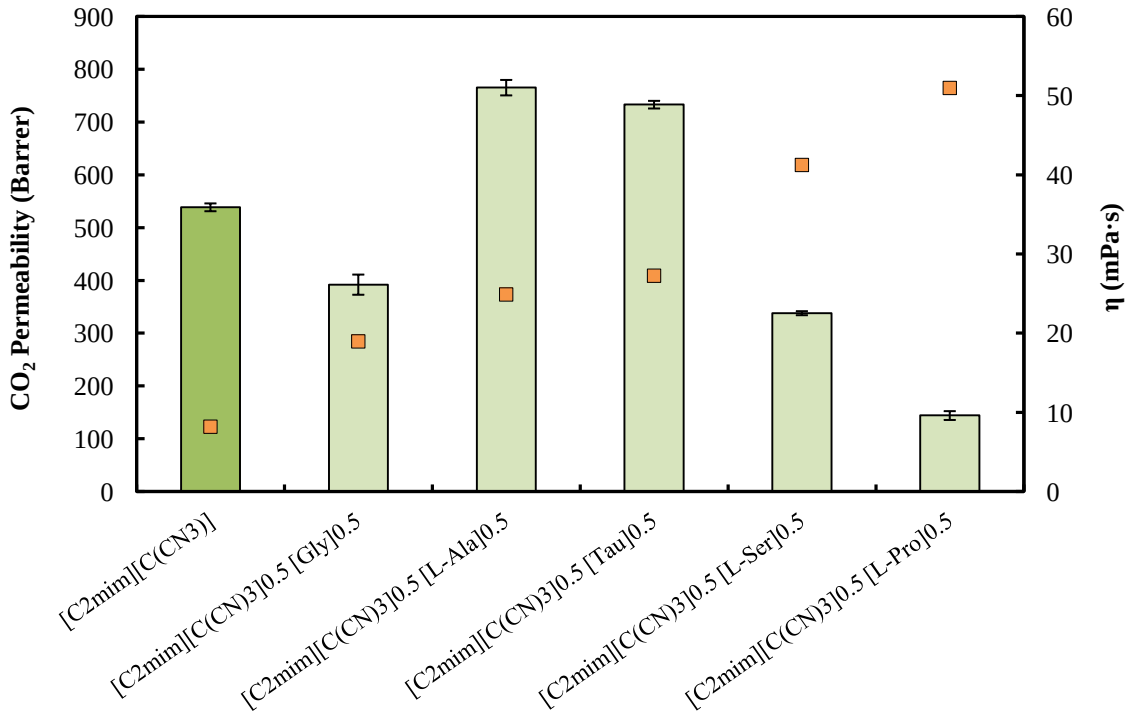

Figure 4.10 - CO_2 permeability values through the prepared SILMs at T = 318.15 K and 2.5 kPa of feed pressure as a function of viscosity (η).

4.3.3 Gas Diffusivity

Gas diffusivity is a mass transfer property that directly affects gas permeability through SILMs as described by Equation 4.4. In fact, gas diffusivity is the parameter that indicates the gas mobility through the membrane. The higher is the diffusivity, the faster is the gas flux through the SILM.

The gas diffusivity (D) was determined from the time-lag parameter (θ), which can be obtained before achieving steady state flux, using Equation 4.4. The time-lag parameter was deduced by extrapolating the slope of the linear portion of the p_d vs. t curve back to the time axis, where the intercept is equal to θ.

$$\boldsymbol{D = \frac{\ell^2}{6\theta}} \qquad \textbf{(4.4)}$$

Temperature dependence on gas diffusion is expressed in terms of an Arrhenius type relationship, seeing that the movement of gas molecules through liquid membranes is a thermally activated process. Mathematically, the temperature dependence of diffusion is given by Equation 4.5:[45]

$$\boldsymbol{D = D_0 e^{\left(-\frac{Ea}{RT}\right)}} \qquad \textbf{(4.5)}$$

where D_0 is the pre exponential factor, Ea is the activation energy, R is the gas constant and T is the temperature. In general, the diffusion coefficient increases with increasing temperature.[45, 92]

Considering that N_2 gas molecules diffuses faster than those of CO_2 through the SILMs due to its smaller sizes, it is generally more difficult to precisely determine the N_2 time-lag parameter (θ) than that of CO_2. In this work, it was not possible to determine N_2 time-lag parameters through any of the SILMs prepared. Although the apparatus available in our lab allows the determination of N_2 diffusivities at T = 293.15 K,[7, 38, 53] it was found that at T = 318.15 K, the N_2 diffusivities are too faster to be accurately determined using this set-up. In view of that, only the CO_2 diffusivity and solubility values are presented and discussed herein.

The CO_2 diffusivity values through the prepared SILMs at T = 318.15 K and 2.5 kPa of feed pressure are presented in Table 4.3 and depicted in Figure 4.11 as a function of viscosity (η).

Table 4.3 - CO_2 diffusivity values through the prepared SILMs at T = 318.15 K and 2.5 kPa of feed pressure.

Diffusivity (x10^{12}) ($m^2 \cdot s^{-1}$) at T = 318.15K		
SILM sample	**Feed Pressure: 2.5 kPa**	
	CO_2	**STDEV**
$[C_2mim][C(CN)_3]$	3.966	0.087
$[C_2mim][C(CN)_3]_{0.5}$ $[Gly]_{0.5}$	1.301	0.065
$[C_2mim][C(CN)_3]_{0.5}$ $[L\text{-}Ala]_{0.5}$	2.381	0.030
$[C_2mim][C(CN)_3]_{0.5}$ $[Tau]_{0.5}$	2.851	0.062
$[C_2mim][C(CN)_3]_{0.5}$ $[L\text{-}Ser]_{0.5}$	0.818	0.030
$[C_2mim][C(CN)_3]_{0.5}$ $[L\text{-}Pro]_{0.5}$	0.369	0.019

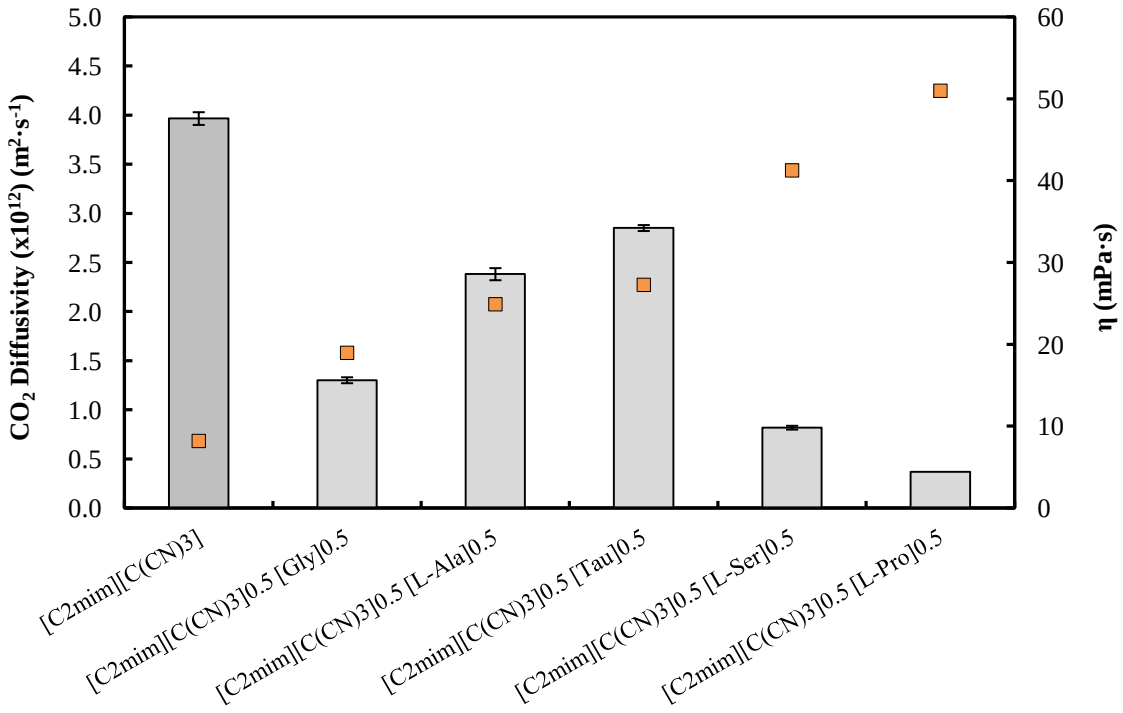

Figure 4.11 - CO_2 diffusivity values through the prepared SILMs at T = 318.15 K and 2.5 kPa of feed pressure as a function of viscosity (η).

It is well know that the liquid phase viscosity can strongly affect gas diffusivity through SILMs.

From Figure 4.9, it can be seen that the pure $[C_2mim][C(CN)_3]$, which has the lowest viscosity within the IL mixtures, presents the higher CO_2 diffusivity. This behaviour is in agreement to what has been reported for SILMs made of pure ILs.[53] In the same way, the $[C_2mim][C(CN)_3]_{0.5}[L\text{-}Pro]_{0.5}$ mixture has the highest viscosity and thus exhibits the lowest CO_2 diffusivities and permeabilities. It depicts the inversely proportional relation between the gas diffusivity and the IL viscosity, in which the lower is the solvent viscosity, the faster the gas passes through it. However, different behaviours were obtained with the $[C_2mim][C(CN)_3]_{0.5}[Gly]_{0.5}$ and the $[C_2mim][C(CN)_3]_{0.5}[Tau]_{0.5}$ mixtures. For instance, the $[C_2mim][C(CN)_3]_{0.5}[Gly]_{0.5}$ mixture shows lower viscosity compared to that of $[C_2mim][C(CN)_3]_{0.5}[Tau]_{0.5}$ mixture, but present lower CO_2 diffusivity, meaning that in this case the CO_2 diffusivities are not entirely controlled by the respective IL viscosities.

Several different correlations for gas diffusivity in different IL families have been developed considering different parameters such as the effect of temperature, gas molar volume, IL viscosity, density and molecular weight, taking into account that gas diffusivities in ILs are one or more order of magnitude smaller than in traditional solvents. This behavior is essentially due to the higher viscosities of ILs as already showed by Scovazzo[43, 50, 52] and Baltus.[49, 93] In conclusion, literature correlations for gas diffusivity in conventional solvents are not adequate to describe gas diffusivity in ILs and thus specific correlations need to be used. Therefore, Scovazzo and co-authors proposed the following general correlation[39]:

$$\boldsymbol{D = A\frac{V_{IL}^{a}}{\eta_{IL}^{b}V_{gas}^{c}}} \qquad \textbf{(4.6)}$$

where A, a, b and c are IL-class specific parameters, η_{IL} is the IL viscosity, V_{IL} is the IL molar volume and V_{gas} is the solute gas molar volume. In the case of ionic liquids with 1-alkyl-3-methylimidazolium cations having an alkyl chain length smaller than four carbon atoms, a is equal to zero, which means that the gas diffusivity is inversely proportional to the IL viscosity. In this context, the relation between the CO_2 diffusivity and IL viscosity at T=318.15K and 100 kPa of feed pressure was discussed.

In Table 4.4 are presented the CO_2 diffusivity values at T = 318.15 K and 100 kPa of feed pressure of the pure $[C_2mim][C(CN)_3]$ and $[C_2mim][C(CN)_3]_{0.5}[Tau]_{0.5}$, and the following mixtures $[C_2mim][C(CN)_3]_{0.5}[L\text{-}Ser]_{0.5}$ and $[C_2mim][C(CN)_3]_{0.5}[L\text{-}Pro]_{0.5}$.

Table 4.4 - CO_2 diffusivity values through the prepared SILMs at T = 318.15 K and 100 kPa of feed pressure.

Diffusivity (Barrer) at T = 318.15 K		
SILM sample	**Feed Pressure: 100 kPa**	
	CO_2	STDEV
$[C_2mim][C(CN)_3]$	87.943	7.389
$[C_2mim][C(CN)_3]_{0.5}$ $[Tau]_{0.5}$	1.981	0.022
$[C_2mim][C(CN)_3]_{0.5}$ $[L\text{-}Ser]_{0.5}$	1.172	0.038
$[C_2mim][C(CN)_3]_{0.5}$ $[L\text{-}Pro]_{0.5}$	0.757	0.017

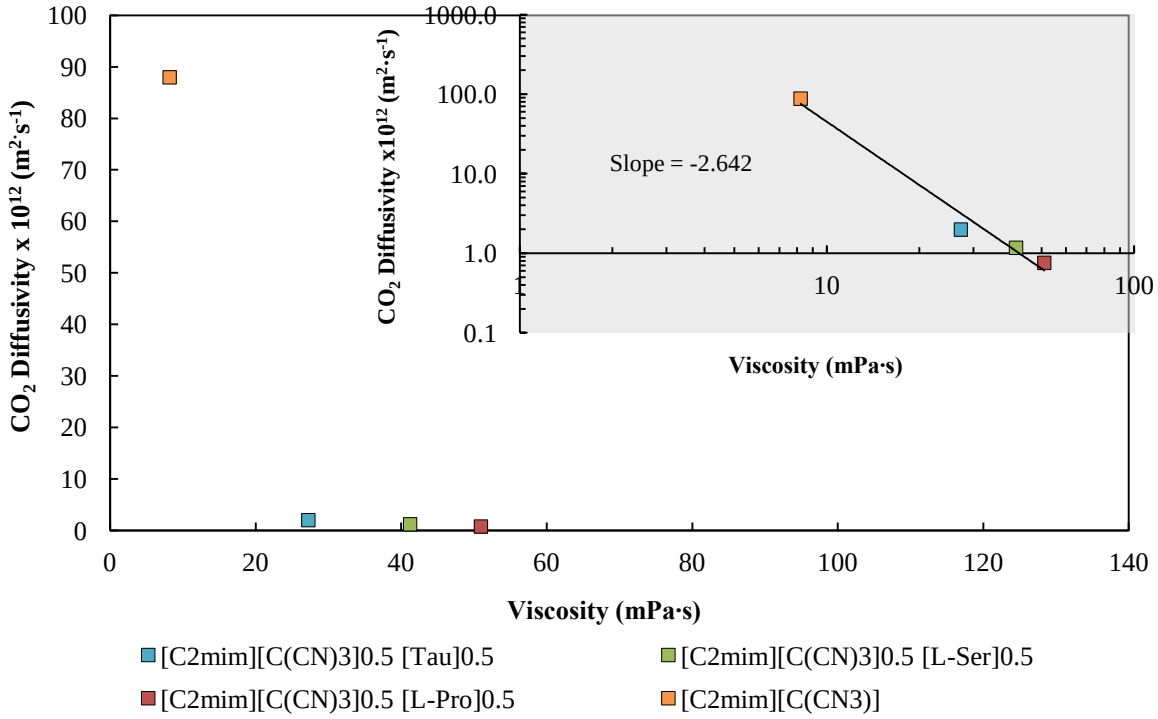

Figure 4.12 – Experimental CO_2 diffusivities in the SILMs as a function of IL viscosity measured at T = 318.15 K.

Morgan *et al*[43] showed, by using a series of imidazolium-based ILs, that gas diffusivity is inversely proportional to IL viscosity with an average power of 0.6. The fit depicted in log-log plot of Figure 4.12 show that experimental CO_2 diffusivities of the pure $[C_2mim][C(CN)_3]$ and the $[C_2mim][C(CN)_3]_{0.5}[Tau]_{0.5}$, $[C_2mim][C(CN)_3]_{0.5}[L\text{-}Ser]_{0.5}$ and $[C_2mim][C(CN)_3]_{0.5}[L\text{-}Pro]_{0.5}$ mixtures vary inversely with IL viscosity to the power of 2.642. This obtained power value is much higher that that reported in literature. However, the power reported is not a theoretical value but an empirical observation based on data for a series of pure imidazolium-ILs, which did not include amino acid or cyano anions. Thus, a truly direct comparison cannot be made.

4.3.4 Gas Solubility

Solubility (m^3 (STP) m^{-3} Pa^{-1}) is a thermodynamic parameter that reflects the number of gas molecules dissolved in the IL sample inside the membrane pores when equilibrated at a given gas pressure and temperature.[94]

The gas solubility was determined by Equation 4.1. Given that the N_2 time-lag parameters were not possible to determine in this work, only the CO_2 solubilities are presented and discussed.

The CO_2 solubility in the prepared SILMs measured at T = 318.15 K and different trans-membrane pressure differentials (2.5, 5, 10, 25, 50 and 100 kPa) are presented in Table 4.5.

Table 4.5 – CO_2 Solubility at T = 318.15 K and different feed pressures.

CO_2 Solubility ($x10^6$) (m^3(STP).m^{-3}.Pa^{-1}) at T = 318.15 K		
SILM sample	**Feed Pressure: 2.5 kPa**	
	CO_2	**STDEV**
$[C_2mim][C(CN)_3]_{0.5}$ $[Gly]_{0.5}$	2262	83.0
$[C_2mim][C(CN)_3]_{0.5}$ $[L\text{-}Ala]_{0.5}$	2410	32.9
$[C_2mim][C(CN)_3]_{0.5}$ $[Tau]_{0.5}$	1929	3.8
$[C_2mim][C(CN)_3]_{0.5}$ $[L\text{-}Ser]_{0.5}$	3099	50.1
$[C_2mim][C(CN)_3]_{0.5}$ $[L\text{-}Pro]_{0.5}$	2930	91.5
$[C_2mim][C(CN_3)]$	1019	24.4
	Feed Pressure: 5 kPa	
$[C_2mim][C(CN)_3]_{0.5}$ $[Gly]_{0.5}$	1682	28.0
$[C_2mim][C(CN)_3]_{0.5}$ $[L\text{-}Ala]_{0.5}$	1821	67.9
$[C_2mim][C(CN)_3]_{0.5}$ $[Tau]_{0.5}$	1471	53.6
$[C_2mim][C(CN)_3]_{0.5}$ $[L\text{-}Ser]_{0.5}$	2703	37.6
$[C_2mim][C(CN)_3]_{0.5}$ $[L\text{-}Pro]_{0.5}$	2256	52.7
$[C_2mim][C(CN_3)]$	807	27.6
	Feed Pressure: 10 kPa	
$[C_2mim][C(CN)_3]_{0.5}$ $[Gly]_{0.5}$	1401	57.8
$[C_2mim][C(CN)_3]_{0.5}$ $[L\text{-}Ala]_{0.5}$	1420	6.4
$[C_2mim][C(CN)_3]_{0.5}$ $[Tau]_{0.5}$	1162	9.4
$[C_2mim][C(CN)_3]_{0.5}$ $[L\text{-}Ser]_{0.5}$	1971	35.8
$[C_2mim][C(CN)_3]_{0.5}$ $[L\text{-}Pro]_{0.5}$	1729	49.9
$[C_2mim][C(CN_3)]$	476	4.9

	Feed Pressure: 25 kPa	
$[C_2mim][C(CN)_3]_{0.5}$ $[Gly]_{0.5}$	1134	43.0
$[C_2mim][C(CN)_3]_{0.5}$ $[L\text{-}Ala]_{0.5}$	1001	28.1
$[C_2mim][C(CN)_3]_{0.5}$ $[Tau]_{0.5}$	826	5.2
$[C_2mim][C(CN)_3]_{0.5}$ $[L\text{-}Ser]_{0.5}$	1668	41.6
$[C_2mim][C(CN)_3]_{0.5}$ $[L\text{-}Pro]_{0.5}$	1201	17.4
$[C_2mim][C(CN_3)]$	204	2.2
	Feed Pressure: 50 kPa	
$[C_2mim][C(CN)_3]_{0.5}$ $[Gly]_{0.5}$	778	15.4
$[C_2mim][C(CN)_3]_{0.5}$ $[L\text{-}Ala]_{0.5}$	1001	28.1
$[C_2mim][C(CN)_3]_{0.5}$ $[Tau]_{0.5}$	621	4.4
$[C_2mim][C(CN)_3]_{0.5}$ $[L\text{-}Ser]_{0.5}$	1180	8.2
$[C_2mim][C(CN)_3]_{0.5}$ $[L\text{-}Pro]_{0.5}$	897	13.5
$[C_2mim][C(CN_3)]$	113	4.3
	Feed Pressure: 100 kPa	
$[C_2mim][C(CN)_3]_{0.5}$ $[Gly]_{0.5}$	-	-
$[C_2mim][C(CN)_3]_{0.5}$ $[L\text{-}Ala]_{0.5}$	-	-
$[C_2mim][C(CN)_3]_{0.5}$ $[Tau]_{0.5}$	413	2.8
$[C_2mim][C(CN)_3]_{0.5}$ $[L\text{-}Ser]_{0.5}$	757	4.4
$[C_2mim][C(CN)_3]_{0.5}$ $[L\text{-}Pro]_{0.5}$	582	8.2
$[C_2mim][C(CN_3)]$	48	3.7

In Figure 4.13 the CO_2 solubilities obtained in the prepared SILMs are represented in function of the feed pressure (kPa).

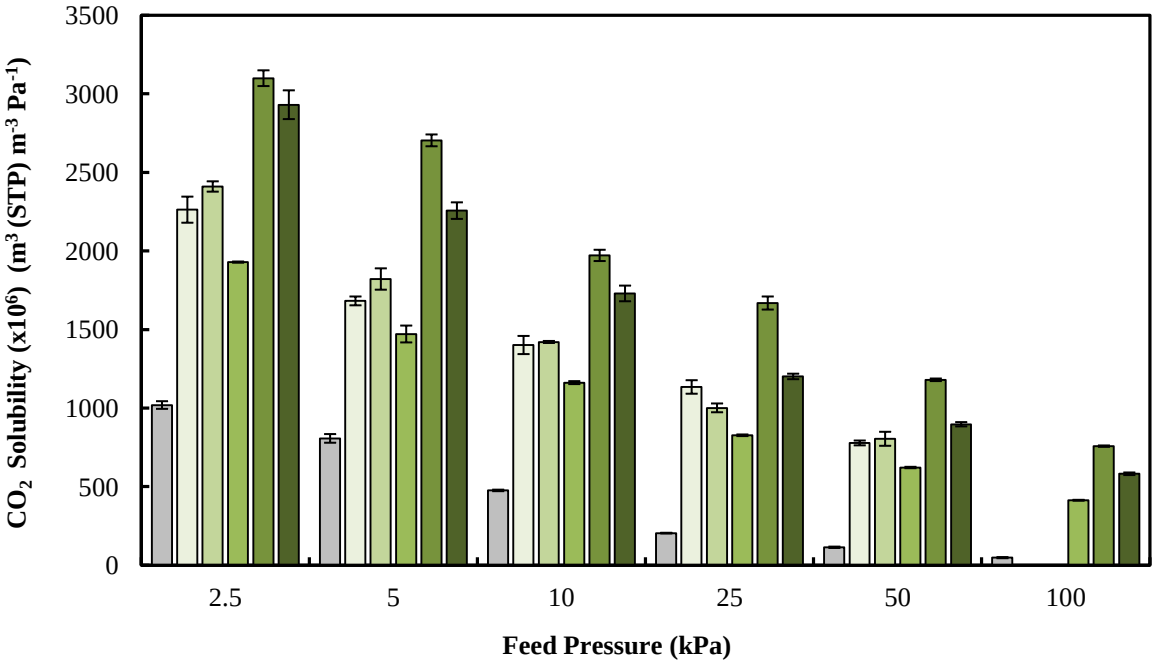

Figure 4.13 - CO_2 solubilities (m^3 (STP) m^{-3} Pa^{-1}) in the prepared SILMs as a function of feed pressure (kPa): $[C_2mim][C(CN)_3]$ (■), $[C_2mim][C(CN)_3]_{0.5}[Gly]_{0.5}$ (■), $[C_2mim][C(CN)_3]_{0.5}[L\text{-}Ala]_{0.5}$ (■), $[C_2mim][C(CN)_3]_{0.5}[Tau]_{0.5}$ (■), $[C_2mim][C(CN)_3]_{0.5}[L\text{-}Ser]_{0.5}$ (■), $[C_2mim][C(CN)_3]_{0.5}[L\text{-}Pro]_{0.5}$ (■).

As it can be seen in Figure 4.13, the CO_2 solubility decreases as the feed pressure increases in all the prepared SILMs. As expected, IL mixtures exhibit higher CO_2 solubility compared to that of the pure $[C_2mim][C(CN)_3]$. It happens due to the addition of the amino acid-based anions, which significantly increase the CO_2 solubility. The $[C_2mim][C(CN)_3]_{0.5}[L\text{-}Ser]_{0.5}$ mixture presents the highest CO_2 solubility, while the $[C_2mim][C(CN)_3][Tau]$ mixture has the lowest CO_2 solubility, meaning that an amino acid-based anion containing the sulfonate group instead of carboxylate promotes lower CO_2 solubilities. Thus, the CO_2 solubility can be ordered as follows: $[C_2mim][C(CN)_3] < [C_2mim][C(CN)_3]_{0.5}[Tau]_{0.5} < [C_2mim][C(CN)_3]_{0.5}[Gly]_{0.5} < [C_2mim][C(CN)_3]_{0.5}[L\text{-}Ala]_{0.5} < [C_2mim][C(CN)_3]_{0.5}[L\text{-}Pro]_{0.5} < [C_2mim][C(CN)_3]_{0.5}[L\text{-}Ser]_{0.5}$.

It has been recognized that gas solubility in SILMs is related to IL molar volume.[95] Two correlations for gas solubilities in ionic liquids based on the regular solution theory, with direct application to SILMs, have been proposed. Camper *et al*.[95] developed a model that uses only the IL molar volume to predict CO_2 gas solubility and solubility selectivity. However, only imidazolium-based ILs data having non-coordinating anions such as $[DCA]^-$, $[NTf_2]^-$, $[BF_4]^-$ or $[CF_3SO_3]^-$ were used in the establishment of this correlation. On the other hand, Kilaru and Scovazzo proposed a two parameter model (the so-called Universal Model) that includes not only the IL molar volume but also the IL viscosity, covering an extended set of ionic liquid families instead of just imidazolium-based ILs.[96] The Universal Model proposed a minimal influence of IL viscosity on the gas solubility but a significant dependence on the IL molar

volume, in consistency with the Camper Model. As a result, both models predict an exponential increase in the solubility selectivity as the IL molar volume decreases.[39, 95]

Due to the presence of amino acid-based anions, higher CO_2 solubility values were obtained for the SILMs prepared with IL mixtures (between 500 and 3000 $m^3(STP)\cdot m^{-3}\cdot Pa^{-1}$). In fact, CO_2/N_2 solubility selectivity cannot be determined since it was not possible to calculate the N_2 solubilities, but considering that both models (Camper and Universal) are based on CO_2 solubility values which are much lower than those obtained in this work, probably these models can not be entirely suitable to predict the solubility selectivities of all the SILMs used in this work.

4.3.5 CO_2 separation performance

An important parameter of a membrane is its ability to separate two gases. Generally, membranes have different permeabilities for each gas, and the faster permeation of some gases relative to others provides their selectivity basis in gas separation.

The ideal permeability selectivity (or permselectivity), $\alpha_{i/j}$, is a measure of how well a membrane discerns one gas from another and can be determined by dividing the permeability of the more permeable specie *i* by the permeability of the less permeable specie *j*. The permselectivity can also be expressed as the product of solubility selectivity (S_i/S_j) and diffusivity selectivity (D_i/D_j) as follows:

$$\boldsymbol{\alpha_{i/j} = \frac{P_i}{P_j} = \left(\frac{D_i}{D_j}\right) \times \left(\frac{S_i}{S_j}\right)} \quad \textbf{(4.7)}$$

The single gas permeabilities (in Barrer units) measured at T = 318.15 K and the ideal CO_2/N_2 permselectivities through the prepared SILMs are presented in Table 4.6 and depicted in Figure 4.14 in function of the different feed pressure (kPa) tested.

Table 4.6 - Single gas permeabilities measured at T = 318.15 K and ideal CO_2/N_2 permselectivity in the prepared SILMs.

Gas Permeability (Barrer) and CO_2/N_2 permselectivity at T = 318.15 K						
SILM sample	**Feed Pressure: 2.5 kPa**					
	CO_2	STDEV	**N_2**	STDEV	**CO_2/N_2**	Error
$[C_2mim][C(CN)_3]_{0.5}$ $[Gly]_{0.5}$	392	7.41	14.5	0.40	27.0	1.25
$[C_2mim][C(CN)_3]_{0.5}$ $[L\text{-}Ala]_{0.5}$	765	19.11	16.97	0.61	45.1	2.75
$[C_2mim][C(CN)_3]_{0.5}$ $[Tau]_{0.5}$	733	14.62	10.6	0.22	69.1	2.85
$[C_2mim][C(CN)_3]_{0.5}$ $[L\text{-}Ser]_{0.5}$	338	7.25	10.0	0.27	33.9	1.65
$[C_2mim][C(CN)_3]_{0.5}$ $[L\text{-}Pro]_{0.5}$	144	3.80	7.8	0.07	18.5	0.65
$[C_2mim][C(CN_3)]$	539	8.38	25.4	0.58	21.2	0.81
	Feed Pressure: 5 kPa					
$[C_2mim][C(CN)_3]_{0.5}$ $[Gly]_{0.5}$	262	1.06	9.6	0.04	27.2	0.23
$[C_2mim][C(CN)_3]_{0.5}$ $[L\text{-}Ala]_{0.5}$	517	17.84	13.5	0.04	38.3	1.44
$[C_2mim][C(CN)_3]_{0.5}$ $[Tau]_{0.5}$	460	16.35	8.7	0.03	52.8	2.07
$[C_2mim][C(CN)_3]_{0.5}$ $[L\text{-}Ser]_{0.5}$	231	7.11	8.6	0.08	26.7	1.06
$[C_2mim][C(CN)_3]_{0.5}$ $[L\text{-}Pro]_{0.5}$	105	2.15	6.6	0.10	16.0	0.57
$[C_2mim][C(CN_3)]$	570	3.94	21.6	0.12	26.4	0.33

			Feed Pressure: 10 kPa			
$[C_2mim][C(CN)_3]_{0.5}$ $[Gly]_{0.5}$	198	1.87	9.0	0.10	21.9	0.44
$[C_2mim][C(CN)_3]_{0.5}$ $[L\text{-}Ala]_{0.5}$	351	12.67	13.4	0.12	26.2	1.19
$[C_2mim][C(CN)_3]_{0.5}$ $[Tau]_{0.5}$	297	3.65	7.9	0.04	37.6	0.65
$[C_2mim][C(CN)_3]_{0.5}$ $[L\text{-}Ser]_{0.5}$	160	3.37	8.1	0.02	19.9	0.46
$[C_2mim][C(CN)_3]_{0.5}$ $[L\text{-}Pro]_{0.5}$	75	1.85	5.9	0.04	12.7	0.39
$[C_2mim][C(CN_3)]$	561	1.94	21.1	0.19	26.6	0.34
			Feed Pressure: 25 kPa			
$[C_2mim][C(CN)_3]_{0.5}$ $[Gly]_{0.5}$	148	3.49	8.6	0.05	17.2	0.50
$[C_2mim][C(CN)_3]_{0.5}$ $[L\text{-}Ala]_{0.5}$	351	12.67	12.5	0.03	28.1	1.09
$[C_2mim][C(CN)_3]_{0.5}$ $[Tau]_{0.5}$	175	1.25	7.4	0.05	23.9	0.32
$[C_2mim][C(CN)_3]_{0.5}$ $[L\text{-}Ser]_{0.5}$	127	2.59	7.3	0.03	17.5	0.43
$[C_2mim][C(CN)_3]_{0.5}$ $[L\text{-}Pro]_{0.5}$	64	1.29	5.6	0.35	11.5	0.95
$[C_2mim][C(CN_3)]$	564	4.18	19.4	0.03	29.0	0.27
			Feed Pressure: 50 kPa			
$[C_2mim][C(CN)_3]_{0.5}$ $[Gly]_{0.5}$	123	0.90	7.3	0.11	16.8	0.37
$[C_2mim][C(CN)_3]_{0.5}$ $[L\text{-}Ala]_{0.5}$	199	3.18	13.5	0.40	14.7	0.66
$[C_2mim][C(CN)_3]_{0.5}$ $[Tau]_{0.5}$	127	1.85	7.0	0.01	18.1	0.29
$[C_2mim][C(CN)_3]_{0.5}$ $[L\text{-}Ser]_{0.5}$	103	2.07	7.1	0.03	14.5	0.35
$[C_2mim][C(CN)_3]_{0.5}$ $[L\text{-}Pro]_{0.5}$	60	0.25	5.2	0.07	11.6	0.20
$[C_2mim][C(CN_3)]$	562	5.16	19.1	0.03	29.4	0.31
			Feed Pressure: 100 kPa			
$[C_2mim][C(CN)_3]_{0.5}$ $[Gly]_{0.5}$	-	-	-	-	-	-
$[C_2mim][C(CN)_3]_{0.5}$ $[L\text{-}Ala]_{0.5}$	-	-	-	-	-	-
$[C_2mim][C(CN)_3]_{0.5}$ $[Tau]_{0.5}$	109	0.53	6.9	0.03	15.8	0.14
$[C_2mim][C(CN)_3]_{0.5}$ $[L\text{-}Ser]_{0.5}$	118	3.26	7.3	0.01	16.2	0.46
$[C_2mim][C(CN)_3]_{0.5}$ $[L\text{-}Pro]_{0.5}$	59	1.04	5.03	0.12	11.7	0.50
$[C_2mim][C(CN_3)]$	556	5.99	18.1	0.02	30.8	0.37

The errors of CO_2/N_2 permselectivities were estimated using the error propagation method:[97]

$$\Delta \boldsymbol{S} = \left|\frac{\partial S}{\boldsymbol{P_{CO_2}}}\right| \Delta \boldsymbol{P_{CO_2}} + \left|\frac{\partial S}{\boldsymbol{P_{N_2}}}\right| \Delta \boldsymbol{P_{N_2}} = \left|\frac{1}{\boldsymbol{P_{N_2}}}\right| \Delta \boldsymbol{P_{CO_2}} + \left|-\frac{\boldsymbol{P_{CO_2}}}{\boldsymbol{P_{N_2}^2}}\right| \Delta \boldsymbol{P_{N_2}} = \left(\frac{1}{\boldsymbol{P_{N_2}}}\right) \Delta \boldsymbol{P_{CO_2}} + \left(\frac{\boldsymbol{P_{CO_2}}}{\boldsymbol{P_{N_2}^2}}\right) \Delta \boldsymbol{P_{N_2}} \quad \textbf{(4.8)}$$

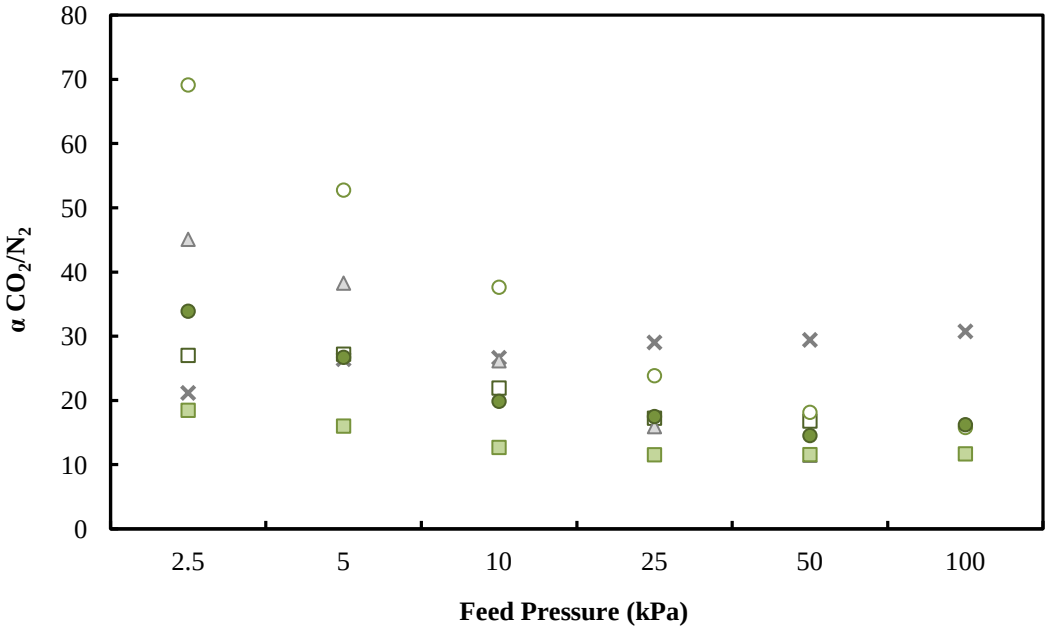

Figure 4.14 - CO_2/N_2 permselectivities through the prepared SILMs in function of feed pressure (kPa): $[C_2mim][C(CN)_3]$ (×), $[C_2mim][C(CN)_3]_{0.5}[Gly]_{0.5}$ (□), $[C_2mim][C(CN)_3]_{0.5}[L\text{-}Ala]_{0.5}$ (▲), $[C_2mim][C(CN)_3]_{0.5}[Tau]_{0.5}$ (○), $[C_2mim][C(CN)_3]_{0.5}[L\text{-}Ser]_{0.5}$ (●), $[C_2mim][C(CN)_3]_{0.5}[L\text{-}Pro]_{0.5}$ (■).

From Figure 4.14, it can be seen that the CO_2/N_2 permselectivity of the SILMs prepared with IL + IL mixtures increases as the feed pressure decreases. Conversely, CO_2/N_2 permselectivity of the pure $[C_2mim][C(CN)_3]$-based SILMs slightly increases with increasing the feed pressure.

Particularly, at 2.5 kPa of feed pressure, the CO_2/N_2 permselectivity of the prepared SILMs can be ordered as: $[C_2mim][C(CN)_3]_{0.5}[L\text{-}Pro]_{0.5}$ < $[C_2mim][C(CN)_3]$ < $[C_2mim][C(CN)_3]_{0.5}[Gly]_{0.5}$ < $[C_2mim][C(CN)_3]_{0.5}[L\text{-}Ser]_{0.5}$ < $[C_2mim][C(CN)_3]_{0.5}[L\text{-}Ala]_{0.5}$ < $[C_2mim][C(CN)_3]_{0.5}[Tau]_{0.5}$, which means that only the $[C_2mim][C(CN)_3]_{0.5}[L\text{-}Pro]_{0.5}$ mixture exhibits lower CO_2/N_2 permselectivity compared to that of the pure $[C_2mim][C(CN)_3]$. Among all the SILMs tested, the largest CO_2/N_2 permselectivity (69.1) was achieved for the $[C_2mim][C(CN)_3]_{0.5}[Tau]_{0.5}$ mixture. However, the $[C_2mim][C(CN)_3]_{0.5}[L\text{-}Ala]_{0.5}$ mixture presents higher CO_2 permeability compared to that of $[C_2mim][C(CN)_3]_{0.5}[Tau]_{0.5}$ mixture. Taking into account the results obtained for both CO_2 diffusivities and solubilities, the $[C_2mim][C(CN)_3]_{0.5}[L\text{-}Ala]_{0.5}$ mixture shows higher CO_2 solubility, but presents lower CO_2 diffusivity compared to that of $[C_2mim][C(CN)_3]_{0.5}[Tau]_{0.5}$. Looking at the ratio between the obtained values, the difference between both CO_2 solubility values is 25% while the difference among the CO_2 diffusivity values is about 20 %. Thus, it can be conclude that the CO_2 solubility is, in this case, the parameter that contributes more to the highest CO_2 permeability of the $[C_2mim][C(CN)_3]_{0.5}[L\text{-}Ala]_{0.5}$ mixture.

In Figure 4.15, the CO_2/N_2 permselectivity values are plotted against CO_2 permeabilities on the so-called Robeson plot.[98] This type of plots is commonly used to evaluate the performance of membrane materials given a particular gas separation, illustrating the progress in membrane science. These plots display the tradeoff line between permeability and selectivity for gas separation using polymeric membranes. Also referred as ‘‘upper bound’’, this tradeoff relationship shows that the permselectivity for a gas pair of interest ($a_{i/j}$) changes inversely with the permeability of the more permeable species (P_i), as described by Robeson:[98]

$$\boldsymbol{P_i = k a_{i/j}^{n}} \qquad \textbf{(4.9)}$$

where the *n* is the slope and *k* is the front factor. Below this line, virtually all the data points exist. Since the performance of the vast majority of membranes falls below the upper bound, which is based on large amounts of experimental data for each separation, data points above this line can be considered as an improvement over the current membrane state of the art.

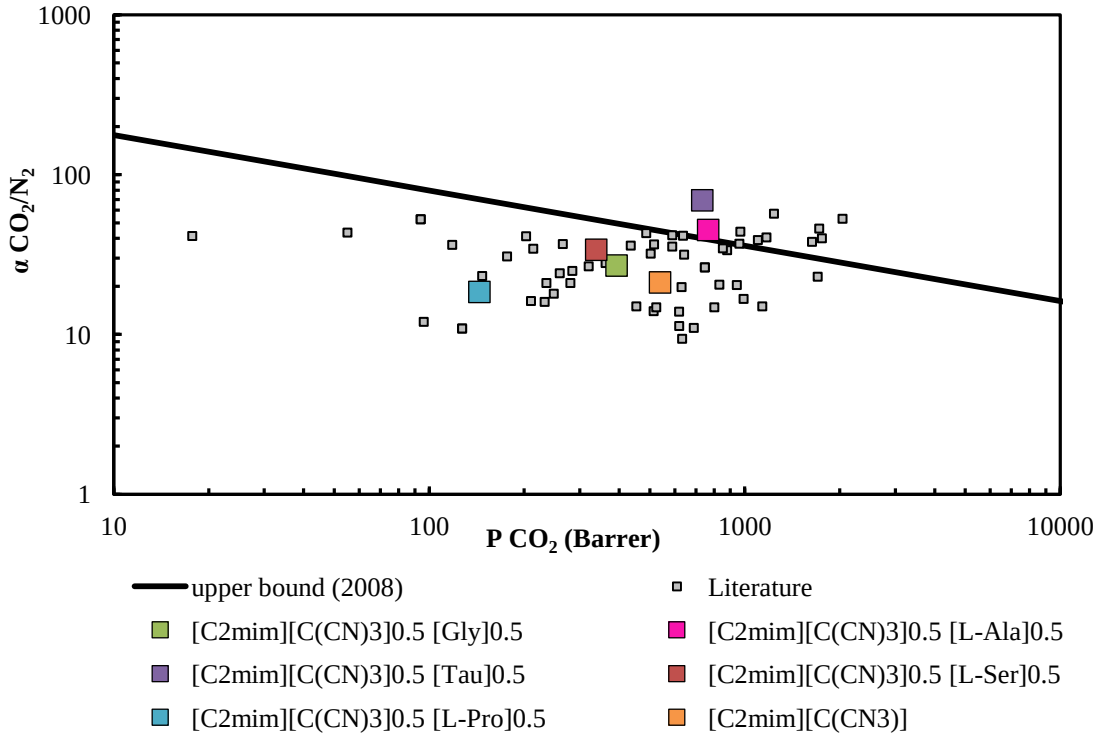

Figure 4.15 - CO_2 separation performance of the SILMs studied at *T* = 318.15 K and 2.5 of feed pressure potted on CO_2/N_2 Robeson plot. Data are plotted on a log–log scale and the upper bound is adapted from Robeson[98] Literature data reported for other supported ionic liquid membranes are also plotted.[7, 45, 47, 50-54, 57, 89, 99]

It should be noted that the literature values illustrated in Figure 4.15 were obtained at different temperatures (between 293 and 303 K) and gas feed pressures (between 85 and 200 kPa), while the values of this work were determined at *T* = 318.15 K and 2.5 of feed pressure. These values were selected because higher CO_2 permeabilities were obtained at lower feed

pressures where in fact the CO_2-facilitated transport is more pronounced. Although a direct comparison cannot be exactly made, it can be observed from Figure 4.15 that both the $[C_2mim][C(CN)_3]_{0.5}[L\text{-}Ala]_{0.5}$ and $[C_2mim][C(CN)_3]_{0.5}[Tau]_{0.5}$-based SILMs are above the upper bond, meaning that, though the results were obtained under conditions of low feed pressure, these IL mixtures are potential candidates as liquid phases for CO_2 separation**.** Nevertheless, the study of temperature effect is essential in order to improve the achieved results and obtain the same trends at higher feed pressures.

5

Final Remarks

5.1 Conclusions and Future Work

The main goal of this work was to evaluate the performance of IL + IL mixtures as new liquid phases to prepare facilitated SILMs for flue gas separation (CO_2/N_2). For this purpose, five AA-based ILs: [C_2mim][Gly], [C_2mim][L-Ala], [C_2mim][Tau], [C_2mim][L-Ser] and [C_2mim][L-Pro], were synthesized via a two-step anion exchange reaction and characterized by ^{1}H and ^{13}C NMR. AAILs were selected, so that CO_2 facilitated transport could be attained, and mixed with [C_2mim][$C(CN)_3$], a low viscous IL. The thermogravimetric analysis (TGA) of the pure ILs and their mixtures was also measured in order to establish the degradation temperature of these liquid phases and thus their upper working temperature limit. The study of thermophysical properties namely, density, viscosity and refractive index, of all the pure ILs and their mixtures as well as gas permeation properties (permeability, diffusivity and solubility) of SILMs was also performed and trends were evaluated.

From the study of thermophysical properties, it can be concluded that the presence of [C_2mim][$C(CN)_3$] in the IL mixtures dramatically decreases the viscosity of AAILs, as expected. It was also observed that [C_2mim][Gly] exhibits the lowest viscosity and molar volume, while [C_2mim][L-Pro] has the highest viscosity and molar volume. This trend was also observed for the IL mixtures. Overall, density, viscosity and refractive index values of pure AAILs were in a good agreement with those reported in literature.

In what concerns the gas permeation properties, the results obtained showed that CO_2 permeability decreases with increasing IL viscosity, with the exception of the [C_2mim][$C(CN)_3$]$_{0.5}$[Gly]$_{0.5}$ mixture. Conversely to what would be expected, diffusivity does not present an inversely proportional relation with IL viscosity, with the exception of [C_2mim][$C(CN)_3$]$_{0.5}$[L-Ser]$_{0.5}$ and [C_2mim][$C(CN)_3$]$_{0.5}$[L-Pro]$_{0.5}$ mixtures and the pure [C_2mim][$C(CN)_3$]. Moreover, IL mixtures displayed an dramatically increase in CO_2 solubility compared to the pure [C_2mim][$C(CN)_3$] due to the addition of the amino acid-based anions. Besides physical solubility, the presence of amine and carboxylic acid groups also provides a chemical solubility mechanism. Although the best CO_2/N_2 separation performance was obtained at low feed pressure, two IL mixtures, [C_2mim][$C(CN)_3$]$_{0.5}$[L-Ala]$_{0.5}$ and [C_2mim][$C(CN)_3$]$_{0.5}$[Tau]$_{0.5}$, presented CO_2/N_2 permselectivities above the Robeson upper bond, showing that mixing ionic liquids is a promising strategy for CO_2/N_2 separation processes, since the IL properties can be tuned by mixing anions with different chemical character.

As future work, in order to fully realize the potential of these IL mixtures for CO_2/N_2 separation, the prepared SILMs need to be evaluated at higher temperature ($\simeq$100 °C). At these temperature conditions, probably the same behaviour can be obtained under higher feed pressures. Another important issue is the chemical and integrity stability study of the most

promising SILMs via long-term membrane module testing at the desired operating temperature and pressure conditions.

6

References

1. Torralba-Calleja, E.; Skinner, J.; Guti; rrez-Tauste, D., CO2 Capture in Ionic Liquids: A Review of Solubilities and Experimental Methods. *Journal of Chemistry* **2013,** 2013, 16.
2. Songolzadeh, M.; Soleimani, M.; Takht Ravanchi, M.; Songolzadeh, R., Carbon Dioxide Separation from Flue Gases: A Technological Review Emphasizing Reduction in Greenhouse Gas Emissions. *The Scientific World Journal* **2014,** 2014, 34.
3. Davidson, R. *Pre-combustion capture of CO2 in IGCC plants*; 2011.
4. http://www.globalccsinstitute.com/content/how-ccs-works-capture (1 September),
5. de Coninck, H.; Stephens, J. C.; Metz, B., Global learning on carbon capture and storage: A call for strong international cooperation on CCS demonstration. *Energy Policy* **2009,** 37, (6), 2161-2165.
6. MacDowell, N.; Florin, N.; Buchard, A.; Hallett, J.; Galindo, A.; Jackson, G.; Adjiman, C. S.; Williams, C. K.; Shah, N.; Fennell, P., An overview of CO2 capture technologies. *Energy & Environmental Science* **2010,** 3, (11), 1645-1669.
7. Tome, L. C.; Patinha, D. J. S.; Freire, C. S. R.; Rebelo, L. P. N.; Marrucho, I. M., CO2 separation applying ionic liquid mixtures: the effect of mixing different anions on gas permeation through supported ionic liquid membranes. *RSC Advances* **2013,** 3, (30), 12220-12229.
8. C. Wang, X. L., X. Zhu, G. Cui, D.-e. Jiang, D. Deng, H. Li and S. Dai, The strategies for improving carbon dioxide chemisorption by functionalized ionic liquids. *RSC Advances* **2013,** 3, 15518-15527.
9. Barbieri G., B. A., Scura F., Drioli E., CO2 Separation by Membrane Technologies: Applications and Potentialities.
10. Brunetti, A.; Scura, F.; Barbieri, G.; Drioli, E., Membrane technologies for CO 2 separation. *Journal of Membrane Science* **2010,** 359, (1), 115-125.
11. Phair, J. W.; Badwal, S. P. S., Materials for separation membranes in hydrogen and oxygen production and future power generation. *Science and Technology of Advanced Materials* **2006,** 7, (8), 792-805.
12. Oyama, S. T.; Stagg-Williams, S. M., *Inorganic, Polymeric and Composite Membranes: Structure, Function and Other Correlations*. Elsevier: 2011.
13. Mohshim, D. F.; Mukhtar, H. b.; Man, Z.; Nasir, R., Latest Development on Membrane Fabrication for Natural Gas Purification: A Review. *Journal of Engineering* **2013,** 2013, 7.
14. Krull, F. F.; Fritzmann, C.; Melin, T., Liquid membranes for gas/vapor separations. *Journal of Membrane Science* **2008,** 325, (2), 509-519.
15. Kocherginsky, N. M.; Yang, Q.; Seelam, L., Recent advances in supported liquid membrane technology. *Separation and Purification Technology* **2007,** 53, (2), 171-177.
16. Araki, T.; Tsukube, H., *Liquid Membranes: Chemical Applications*. Taylor & Francis: 1990.
17. Ramdin, M.; de Loos, T. W.; Vlugt, T. J. H., State-of-the-Art of CO2 Capture with Ionic Liquids. *Industrial & Engineering Chemistry Research* **2012,** 51, (24), 8149-8177.
18. Scovazzo, P.; Kieft, J.; Finan, D. A.; Koval, C.; DuBois, D.; Noble, R., Gas separations using non-hexafluorophosphate [PF6]− anion supported ionic liquid membranes. *Journal of Membrane Science* **2004,** 238, (1–2), 57-63.
19. Neves, L. A.; Crespo, J. G.; Coelhoso, I. M., Gas permeation studies in supported ionic liquid membranes. *Journal of Membrane Science* **2010,** 357, (1–2), 160-170.
20. Luis, P.; Van Gerven, T.; Van der Bruggen, B., Recent developments in membrane-based technologies for CO2 capture. *Progress in Energy and Combustion Science* **2012,** 38, (3), 419-448.
21. Wasserscheid, P.; Keim, W., Ionic Liquids—New "Solutions" for Transition Metal Catalysis. *Angewandte Chemie International Edition* **2000,** 39, (21), 3772-3789.
22. Tavares, A. P. M.; Rodríguez, O.; Macedo, E. A., *New Generations of Ionic Liquids Applied to Enzymatic Biocatalysis*. 2013.
23. Zhang S., L. X., Zhou Q., Li X., Zhang X., Li S., *Ionic Liquids: Physicochemical Properties*. 2009.

24. Zhang, S.; Sun, N.; He, X.; Lu, X.; Zhang, X., Physical Properties of Ionic Liquids: Database and Evaluation. *Journal of Physical and Chemical Reference Data* **2006,** 35, (4), 1475-1517.
25. Earle, M. J.; Esperanca, J. M. S. S.; Gilea, M. A.; Canongia Lopes, J. N.; Rebelo, L. P. N.; Magee, J. W.; Seddon, K. R.; Widegren, J. A., The distillation and volatility of ionic liquids. *Nature* **2006,** 439, (7078), 831-834.
26. Anderson, J. L.; Ding, R.; Ellern, A.; Armstrong, D. W., Structure and Properties of High Stability Geminal Dicationic Ionic Liquids. *Journal of the American Chemical Society* **2004,** 127, (2), 593-604.
27. S., H., *Applications of Ionic Liquids in Science and Technology*. InTech: 2011.
28. MacFarlane, D. R.; Tachikawa, N.; Forsyth, M.; Pringle, J. M.; Howlett, P. C.; Elliott, G. D.; Davis, J. H.; Watanabe, M.; Simon, P.; Angell, C. A., Energy applications of ionic liquids. *Energy & Environmental Science* **2014,** 7, (1), 232-250.
29. Malik, M. A.; Hashim, M. A.; Nabi, F., Ionic liquids in supported liquid membrane technology. *Chemical Engineering Journal* **2011,** 171, (1), 242-254.
30. Zhang, X.; Zhang, X.; Dong, H.; Zhao, Z.; Zhang, S.; Huang, Y., Carbon capture with ionic liquids: overview and progress. *Energy & Environmental Science* **2012,** 5, (5), 6668-6681.
31. Hu, Y.-F.; Liu, Z.-C.; Xu, C.-M.; Zhang, X.-M., The molecular characteristics dominating the solubility of gases in ionic liquids. *Chemical Society Reviews* **2011,** 40, (7), 3802-3823.
32. Shannon, M. S.; Bara, J. E., Reactive and Reversible Ionic Liquids for CO2 Capture and Acid Gas Removal. *Separation Science and Technology* **2011,** 47, (2), 178-188.
33. Sistla, Y. S.; Jain, L.; Khanna, A., Validation and prediction of solubility parameters of ionic liquids for CO2 capture. *Separation and Purification Technology* **2012,** 97, (0), 51-64.
34. Anderson, J. L.; Dixon, J. K.; Brennecke, J. F., Solubility of CO2, CH4, C2H6, C2H4, O2, and N2 in 1-Hexyl-3-methylpyridinium Bis(trifluoromethylsulfonyl)imide: Comparison to Other Ionic Liquids. *Accounts of Chemical Research* **2007,** 40, (11), 1208-1216.
35. Anthony, J. L.; Anderson, J. L.; Maginn, E. J.; Brennecke, J. F., Anion Effects on Gas Solubility in Ionic Liquids. *The Journal of Physical Chemistry B* **2005,** 109, (13), 6366-6374.
36. Cadena, C.; Anthony, J. L.; Shah, J. K.; Morrow, T. I.; Brennecke, J. F.; Maginn, E. J., Why Is CO2 So Soluble in Imidazolium-Based Ionic Liquids? *Journal of the American Chemical Society* **2004,** 126, (16), 5300-5308.
37. Muldoon, M. J.; Aki, S. N. V. K.; Anderson, J. L.; Dixon, J. K.; Brennecke, J. F., Improving Carbon Dioxide Solubility in Ionic Liquids. *The Journal of Physical Chemistry B* **2007,** 111, (30), 9001-9009.
38. Tome, L. C.; Florindo, C.; Freire, C. S. R.; Rebelo, L. P. N.; Marrucho, I. M., Playing with ionic liquid mixtures to design engineered CO2 separation membranes. *Physical Chemistry Chemical Physics* **2014,** 16, (32), 17172-17182.
39. Scovazzo, P., Determination of the upper limits, benchmarks, and critical properties for gas separations using stabilized room temperature ionic liquid membranes (SILMs) for the purpose of guiding future research. *Journal of Membrane Science* **2009,** 343, (1-2), 199-211.
40. Bernardo, P.; Drioli, E.; Golemme, G., Membrane Gas Separation: A Review/State of the Art. *Industrial & Engineering Chemistry Research* **2009,** 48, (10), 4638-4663.
41. Baltus, R. E.; Counce, R. M.; Culbertson, B. H.; Luo, H.; DePaoli, D. W.; Dai, S.; Duckworth, D. C., Examination of the Potential of Ionic Liquids for Gas Separations. *Separation Science and Technology* **2005,** 40, (1-3), 525-541.
42. Luis, P.; Neves, L. A.; Afonso, C. A. M.; Coelhoso, I. M.; Crespo, J. G.; Garea, A.; Irabien, A., Facilitated transport of CO2 and SO2 through Supported Ionic Liquid Membranes (SILMs). *Desalination* **2009,** 245, (1–3), 485-493.
43. Morgan, D.; Ferguson, L.; Scovazzo, P., Diffusivities of Gases in Room-Temperature Ionic Liquids: Data and Correlations Obtained Using a Lag-Time Technique. *Industrial & Engineering Chemistry Research* **2005,** 44, (13), 4815-4823.
44. Neves, L. A.; Nemestóthy, N.; Alves, V. D.; Cserjési, P.; Bélafi-Bakó, K.; Coelhoso, I. M., Separation of biohydrogen by supported ionic liquid membranes. *Desalination* **2009,** 240, (1–3), 311-315.

45. Santos, E.; Albo, J.; Irabien, A., Acetate based Supported Ionic Liquid Membranes (SILMs) for CO2 separation: Influence of the temperature. *Journal of Membrane Science* **2014,** 452, (0), 277-283.
46. Hojniak, S. D.; Khan, A. L.; Hollóczki, O.; Kirchner, B.; Vankelecom, I. F.; Dehaen, W.; Binnemans, K., Separation of Carbon Dioxide from Nitrogen or Methane by Supported Ionic Liquid Membranes (SILMs): Influence of the Cation Charge of the Ionic Liquid. *The Journal of Physical Chemistry B* **2013,** 117, (48), 15131-15140.
47. Mahurin, S. M.; Hillesheim, P. C.; Yeary, J. S.; Jiang, D.-e.; Dai, S., High CO2 solubility, permeability and selectivity in ionic liquids with the tetracyanoborate anion. *RSC Advances* **2012,** 2, (31), 11813-11819.
48. Tome, L. C.; Aboudzadeh, M. A.; Rebelo, L. P. N.; Freire, C. S. R.; Mecerreyes, D.; Marrucho, I. M., Polymeric ionic liquids with mixtures of counter-anions: a new straightforward strategy for designing pyrrolidinium-based CO2 separation membranes. *Journal of Materials Chemistry A* **2013,** 1, (35), 10403-10411.
49. Hou, Y.; Baltus, R. E., Experimental Measurement of the Solubility and Diffusivity of CO2 in Room-Temperature Ionic Liquids Using a Transient Thin-Liquid-Film Method. *Industrial & Engineering Chemistry Research* **2007,** 46, (24), 8166-8175.
50. Condemarin, R.; Scovazzo, P., Gas permeabilities, solubilities, diffusivities, and diffusivity correlations for ammonium-based room temperature ionic liquids with comparison to imidazolium and phosphonium RTIL data. *Chemical Engineering Journal* **2009,** 147, (1), 51-57.
51. Cserjési, P.; Nemestóthy, N.; Bélafi-Bakó, K., Gas separation properties of supported liquid membranes prepared with unconventional ionic liquids. *Journal of Membrane Science* **2010,** 349, (1–2), 6-11.
52. Ferguson, L.; Scovazzo, P., Solubility, Diffusivity, and Permeability of Gases in Phosphonium-Based Room Temperature Ionic Liquids: Data and Correlations. *Industrial & Engineering Chemistry Research* **2007,** 46, (4), 1369-1374.
53. Tomé, L. C.; Patinha, D. J. S.; Ferreira, R.; Garcia, H.; Silva Pereira, C.; Freire, C. S. R.; Rebelo, L. P. N.; Marrucho, I. M., Cholinium-based Supported Ionic Liquid Membranes: A Sustainable Route for Carbon Dioxide Separation. *ChemSusChem* **2014,** 7, (1), 110-113.
54. Bara, J. E.; Gabriel, C. J.; Carlisle, T. K.; Camper, D. E.; Finotello, A.; Gin, D. L.; Noble, R. D., Gas separations in fluoroalkyl-functionalized room-temperature ionic liquids using supported liquid membranes. *Chemical Engineering Journal* **2009,** 147, (1), 43-50.
55. Bara, J. E.; Gabriel, C. J.; Lessmann, S.; Carlisle, T. K.; Finotello, A.; Gin, D. L.; Noble, R. D., Enhanced CO2 Separation Selectivity in Oligo(ethylene glycol) Functionalized Room-Temperature Ionic Liquids. *Industrial & Engineering Chemistry Research* **2007,** 46, (16), 5380-5386.
56. Mahurin, S. M.; Lee, J. S.; Baker, G. A.; Luo, H.; Dai, S., Performance of nitrile-containing anions in task-specific ionic liquids for improved CO2/N2 separation. *Journal of Membrane Science* **2010,** 353, (1–2), 177-183.
57. Mahurin, S. M.; Yeary, J. S.; Baker, S. N.; Jiang, D.-e.; Dai, S.; Baker, G. A., Ring-opened heterocycles: Promising ionic liquids for gas separation and capture. *Journal of Membrane Science* **2012,** 401–402, (0), 61-67.
58. Ramasubramanian, K.; Zhao, Y.; Winston Ho, W. S., CO2 capture and H2 purification: Prospects for CO2-selective membrane processes. *AIChE Journal* **2013,** 59, (4), 1033-1045.
59. Xing, H.; Yan, Y.; Yang, Q.; Bao, Z.; Su, B.; Yang, Y.; Ren, Q., Effect of Tethering Strategies on the Surface Structure of Amine-Functionalized Ionic Liquids: Inspiration on the CO2 Capture. *The Journal of Physical Chemistry C* **2013,** 117, (31), 16012-16021.
60. Bates, E. D.; Mayton, R. D.; Ntai, I.; Davis, J. H., CO2 Capture by a Task-Specific Ionic Liquid. *Journal of the American Chemical Society* **2002,** 124, (6), 926-927.
61. Fukumoto, K.; Yoshizawa, M.; Ohno, H., Room Temperature Ionic Liquids from 20 Natural Amino Acids. *Journal of the American Chemical Society* **2005,** 127, (8), 2398-2399.
62. Goodrich, B. F.; de la Fuente, J. C.; Gurkan, B. E.; Lopez, Z. K.; Price, E. A.; Huang, Y.; Brennecke, J. F., Effect of Water and Temperature on Absorption of CO2 by Amine-

Functionalized Anion-Tethered Ionic Liquids. *The Journal of Physical Chemistry B* **2011,** 115, (29), 9140-9150.
63. Goodrich, B. F.; de la Fuente, J. C.; Gurkan, B. E.; Zadigian, D. J.; Price, E. A.; Huang, Y.; Brennecke, J. F., Experimental Measurements of Amine-Functionalized Anion-Tethered Ionic Liquids with Carbon Dioxide. *Industrial & Engineering Chemistry Research* **2010,** 50, (1), 111-118.
64. Zhang, J.; Zhang, S.; Dong, K.; Zhang, Y.; Shen, Y.; Lv, X., Supported Absorption of CO2 by Tetrabutylphosphonium Amino Acid Ionic Liquids. *Chemistry – A European Journal* **2006,** 12, (15), 4021-4026.
65. Ohno, H.; Fukumoto, K., Amino Acid Ionic Liquids. *Accounts of Chemical Research* **2007,** 40, (11), 1122-1129.
66. Tao, G.-h.; He, L.; Sun, N.; Kou, Y., New generation ionic liquids: cations derived from amino acids. *Chemical Communications* **2005**, (28), 3562-3564.
67. Gurkan, B. E.; de la Fuente, J. C.; Mindrup, E. M.; Ficke, L. E.; Goodrich, B. F.; Price, E. A.; Schneider, W. F.; Brennecke, J. F., Equimolar CO2 Absorption by Anion-Functionalized Ionic Liquids. *Journal of the American Chemical Society* **2010,** 132, (7), 2116-2117.
68. Hanioka, S.; Maruyama, T.; Sotani, T.; Teramoto, M.; Matsuyama, H.; Nakashima, K.; Hanaki, M.; Kubota, F.; Goto, M., CO2 separation facilitated by task-specific ionic liquids using a supported liquid membrane. *Journal of Membrane Science* **2008,** 314, (1–2), 1-4.
69. Myers, C.; Pennline, H.; Luebke, D.; Ilconich, J.; Dixon, J. K.; Maginn, E. J.; Brennecke, J. F., High temperature separation of carbon dioxide/hydrogen mixtures using facilitated supported ionic liquid membranes. *Journal of Membrane Science* **2008,** 322, (1), 28-31.
70. Kasahara, S.; Kamio, E.; Ishigami, T.; Matsuyama, H., Amino acid ionic liquid-based facilitated transport membranes for CO2 separation. *Chemical Communications* **2012,** 48, (55), 6903-6905.
71. Wang, X.; Akhmedov, N. G.; Duan, Y.; Luebke, D.; Li, B., Immobilization of amino acid ionic liquids into nanoporous microspheres as robust sorbents for CO2 capture. *Journal of Materials Chemistry A* **2013,** 1, (9), 2978-2982.
72. Niedermeyer, H.; Hallett, J. P.; Villar-Garcia, I. J.; Hunt, P. A.; Welton, T., Mixtures of ionic liquids. *Chemical Society Reviews* **2012,** 41, (23), 7780-7802.
73. Annat, G.; Forsyth, M.; MacFarlane, D. R., Ionic Liquid Mixtures—Variations in Physical Properties and Their Origins in Molecular Structure. *The Journal of Physical Chemistry B* **2012,** 116, (28), 8251-8258.
74. Finotello, A.; Bara, J. E.; Narayan, S.; Camper, D.; Noble, R. D., Ideal Gas Solubilities and Solubility Selectivities in a Binary Mixture of Room-Temperature Ionic Liquids. *The Journal of Physical Chemistry B* **2008,** 112, (8), 2335-2339.
75. Hasib-ur-Rahman, M.; Siaj, M.; Larachi, F., Ionic liquids for CO2 capture—Development and progress. *Chemical Engineering and Processing: Process Intensification* **2010,** 49, (4), 313-322.
76. Neves, C. M. S. S.; Kurnia, K. A.; Coutinho, J. A. P.; Marrucho, I. M.; Lopes, J. N. C.; Freire, M. G.; Rebelo, L. P. N., Systematic Study of the Thermophysical Properties of Imidazolium-Based Ionic Liquids with Cyano-Functionalized Anions. *The Journal of Physical Chemistry B* **2013,** 117, (35), 10271-10283.
77. Dai, S.; Luo, H.; Lee, J. S., Carbon Films Produced from Ionic Liquid Carbon Precursors. In Google Patents: 2011.
78. Oliveira, F. S.; Freire, M. G.; Carvalho, P. J.; Coutinho, J. o. A. P.; Lopes, J. N. C.; Rebelo, L. s. P. N.; Marrucho, I. M., Structural and Positional Isomerism Influence in the Physical Properties of Pyridinium NTf2-Based Ionic Liquids: Pure and Water-Saturated Mixtures†. *Journal of Chemical & Engineering Data* **2010,** 55, (10), 4514-4520.
79. Köddermann, T.; Ludwig, R.; Paschek, D., On the Validity of Stokes–Einstein and Stokes–Einstein–Debye Relations in Ionic Liquids and Ionic-Liquid Mixtures. *ChemPhysChem* **2008,** 9, (13), 1851-1858.
80. Muhammad, A.; Abdul Mutalib, M. I.; Wilfred, C. D.; Murugesan, T.; Shafeeq, A., Thermophysical properties of 1-hexyl-3-methyl imidazolium based ionic liquids with

tetrafluoroborate, hexafluorophosphate and bis(trifluoromethylsulfonyl)imide anions. *The Journal of Chemical Thermodynamics* **2008,** 40, (9), 1433-1438.
81. Muhammad, N.; Man, Z. B.; Bustam, M. A.; Mutalib, M. I. A.; Wilfred, C. D.; Rafiq, S., Synthesis and Thermophysical Properties of Low Viscosity Amino Acid-Based Ionic Liquids. *Journal of Chemical & Engineering Data* **2011,** 56, (7), 3157-3162.
82. Tao, D.-J.; Cheng, Z.; Chen, F.-F.; Li, Z.-M.; Hu, N.; Chen, X.-S., Synthesis and Thermophysical Properties of Biocompatible Cholinium-Based Amino Acid Ionic Liquids. *Journal of Chemical & Engineering Data* **2013,** 58, (6), 1542-1548.
83. Tariq, M.; Forte, P. A. S.; Gomes, M. F. C.; Lopes, J. N. C.; Rebelo, L. P. N., Densities and refractive indices of imidazolium- and phosphonium-based ionic liquids: Effect of temperature, alkyl chain length, and anion. *The Journal of Chemical Thermodynamics* **2009,** 41, (6), 790-798.
84. Mahajan, A. R.; Mirgane, S. R., Excess Molar Volumes and Viscosities for the Binary Mixtures of n-Octane, n-Decane, n-Dodecane, and n-Tetradecane with Octan-2-ol at 298.15K. *Journal of Thermodynamics* **2013,** 2013, 11.
85. Lide, D. R.; Kehiaian, H. V., *CRC Handbook of Thermophysical and Thermochemical Data*. Taylor & Francis: 1994.
86. Santosh, M. S.; Bhat, D. K., Molar volume, compressibility and excess properties of glycylglycine in aqueous NiCl2 solutions. *Fluid Phase Equilibria* **2010,** 299, (1), 102-108.
87. X.-X. Li, G. Z., D.-S. Liu and W.-W. Cao, Excess Molar Volume and Viscosity Deviation for the Binary Mixture of Diethylene Glycol Monobutyl Ether + Water from (293.15 to 333.15) K at Atmospheric Pressure. *J. Chem. Eng. Data* **2009,** 54, 890-892.
88. Wijmans, J. G.; Baker, R. W., The solution-diffusion model: a review. *Journal of Membrane Science* **1995,** 107, (1–2), 1-21.
89. Hillesheim, P. C.; Mahurin, S. M.; Fulvio, P. F.; Yeary, J. S.; Oyola, Y.; Jiang, D.-e.; Dai, S., Synthesis and Characterization of Thiazolium-Based Room Temperature Ionic Liquids for Gas Separations. *Industrial & Engineering Chemistry Research* **2012,** 51, (35), 11530-11537.
90. Mahurin, S. M.; Dai, T.; Yeary, J. S.; Luo, H.; Dai, S., Benzyl-Functionalized Room Temperature Ionic Liquids for CO2/N2 Separation. *Industrial & Engineering Chemistry Research* **2011,** 50, (24), 14061-14069.
91. Santos, E.; Albo, J.; Daniel, C. I.; Portugal, C. A. M.; Crespo, J. G.; Irabien, A., Permeability modulation of Supported Magnetic Ionic Liquid Membranes (SMILMs) by an external magnetic field. *Journal of Membrane Science* **2013,** 430, (0), 56-61.
92. Kasahara, S.; Kamio, E.; Otani, A.; Matsuyama, H., Fundamental Investigation of the Factors Controlling the CO2 Permeability of Facilitated Transport Membranes Containing Amine-Functionalized Task-Specific Ionic Liquids. *Industrial & Engineering Chemistry Research* **2014,** 53, (6), 2422-2431.
93. Moganty, S. S.; Baltus, R. E., Diffusivity of Carbon Dioxide in Room-Temperature Ionic Liquids. *Industrial & Engineering Chemistry Research* **2010,** 49, (19), 9370-9376.
94. Ghosal, K.; Freeman, B. D., Gas separation using polymer membranes: an overview. *Polymers for Advanced Technologies* **1994,** 5, (11), 673-697.
95. Camper, D.; Bara, J.; Koval, C.; Noble, R., Bulk-Fluid Solubility and Membrane Feasibility of Rmim-Based Room-Temperature Ionic Liquids. *Industrial & Engineering Chemistry Research* **2006,** 45, (18), 6279-6283.
96. Kilaru, P. K.; Scovazzo, P., Correlations of Low-Pressure Carbon Dioxide and Hydrocarbon Solubilities in Imidazolium-, Phosphonium-, and Ammonium-Based Room-Temperature Ionic Liquids. Part 2. Using Activation Energy of Viscosity. *Industrial & Engineering Chemistry Research* **2007,** 47, (3), 910-919.
97. Bevington, P. R.; Robinson, D. K., *Data reduction and error analysis for the physical sciences*. McGraw-Hill: 2003.
98. Robeson, L. M., The upper bound revisited. *Journal of Membrane Science* **2008,** 320, (1–2), 390-400.

99. Scovazzo, P.; Havard, D.; McShea, M.; Mixon, S.; Morgan, D., Long-term, continuous mixed-gas dry fed CO2/CH4 and CO2/N2 separation performance and selectivities for room temperature ionic liquid membranes. *Journal of Membrane Science* **2009,** 327, (1–2), 41-48.

7

Appendixes

7.1 Appendix 1

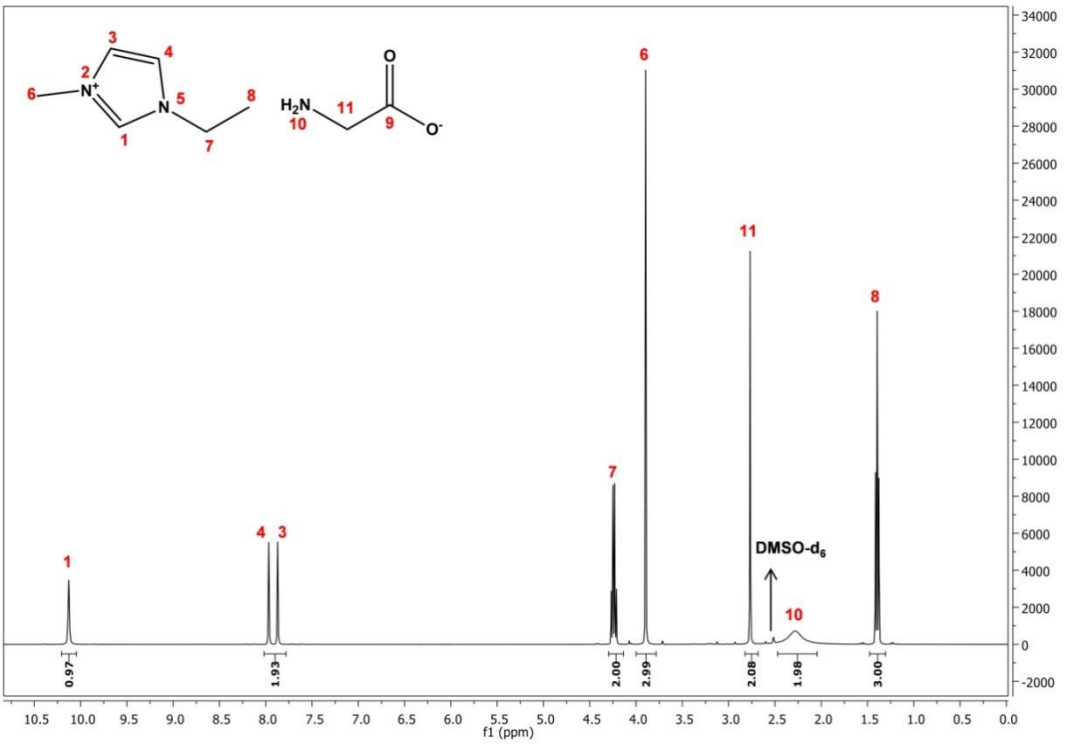

Figure 7.1 - ^{1}H-NMR spectrum of [C_2mim][Gly] in DMSO-d6.

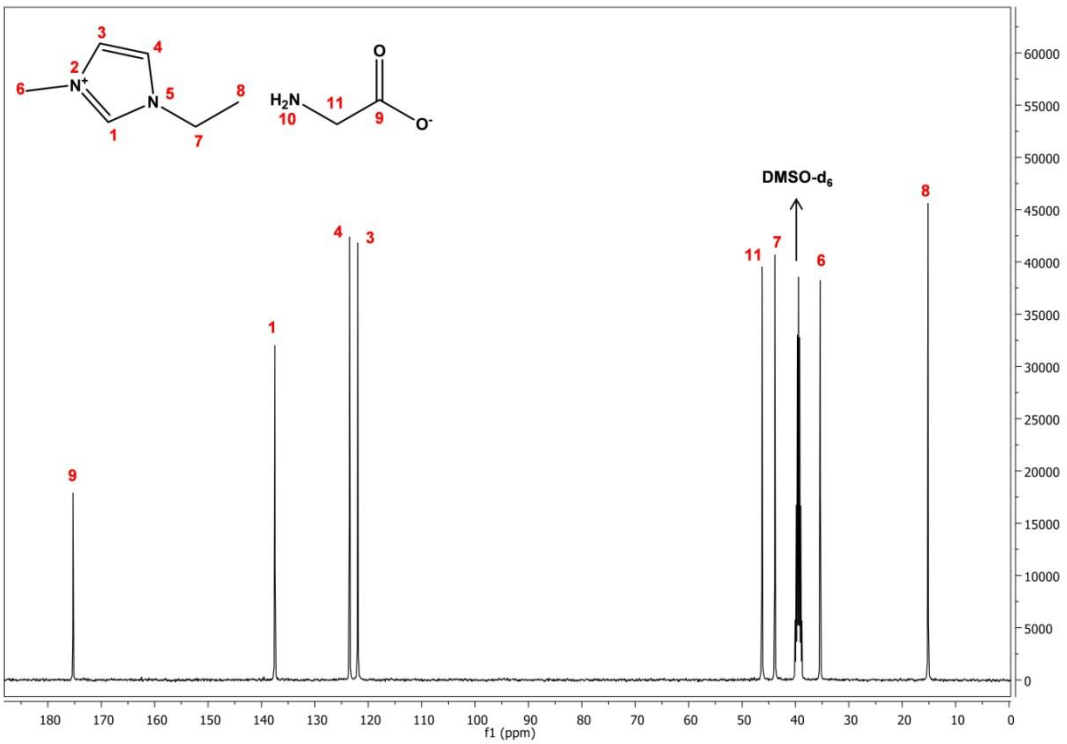

Figure 7.2 - ^{13}C-NMR spectrum of [C_2mim][Gly] in DMSO-d6.

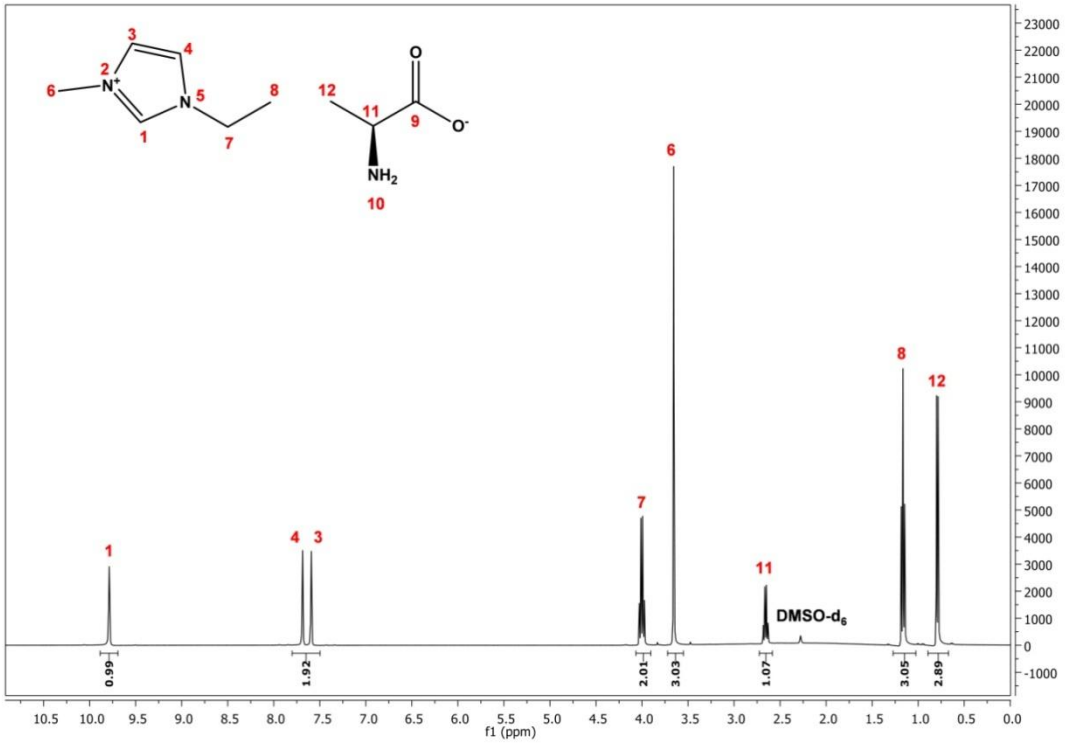

Figure 7.3 - ^{1}H-NMR spectrum of [C_2mim][L-Ala] in DMSO-d6.

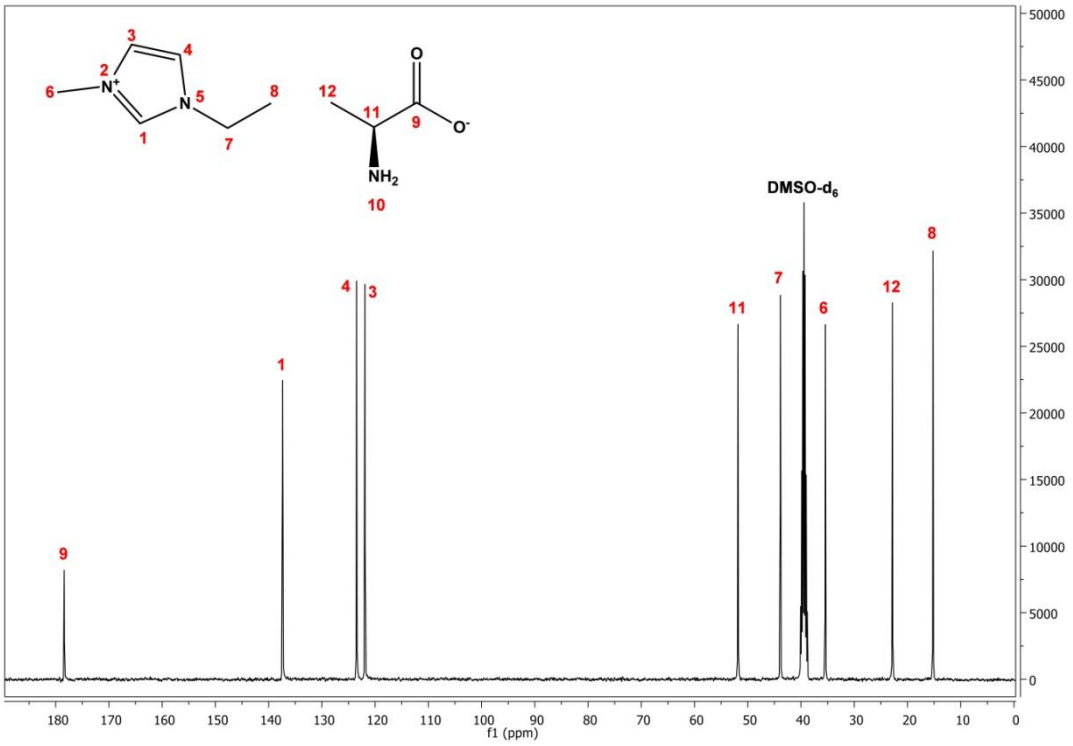

Figure 7.4 - ^{13}C-NMR spectrum of [C_2mim][L-Ala] in DMSO-d6.

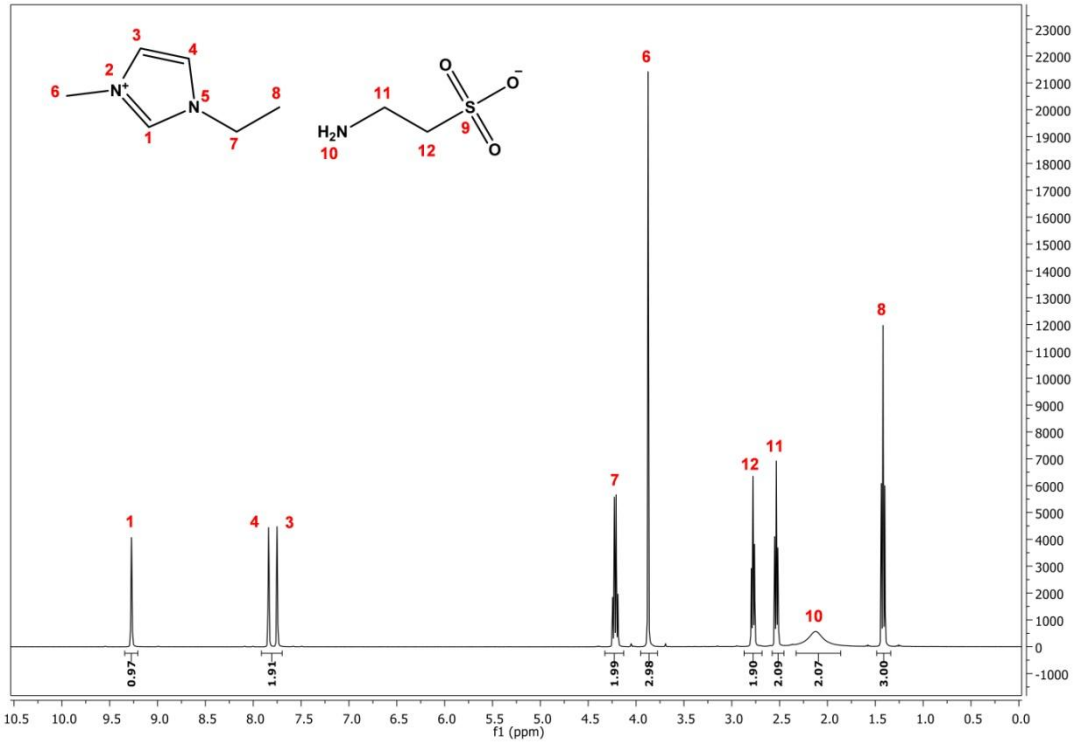

Figure 7.5 - ^{1}H-NMR spectrum of [C_2mim][Tau] in DMSO-d6.

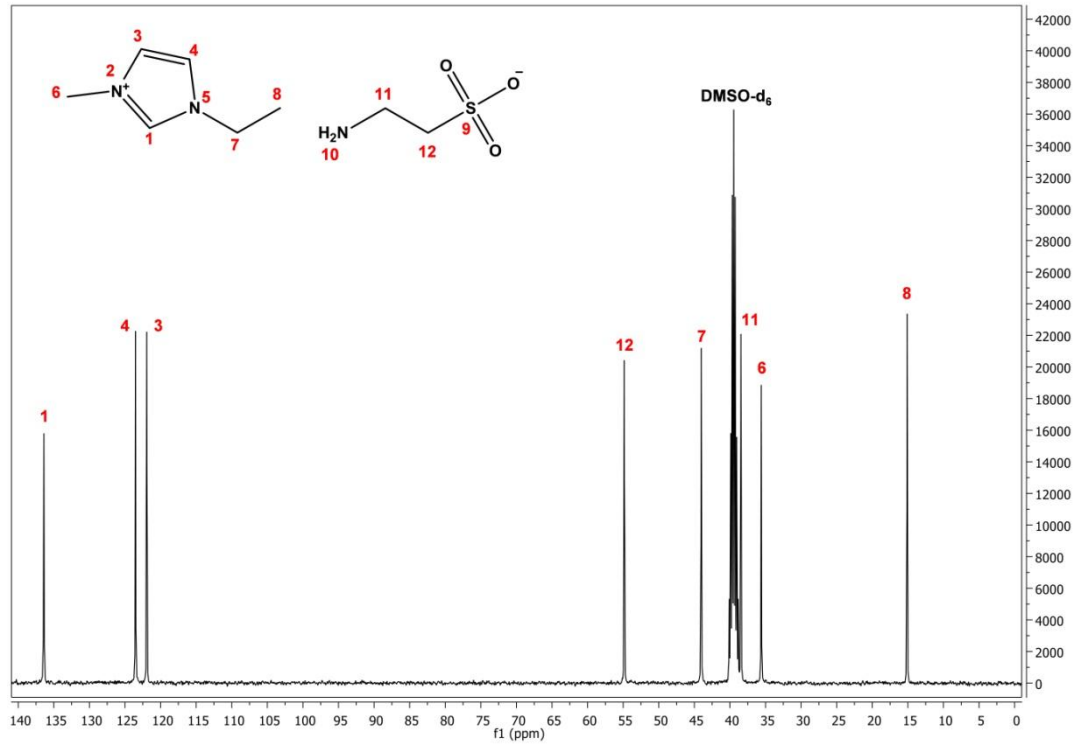

Figure 7.6 - ^{13}C-NMR spectrum of [C_2mim][Tau] in DMSO-d6.

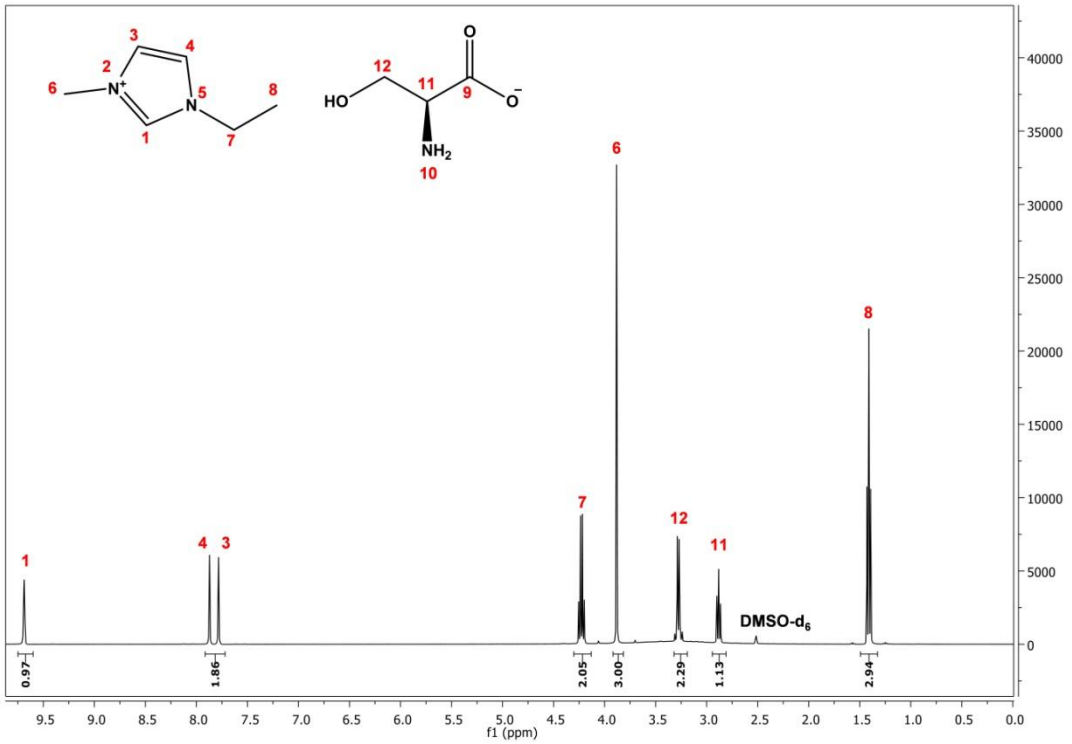

Figure 7.7 - ^{1}H-NMR spectrum of [C_2mim][L-Ser] in DMSO-d6.

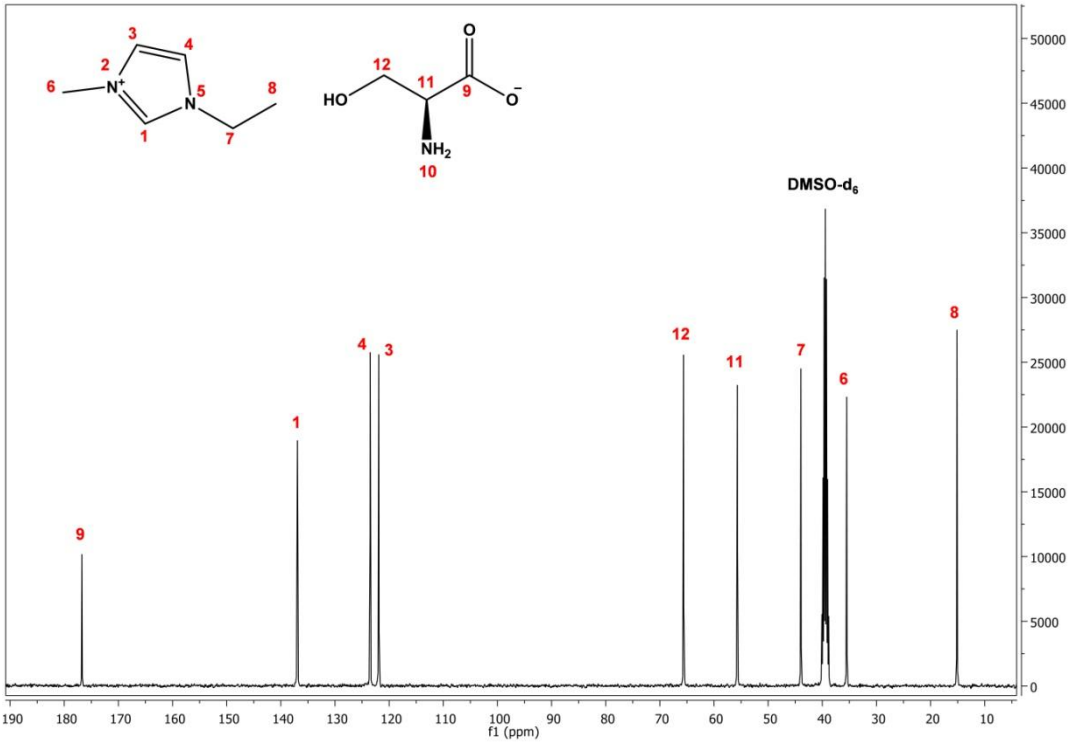

Figure 7.8 - ^{13}C-NMR spectrum of [C_2mim][L-Ser] in DMSO-d6.

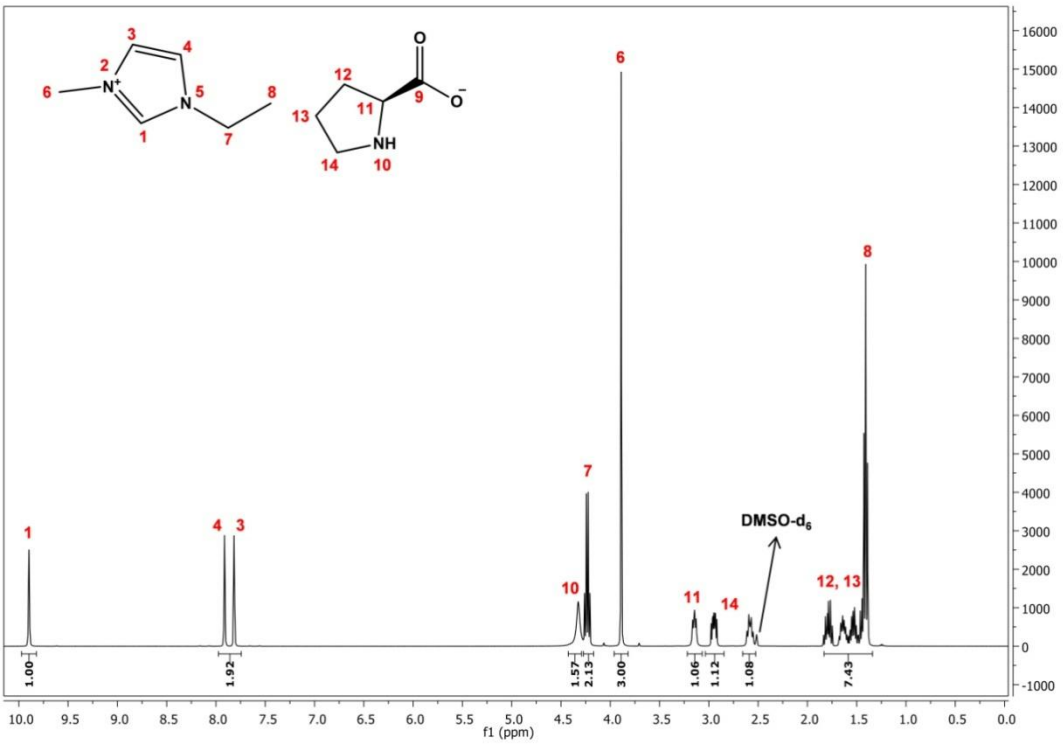

Figure 7.9 - ^{1}H-NMR spectrum of [C_2mim][L-Pro] in DMSO-d6.

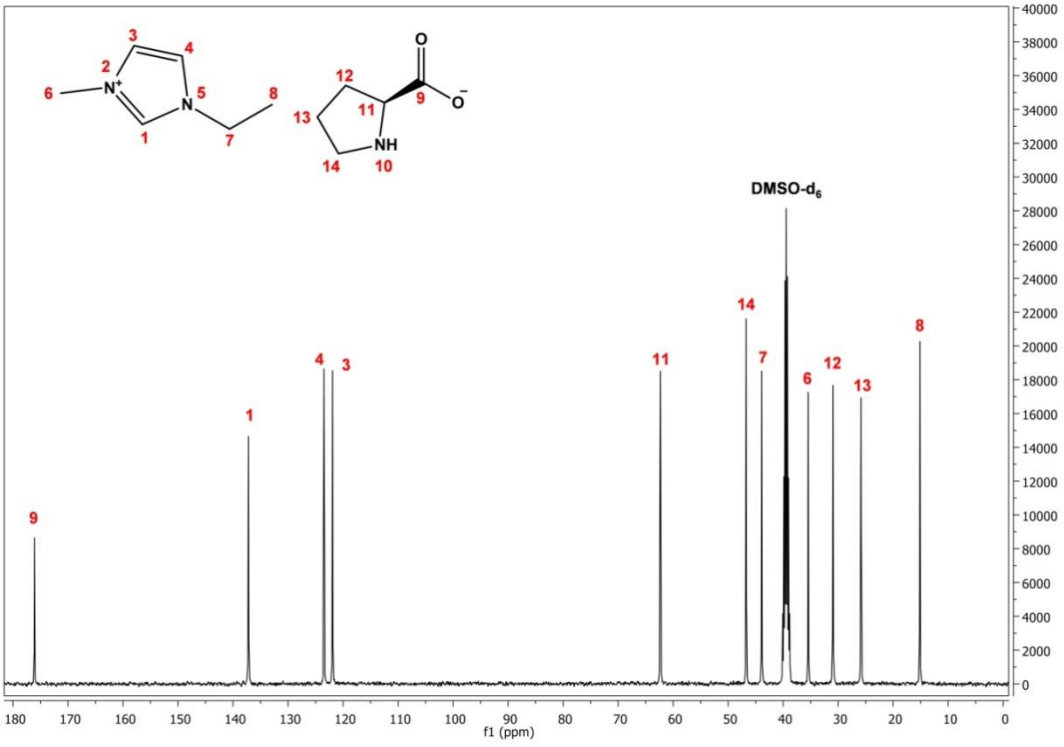

Figure 7.10 - ^{13}C-NMR spectrum of [C_2mim][L-Pro] in DMSO-d6.

7.2 Appendix 2

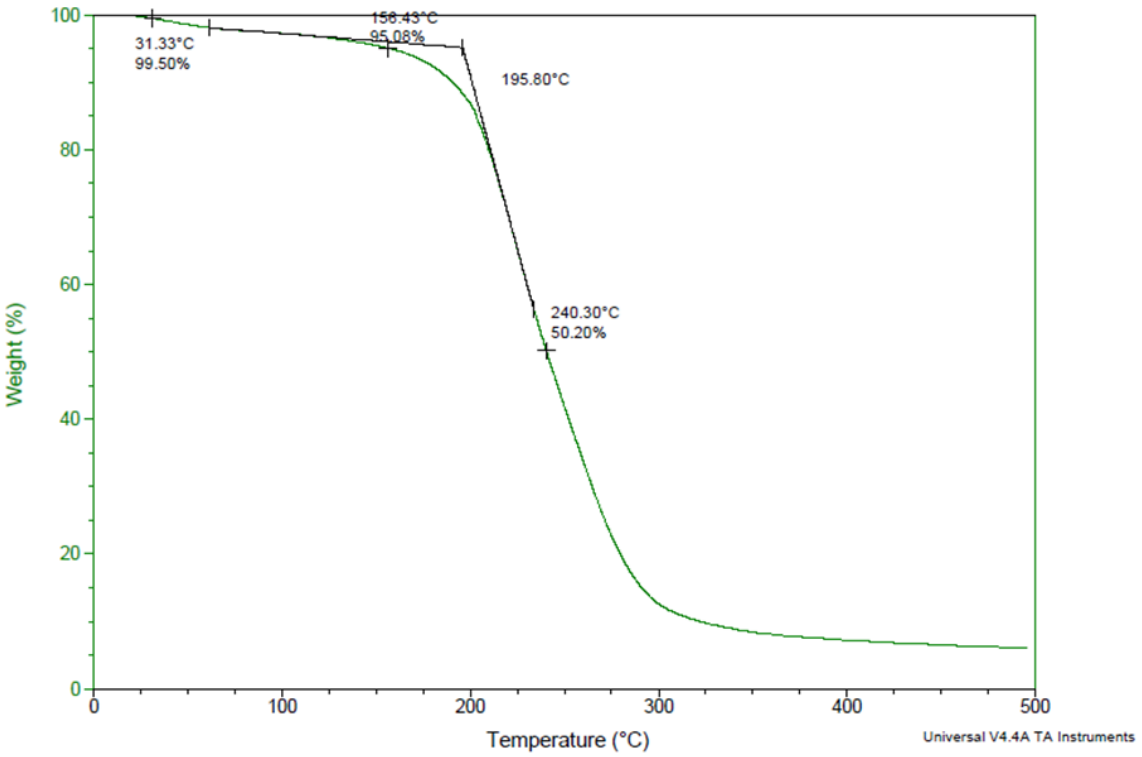

Figure 7.11 – TGA thermogram of the pure [C_2mim][Gly].

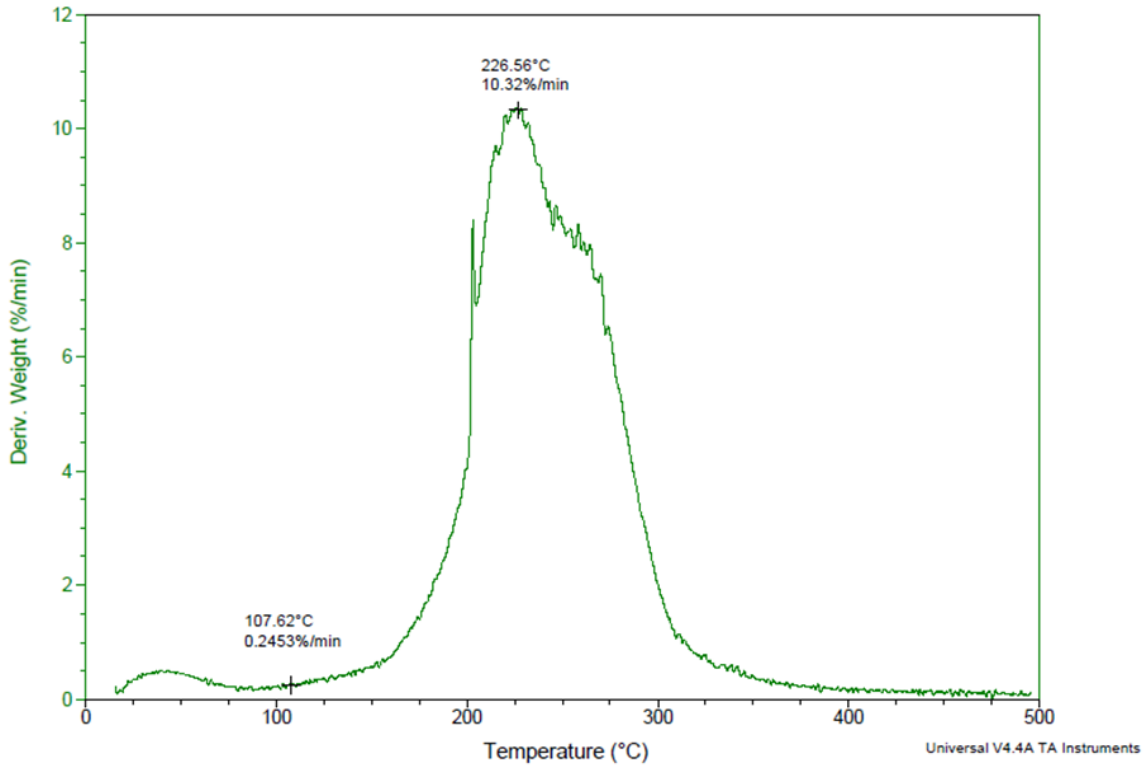

Figure 7.12- Derivative weight (%/min) of the pure [C_2mim][Gly] as a function of temperature (*T*).

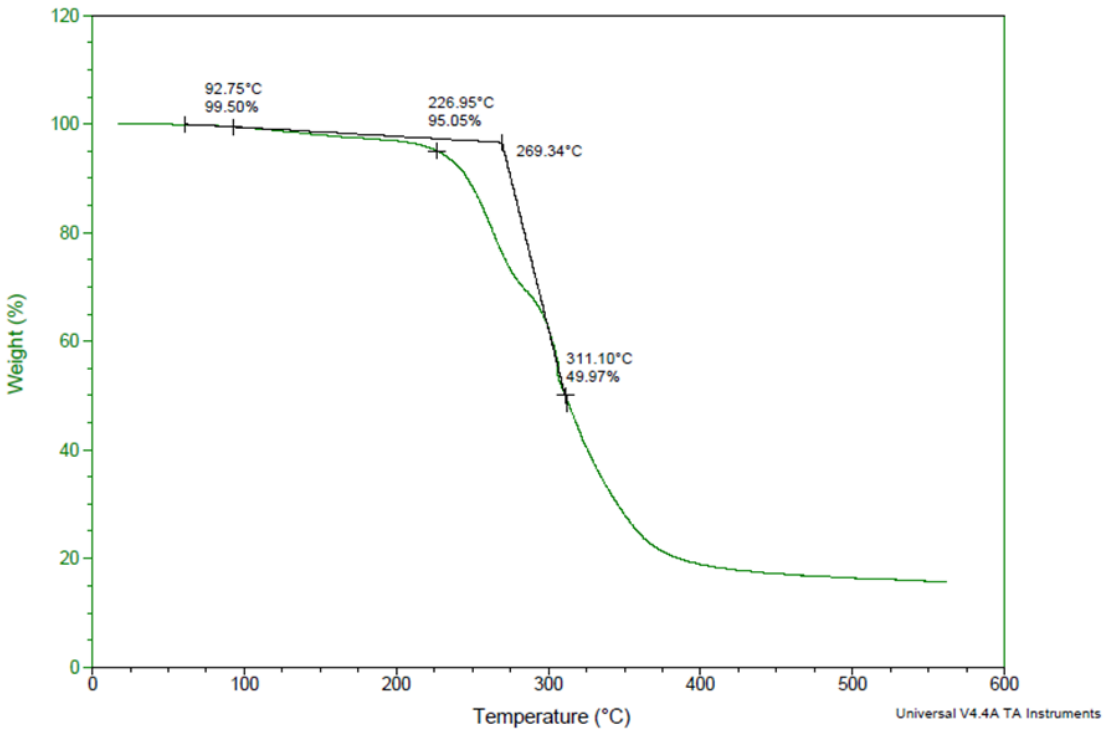

Figure 7.13 - TGA thermogram of the pure [C_2mim][Tau].

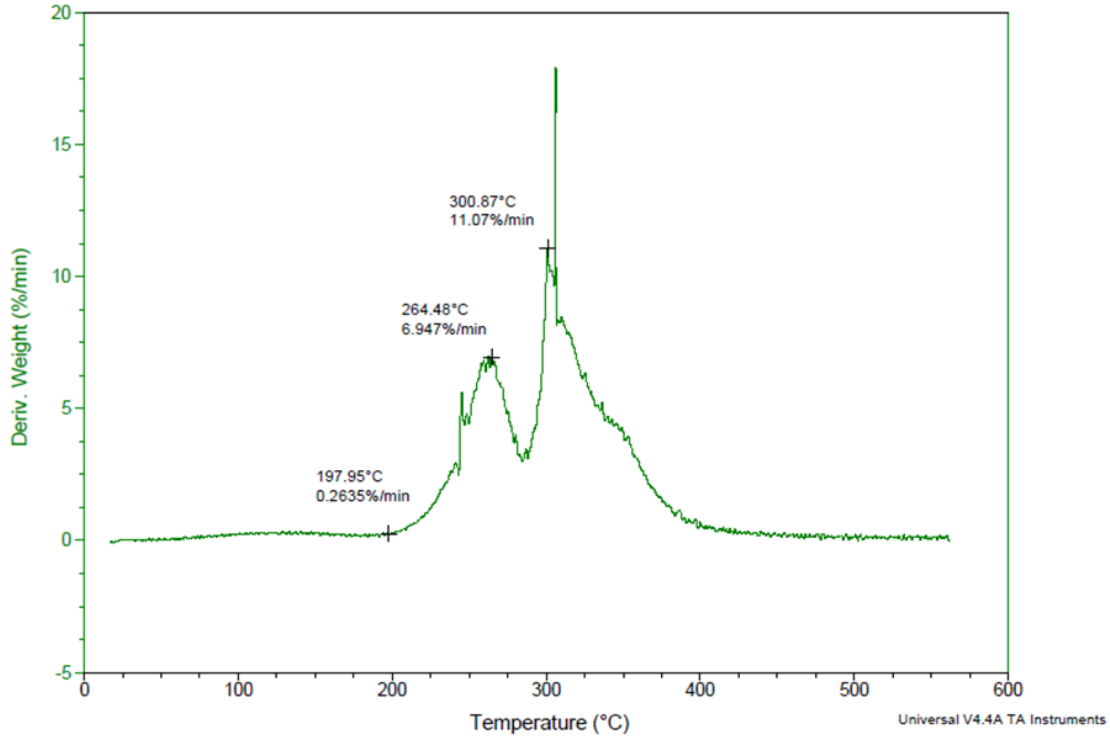

Figure 7.14 - Derivative weight (%/min) of the pure [C_2mim][Tau] as a function of temperature (*T*).

.

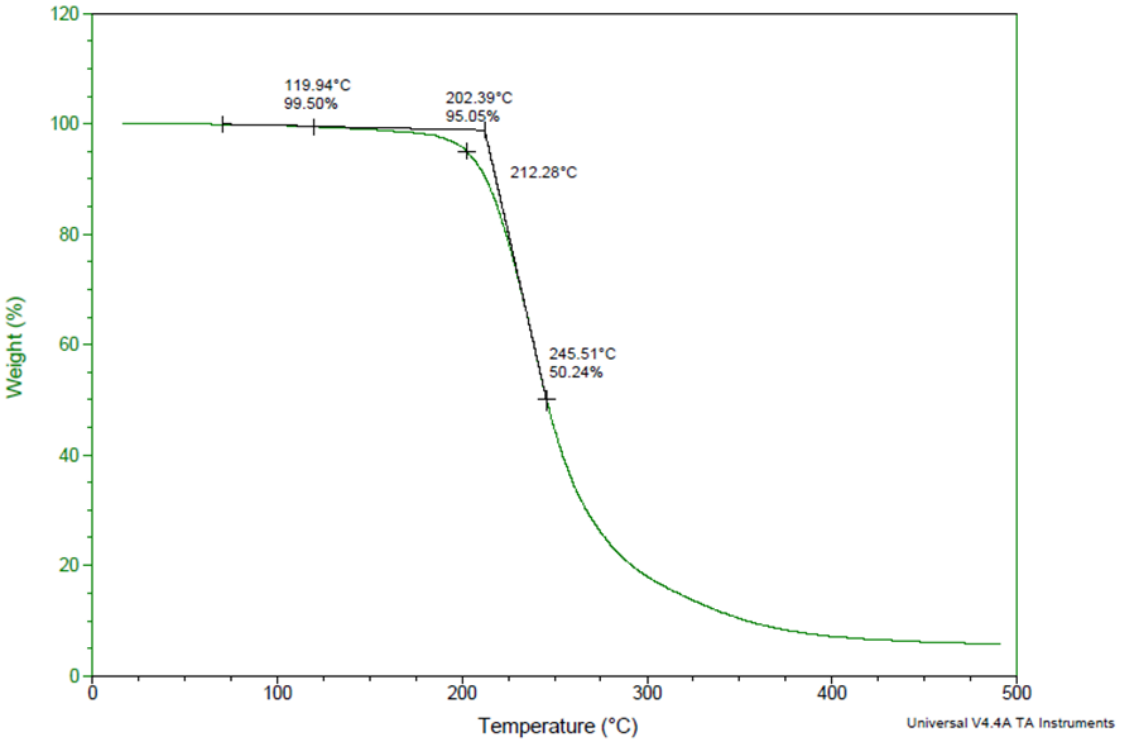

Figure 7.15 - TGA thermogram of the pure [C_2mim][L-Ser].

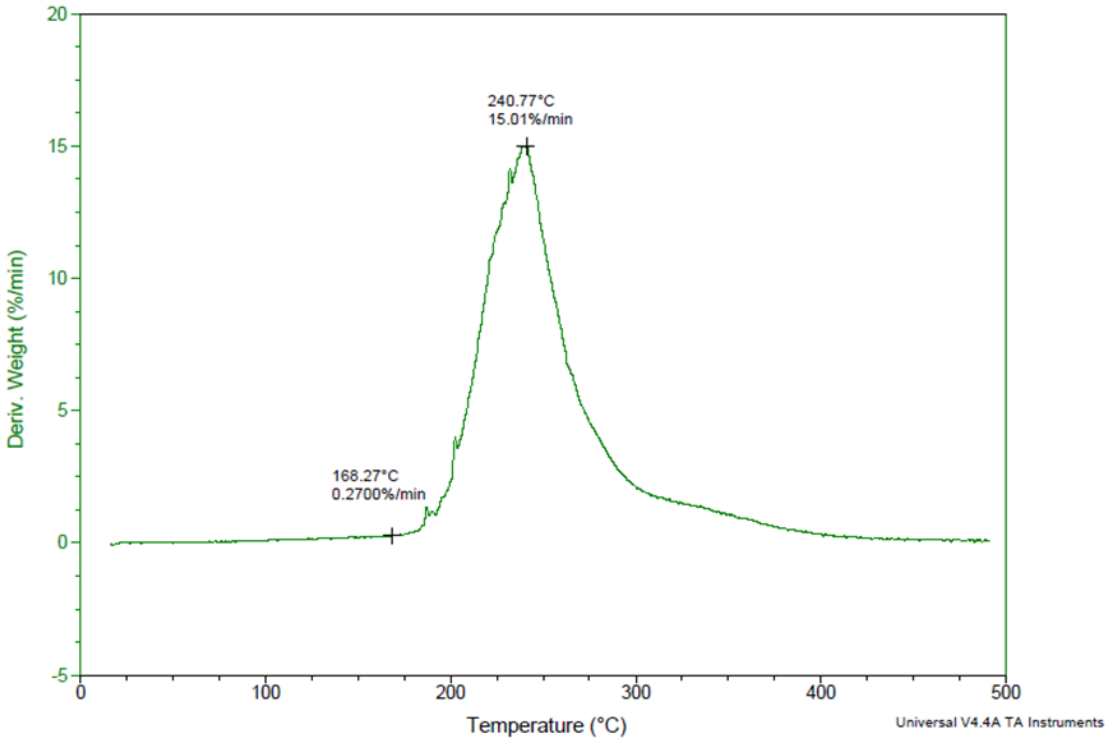

Figure 7.16 - Derivative weight (%/min) of the pure [C_2mim][L-Ser] as a function of temperature (*T*).

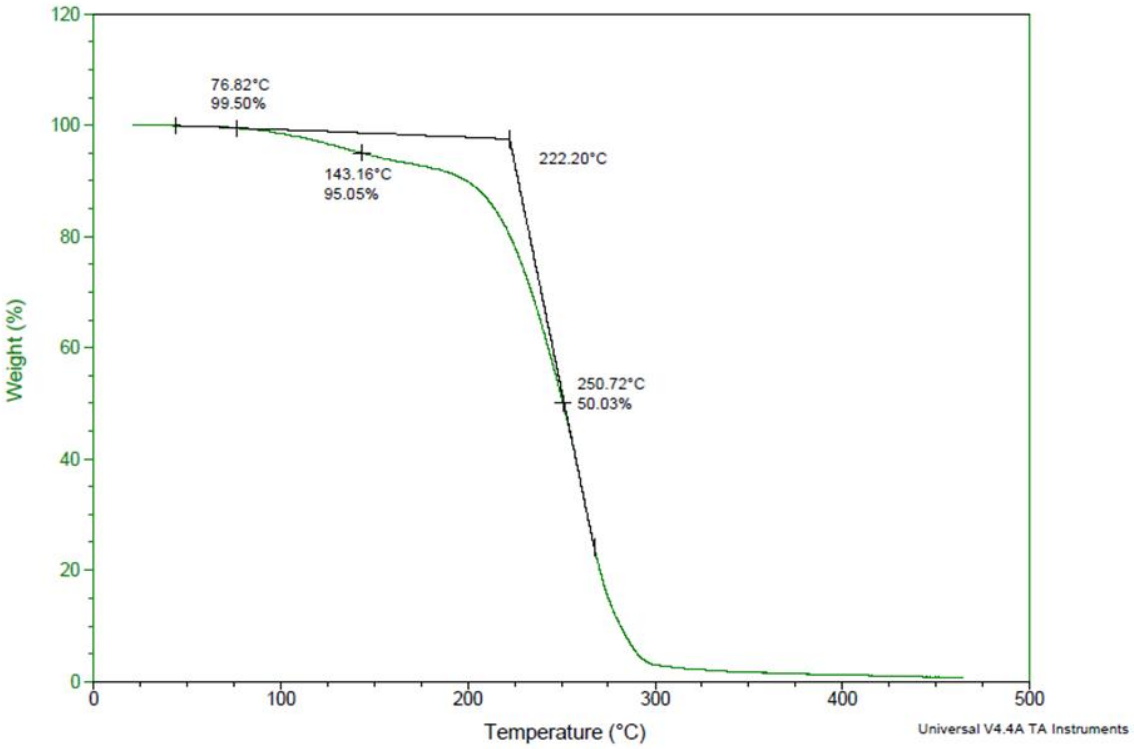

Figure 7.17 - TGA thermogram of the pure [C_2mim][L-Pro].

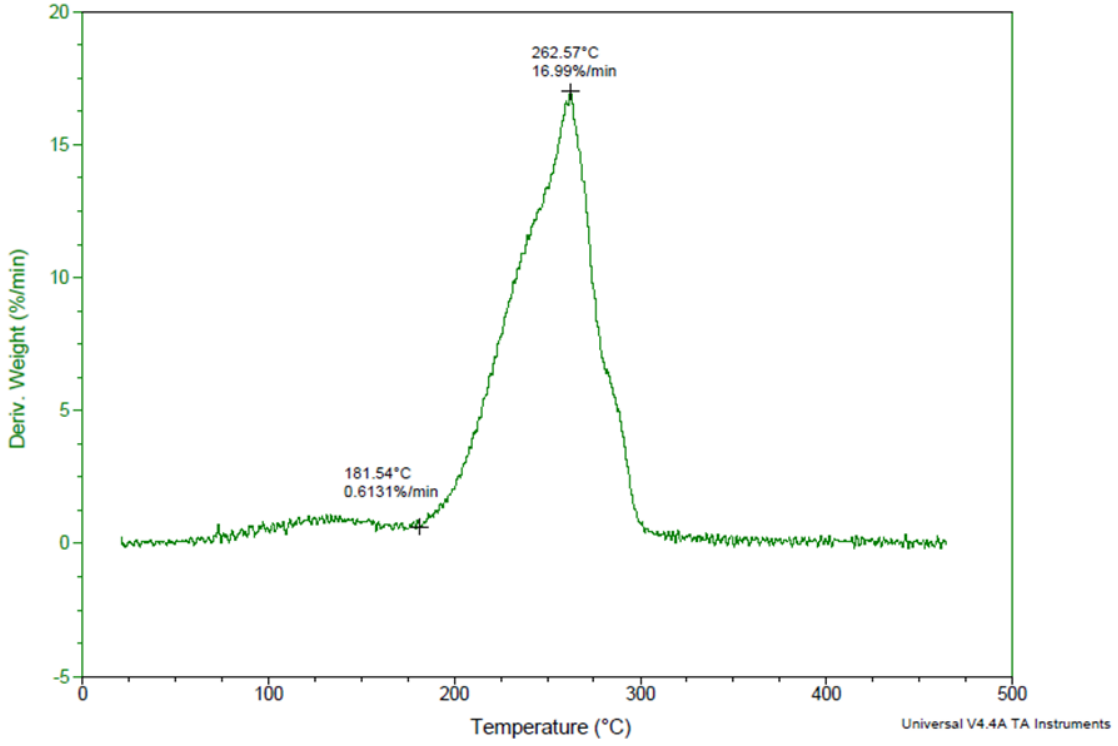

Figure 7.18 - Derivative weight (%/min) of the pure [C_2mim][L-Pro] as a function of temperature (*T*).

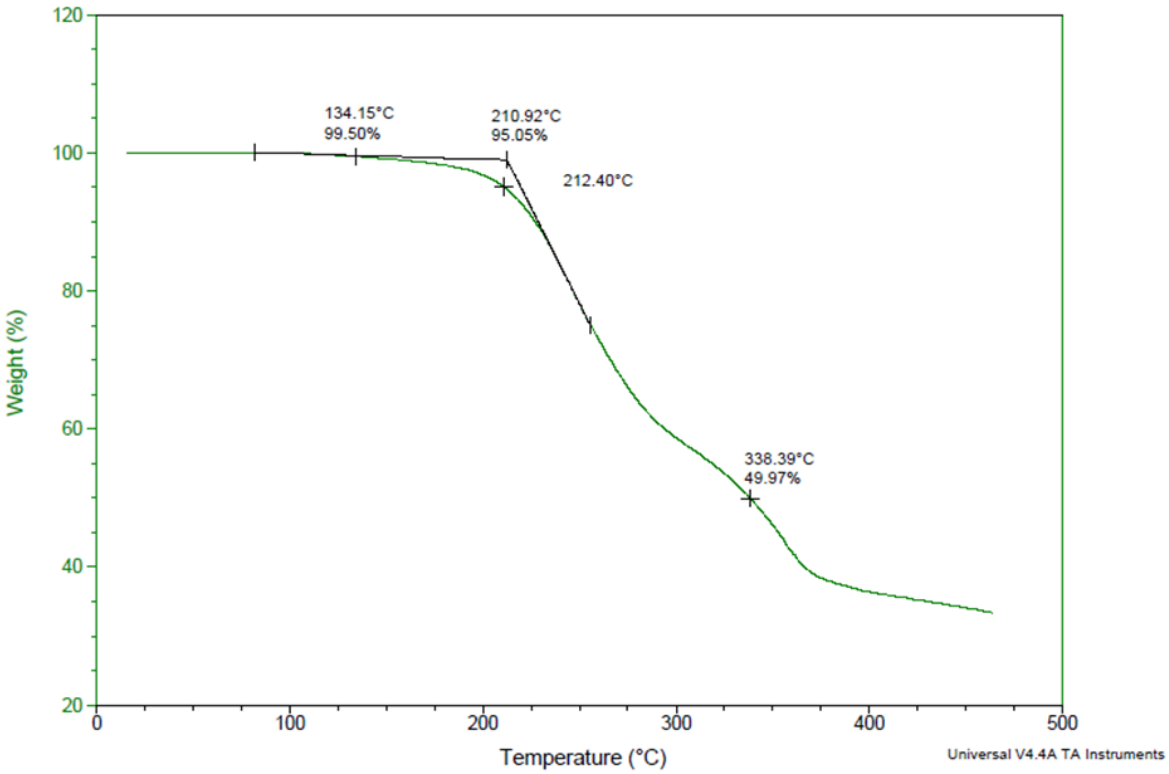

Figure 7.19 - TGA thermogram of the $[C_2mim][C(CN)_3]_{0.5}[Gly]_{0.5}$ mixture.

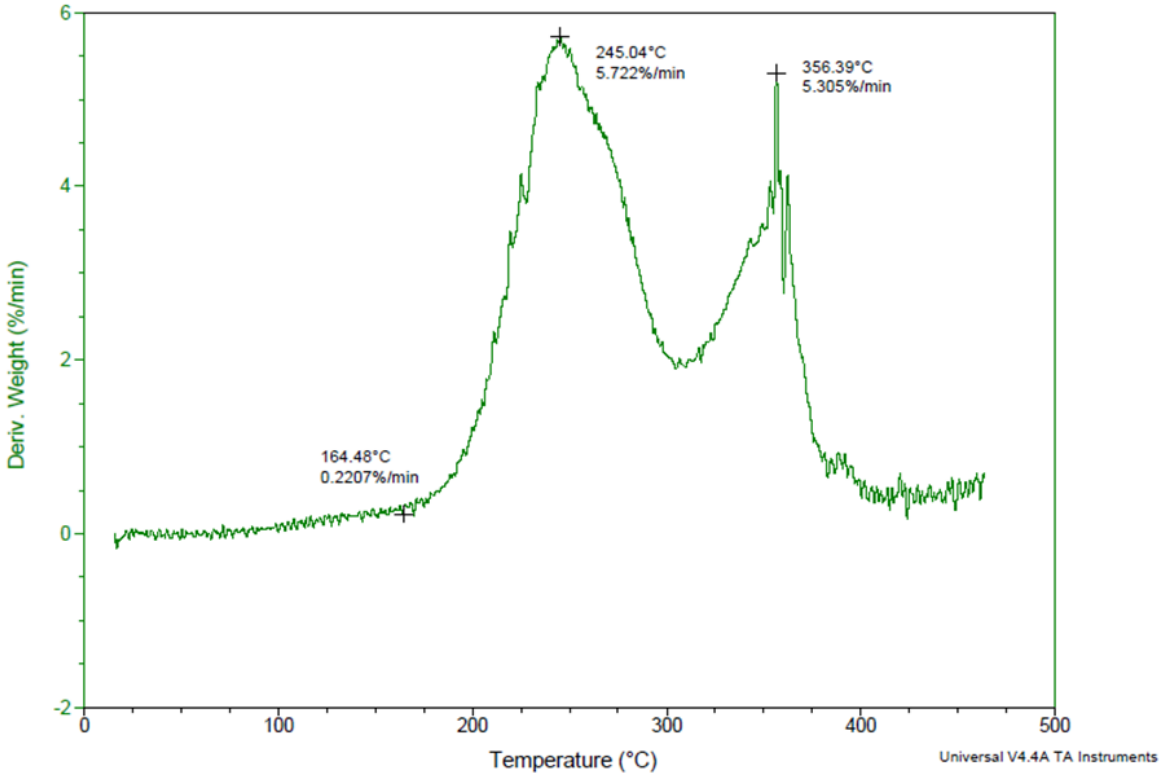

Figure 7.20 - Derivative weight (%/min) of the $[C_2mim][C(CN)_3]_{0.5}[Gly]_{0.5}$ mixture as a function of temperature (*T*).

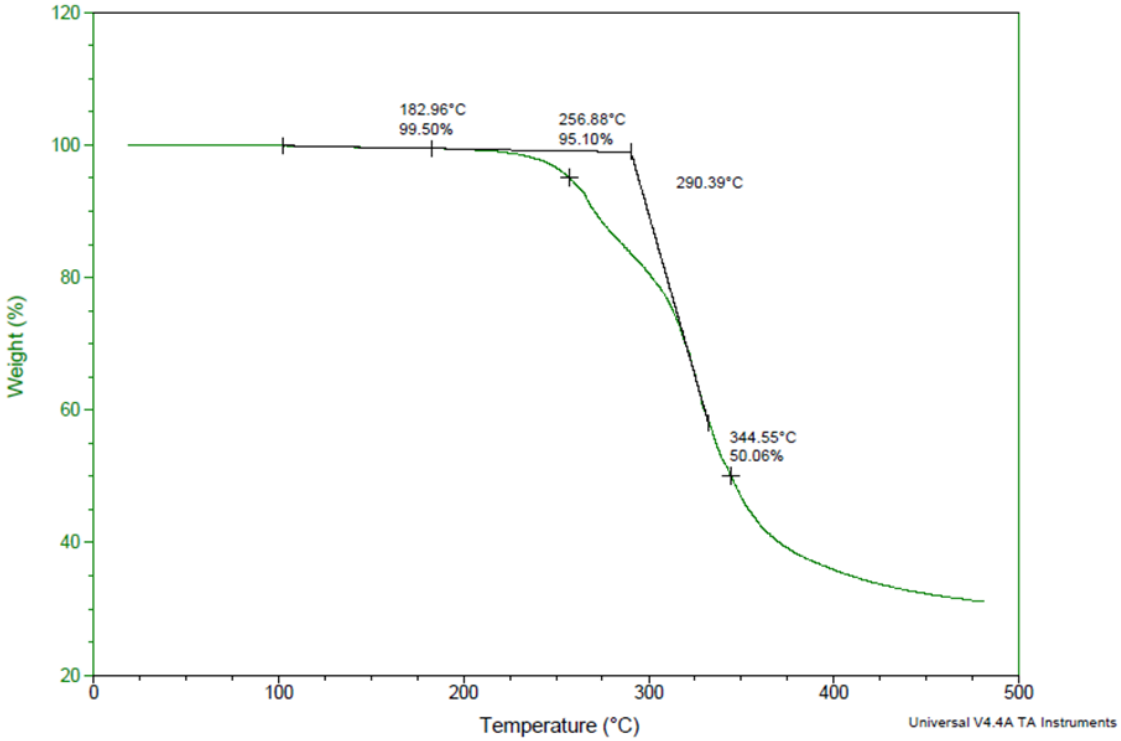

Figure 7.21 - TGA thermogram of the $[C_2mim][C(CN)_3]_{0.5}[Tau]_{0.5}$ mixture.

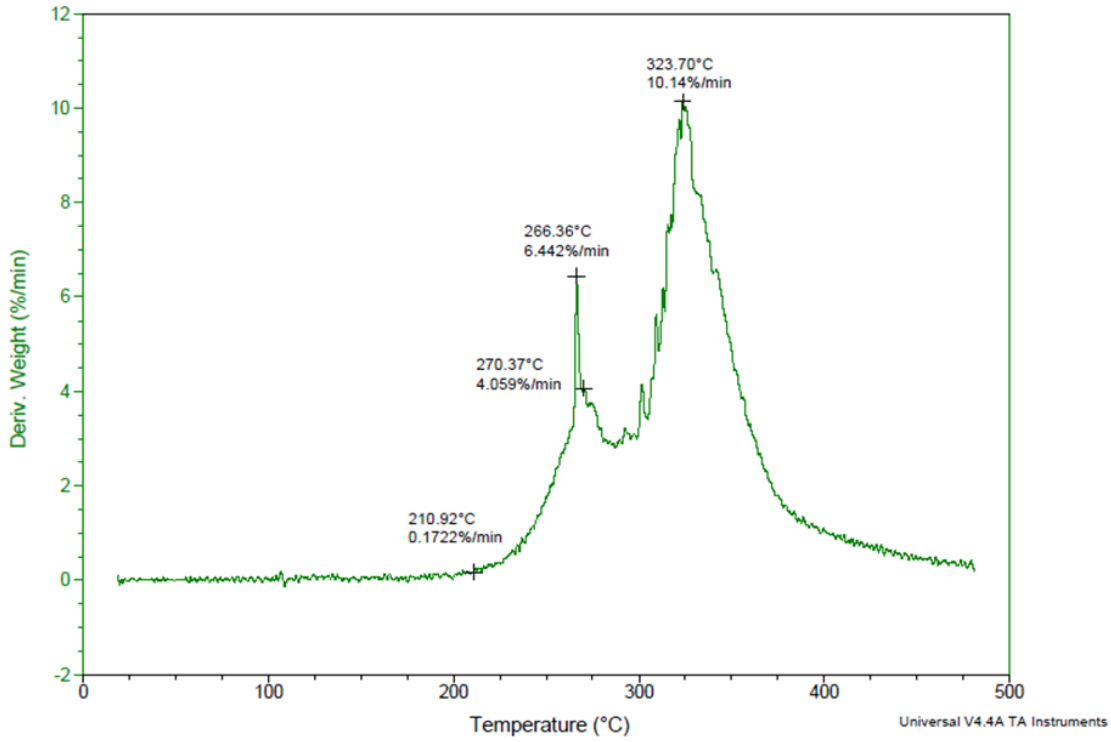

Figure 7.22 - Derivative weight (%/min) of the $[C_2mim][C(CN)_3]_{0.5}[Tau]_{0.5}$ mixture as a function of temperature (*T*).

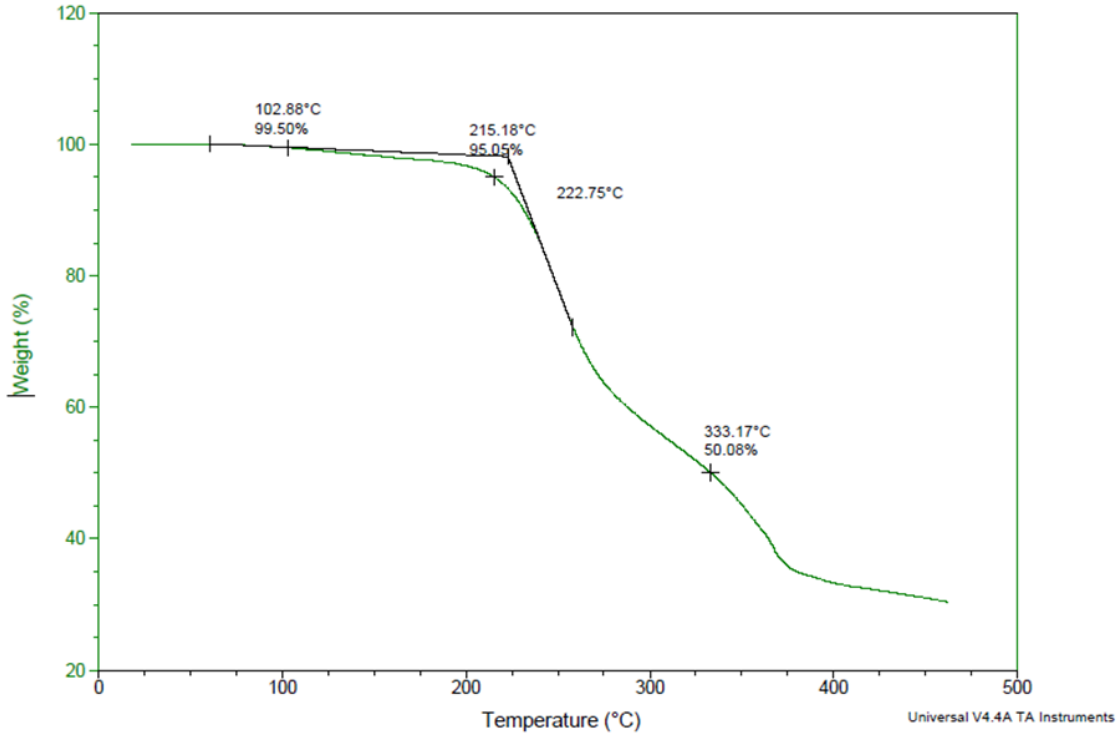

Figure 7.23 - TGA thermogram of the $[C_2mim][C(CN)_3]_{0.5}[L\text{-}Ser]_{0.5}$ mixture.

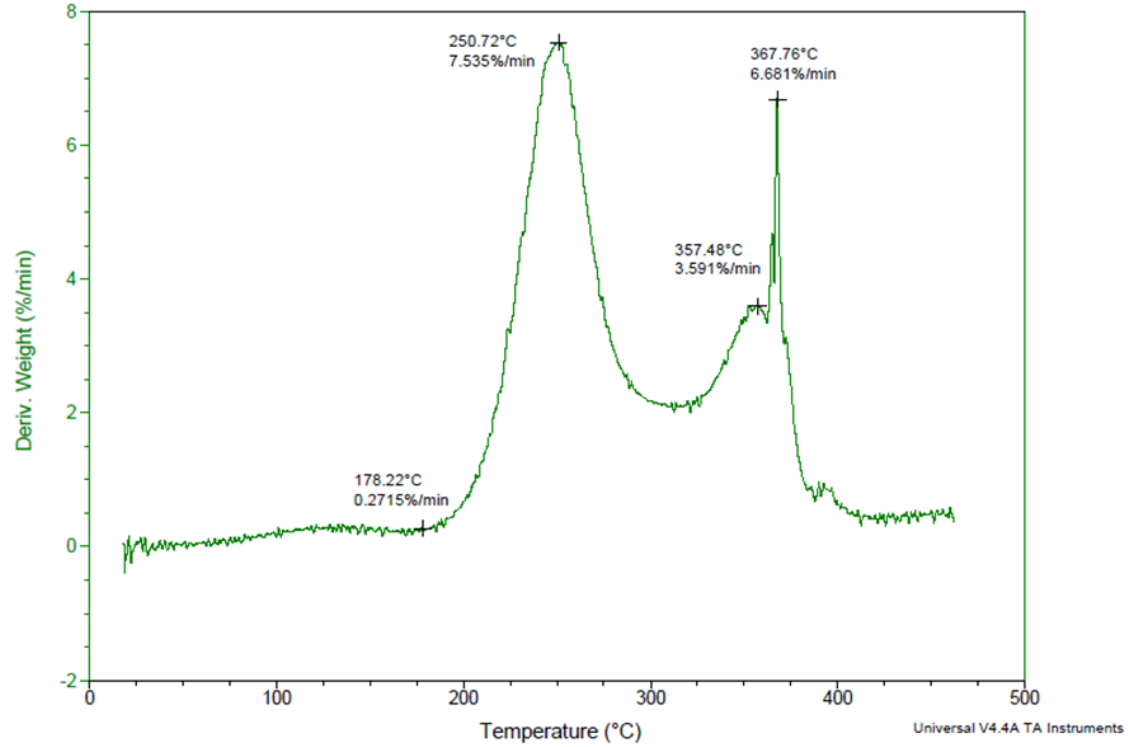

Figure 7.24 - Derivative weight (%/min) of the $[C_2mim][C(CN)_3]_{0.5}[L\text{-}Ser]_{0.5}$ mixture as a function of temperature (*T*).

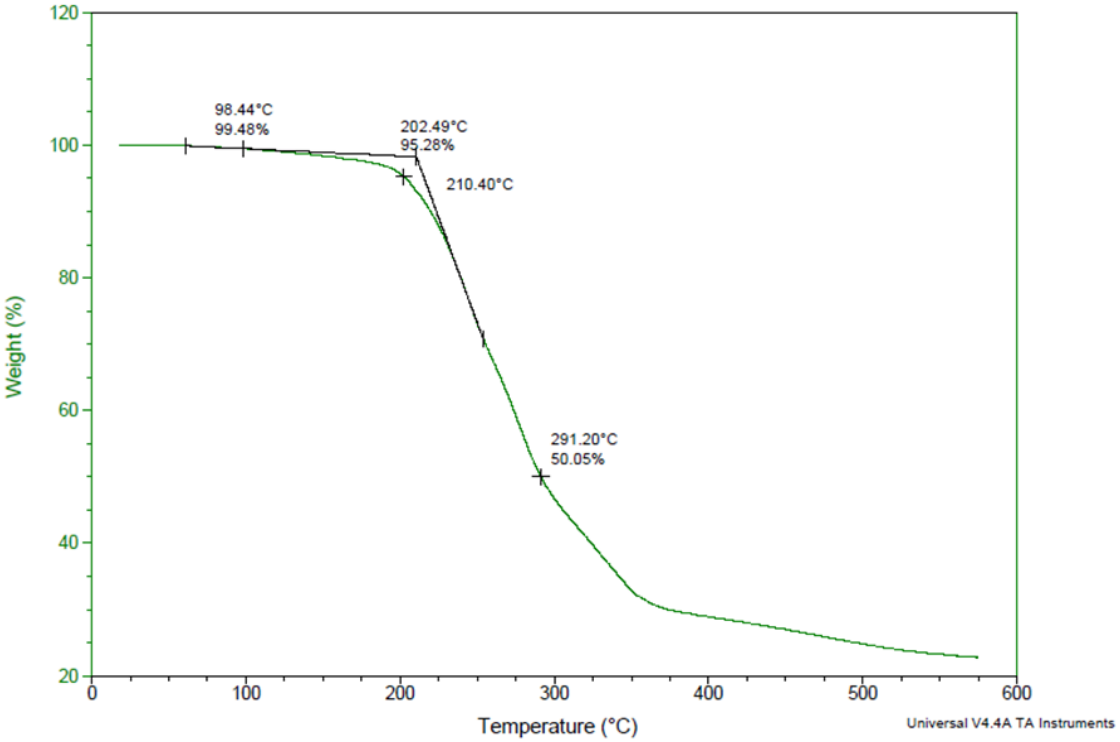

Figure 7.25 - TGA thermogram of the $[C_2mim][C(CN)_3]_{0.5}[L\text{-}Pro]_{0.5}$ mixture.

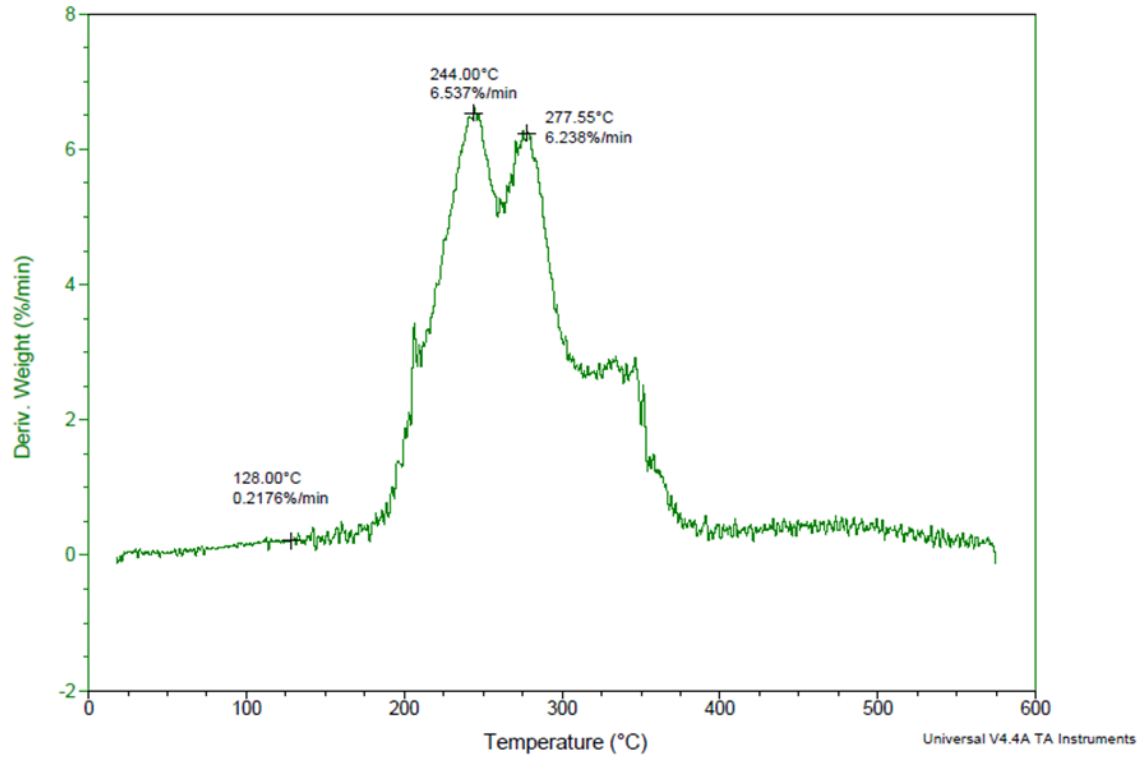

Figure 7.26 - Derivative weight (%/min) of the $[C_2mim][C(CN)_3]_{0.5}[L\text{-}Pro]_{0.5}$ mixture as a function of temperature (*T*).

7.3 Appendix 3

Table 7.1 - Measured densities, ρ (g·cm^{-3}), of the pure ionic liquids studied in this work.

T(K)	ρ (g·cm^{-3})					
	[C_2mim][C(CN)$_3$]	[C_2mim][Gly]	[C_2mim][L-Ala]	[C_2mim][Tau]	[C_2mim][L-Ser]	[C_2mim][L-Pro]
293.15	1.085	1.164	1.126	1.255	1.207	1.144
298.15	1.081	1.161	1.123	1.252	1.204	1.141
303.15	1.077	1.158	1.120	1.248	1.201	1.138
308.15	1.074	1.155	1.117	1.245	1.197	1.135
313.15	1.070	1.152	1.114	1.242	1.194	1.132
318.15	1.067	1.149	1.110	1.239	1.191	1.129
323.15	1.064	1.146	1.107	1.236	1.188	1.126
328.15	1.060	1.143	1.104	1.232	1.185	1.123
333.15	1.057	1.140	1.101	1.229	1.182	1.120
338.15	1.054	1.137	1.098	1.226	1.179	1.117
343.15	1.050	1.134	1.095	1.223	1.176	1.114
348.15	1.047	1.131	1.092	1.220	1.173	1.111
353.15	1.043	1.127	1.089	1.217	1.170	1.108

Table 7.2 - Measured densities, ρ (g·cm^{-3}), of ionic liquid mixtures studied in this work.

T(K)	ρ (g·cm^{-3})				
	[C_2mim][C(CN)$_3$]$_{0.25}$ [C_2mim][Gly]$_{0.75}$	[C_2mim][C(CN)$_3$]$_{0.25}$ [C_2mim][L-Ala]$_{0.75}$	[C_2mim][C(CN)$_3$]$_{0.25}$ [C_2mim][Tau]$_{0.75}$	[C_2mim][C(CN)$_3$]$_{0.25}$ [C_2mim][L-Ser]$_{0.75}$	[C_2mim][C(CN)$_3$]$_{0.25}$ [C_2mim][L-Pro]$_{0.75}$
293.15	1.140	1.114	1.208	1.177	1.138
298.15	1.137	1.110	1.204	1.174	1.134
303.15	1.134	1.107	1.201	1.170	1.131
308.15	1.130	1.104	1.198	1.167	1.128
313.15	1.127	1.101	1.195	1.164	1.125
318.15	1.124	1.098	1.192	1.160	1.122
323.15	1.121	1.095	1.189	1.157	1.119
328.15	1.118	1.092	1.185	1.154	1.116
333.15	1.115	1.088	1.182	1.151	1.113
338.15	1.112	1.085	1.179	1.148	1.110
343.15	1.109	1.082	1.176	1.144	1.106
348.15	1.106	1.079	1.173	1.141	1.103
353.15	1.102	1.076	1.169	1.138	1.100

Table 7.3 - Measured densities, ρ (g·cm^{-3}), of ionic liquid mixtures studied in this work.

T(K)	ρ (g·cm^{-3})				
	$[C_2mim][C(CN)_3]_{0.5}$ $[C_2mim][Gly]_{0.5}$	$[C_2mim][C(CN)_3]_{0.5}$ $[C_2mim][L\text{-}Ala]_{0.5}$	$[C_2mim][C(CN)_3]_{0.5}$ $[C_2mim][Tau]_{0.5}$	$[C_2mim][C(CN)_3]_{0.5}$ $[C_2mim][L\text{-}Ser]_{0.5}$	$[C_2mim][C(CN)_3]_{0.5}$ $[C_2mim][L\text{-}Pro]_{0.5}$
293.15	1.118	1.102	1.165	1.142	1.120
298.15	1.115	1.099	1.161	1.138	1.116
303.15	1.112	1.096	1.158	1.135	1.113
308.15	1.108	1.092	1.155	1.132	1.110
313.15	1.105	1.089	1.151	1.128	1.107
318.15	1.102	1.086	1.148	1.125	1.104
323.15	1.099	1.083	1.145	1.122	1.101
328.15	1.096	1.080	1.142	1.118	1.097
333.15	1.092	1.076	1.138	1.115	1.094
338.15	1.089	1.073	1.135	1.112	1.091
343.15	1.086	1.070	1.132	1.109	1.088
348.15	1.083	1.067	1.129	1.105	1.085
353.15	1.080	1.063	1.126	1.102	1.082

Table 7.4 - Measured densities, ρ (g·cm^{-3}), of ionic liquid mixtures studied in this work.

T(K)	ρ (g·cm^{-3})				
	$[C_2mim][C(CN)_3]_{0.75}$ $[C_2mim][Gly]_{0.25}$	$[C_2mim][C(CN)_3]_{0.75}$ $[C_2mim][L\text{-}Ala]_{0.25}$	$[C_2mim][C(CN)_3]_{0.75}$ $[C_2mim][Tau]_{0.25}$	$[C_2mim][C(CN)_3]_{0.75}$ $[C_2mim][L\text{-}Ser]_{0.25}$	$[C_2mim][C(CN)_3]_{0.75}$ $[C_2mim][L\text{-}Pro]_{0.25}$
293.15	1.101	1.093	1.124	1.113	1.103
298.15	1.098	1.089	1.121	1.109	1.100
303.15	1.094	1.086	1.117	1.106	1.096
308.15	1.091	1.083	1.114	1.102	1.093
313.15	1.088	1.079	1.110	1.099	1.090
318.15	1.084	1.076	1.107	1.096	1.087
323.15	1.081	1.073	1.104	1.092	1.083
328.15	1.078	1.069	1.101	1.089	1.080
333.15	1.074	1.066	1.097	1.086	1.077
338.15	1.071	1.063	1.094	1.082	1.074
343.15	1.068	1.060	1.091	1.079	1.070
348.15	1.065	1.056	1.087	1.076	1.067
353.15	1.061	1.053	1.084	1.072	1.064

7.4 Appendix 4

Table 7.5 – Molar Volumes, V_m ($cm^3 \cdot mol^{-1}$), of the pure ionic liquids studied in this work.

T(K)	V_m ($cm^3 \cdot mol^{-1}$)					
	$[C_2mim][C(CN)_3]$	**$[C_2mim][Gly]$**	**$[C_2mim][L\text{-}Ala]$**	**$[C_2mim][Tau]$**	**$[C_2mim][L\text{-}Ser]$**	**$[C_2mim][L\text{-}Pro]$**
293.15	185.420	159.078	176.912	187.485	178.359	196.886
298.15	186.037	159.512	177.427	188.009	178.819	197.432
303.15	186.642	159.939	177.934	188.522	179.295	197.988
308.15	187.256	160.359	178.438	189.026	179.780	198.540
313.15	187.868	160.781	178.935	189.514	180.276	199.090
318.15	188.461	161.206	179.42	189.973	180.741	199.601
323.15	189.063	161.628	179.915	190.449	181.217	200.133
328.15	189.669	162.052	180.420	190.928	181.686	200.656
333.15	190.273	162.483	180.917	191.420	182.153	201.182
338.15	190.875	162.917	181.422	191.904	182.611	201.704
343.15	191.487	163.362	181.925	192.396	183.077	202.235
348.15	192.109	163.805	182.441	192.879	183.540	202.763
353.15	192.735	164.285	182.983	193.381	184.016	203.312

Table 7.6 - Molar Volumes, V_m ($cm^3 \cdot mol^{-1}$), of the ionic liquids mixtures studied in this work.

T(K)	V_m ($cm^3 \cdot mol^{-1}$)				
	$[C_2mim][C(CN)_3]_{0.25}$ $[C_2mim][Gly]_{0.75}$	**$[C_2mim][C(CN)_3]_{0.25}$ $[C_2mim][L\text{-}Ala]_{0.75}$**	**$[C_2mim][C(CN)_3]_{0.25}$ $[C_2mim][Tau]_{0.75}$**	**$[C_2mim][C(CN)_3]_{0.25}$ $[C_2mim][L\text{-}Ser]_{0.75}$**	**$[C_2mim][C(CN)_3]_{0.25}$ $[C_2mim][L\text{-}Pro]_{0.75}$**
293.15	165.956	179.353	187.775	179.872	192.747
298.15	166.432	179.891	188.290	180.423	193.319
303.15	166.902	180.416	188.807	180.963	193.871
308.15	167.384	180.923	189.317	181.475	194.421
313.15	167.855	181.449	189.824	181.990	194.963
318.15	168.307	181.950	190.302	182.468	195.502
323.15	168.778	182.477	190.814	182.973	196.009
328.15	169.256	183.000	191.329	183.488	196.553
333.15	169.732	183.522	191.842	183.998	197.095
338.15	170.210	184.046	192.352	184.511	197.634
343.15	170.681	184.573	192.864	185.035	198.188
348.15	171.159	185.103	193.390	185.546	198.727
353.15	171.641	185.660	193.925	186.076	199.268

Table 7.7 - Molar Volumes, V_m ($cm^3 \cdot mol^{-1}$), of the ionic liquids mixtures studied in this work.

	V_m ($cm^3 \cdot mol^{-1}$)				
***T*(K)**	**$[C_2mim][C(CN)_3]_{0.5}$ $[C_2mim][Gly]_{0.5}$**	**$[C_2mim][C(CN)_3]_{0.5}$ $[C_2mim][L\text{-}Ala]_{0.5}$**	**$[C_2mim][C(CN)_3]_{0.5}$ $[C_2mim][Tau]_{0.5}$**	**$[C_2mim][C(CN)_3]_{0.5}$ $[C_2mim][L\text{-}Ser]_{0.5}$**	**$[C_2mim][C(CN)_3]_{0.5}$ $[C_2mim][L\text{-}Pro]_{0.5}$**
293.15	172.774	181.681	187.379	182.373	190.456
298.15	173.301	182.224	187.927	182.918	191.019
303.15	173.816	182.767	188.479	183.477	191.574
308.15	174.333	183.314	189.018	184.012	192.126
313.15	174.843	183.864	189.565	184.550	192.682
318.15	175.340	184.394	190.093	185.091	193.217
323.15	175.851	184.939	190.630	185.636	193.779
328.15	176.359	185.488	191.175	186.183	194.332
333.15	176.887	186.039	191.724	186.740	194.900
338.15	177.401	186.594	192.264	187.289	195.454
343.15	177.918	187.158	192.808	187.846	196.017
348.15	178.444	187.743	193.354	188.413	196.595
353.15	178.984	188.361	193.910	188.994	197.183

Table 7.8 - Molar Volumes, V_m ($cm^3 \cdot mol^{-1}$), of the ionic liquids mixtures studied in this work.

	V_m ($cm^3 \cdot mol^{-1}$)				
***T*(K)**	**$[C_2mim][C(CN)_3]_{0.75}$ $[C_2mim][Gly]_{0.25}$**	**$[C_2mim][C(CN)_3]_{0.75}$ $[C_2mim][L\text{-}Ala]_{0.25}$**	**$[C_2mim][C(CN)_3]_{0.75}$ $[C_2mim][Tau]_{0.25}$**	**$[C_2mim][C(CN)_3]_{0.75}$ $[C_2mim][L\text{-}Ser]_{0.25}$**	**$[C_2mim][C(CN)_3]_{0.75}$ $[C_2mim][L\text{-}Pro]_{0.25}$**
293.15	179.102	183.672	186.597	183.971	187.858
298.15	179.657	184.273	187.174	184.557	188.445
303.15	180.221	184.850	187.744	185.141	189.017
308.15	180.777	185.425	188.317	185.729	189.588
313.15	181.320	186.009	188.888	186.309	190.168
318.15	181.883	186.574	189.445	186.870	190.734
323.15	182.443	187.136	190.017	187.446	191.309
328.15	183.002	187.714	190.587	188.020	191.882
333.15	183.559	188.283	191.166	188.597	192.458
338.15	184.113	188.862	191.737	189.178	193.031
343.15	184.676	189.444	192.317	189.757	193.615
348.15	185.237	190.036	192.913	190.333	194.207
353.15	185.807	190.650	193.518	190.937	194.816

Table 7.9 – Excess Molar Volumes, V^E ($cm^3 \cdot mol^{-1}$), of the ionic liquids mixtures studied in this work.

	V^E ($cm^3 \cdot mol^{-1}$)				
***T*(K)**	**$[C_2mim][C(CN)_3]_{0.25}$ $[C_2mim][Gly]_{0.75}$**	**$[C_2mim][C(CN)_3]_{0.25}$ $[C_2mim][L\text{-}Ala]_{0.75}$**	**$[C_2mim][C(CN)_3]_{0.25}$ $[C_2mim][Tau]_{0.75}$**	**$[C_2mim][C(CN)_3]_{0.25}$ $[C_2mim][L\text{-}Ser]_{0.75}$**	**$[C_2mim][C(CN)_3]_{0.25}$ $[C_2mim][L\text{-}Pro]_{0.75}$**
293.15	0.262	0.284	0.777	-0.283	-1.303
298.15	0.259	0.282	0.743	-0.230	-1.295
303.15	0.257	0.276	0.725	-0.199	-1.310
308.15	0.271	0.250	0.703	-0.204	-1.328
313.15	0.271	0.250	0.691	-0.215	-1.352
318.15	0.258	0.233	0.677	-0.233	-1.345
323.15	0.261	0.244	0.681	-0.237	-1.387
328.15	0.269	0.237	0.685	-0.225	-1.387
333.15	0.270	0.235	0.678	-0.216	-1.390
338.15	0.273	0.229	0.674	-0.197	-1.394
343.15	0.256	0.227	0.665	-0.176	-1.391
348.15	0.247	0.214	0.673	-0.168	-1.404
353.15	0.212	0.208	0.674	-0.151	-1.431

Table 7.10 - Excess Molar Volumes, V^E ($cm^3 \cdot mol^{-1}$), of the ionic liquids mixtures studied in this work.

	V^E ($cm^3 \cdot mol^{-1}$)				
***T*(K)**	**$[C_2mim][C(CN)_3]_{0.5}$ $[C_2mim][Gly]_{0.5}$**	**$[C_2mim][C(CN)_3]_{0.5}$ $[C_2mim][L\text{-}Ala]_{0.5}$**	**$[C_2mim][C(CN)_3]_{0.5}$ $[C_2mim][Tau]_{0.5}$**	**$[C_2mim][C(CN)_3]_{0.5}$ $[C_2mim][L\text{-}Ser]_{0.5}$**	**$[C_2mim][C(CN)_3]_{0.5}$ $[C_2mim][L\text{-}Pro]_{0.5}$**
293.15	0.465	0.456	0.866	0.424	-0.757
298.15	0.466	0.432	0.844	0.430	-0.776
303.15	0.465	0.420	0.837	0.448	-0.801
308.15	0.465	0.407	0.816	0.434	-0.832
313.15	0.458	0.402	0.813	0.417	-0.858
318.15	0.446	0.389	0.816	0.430	-0.875
323.15	0.444	0.389	0.813	0.434	-0.880
328.15	0.437	0.382	0.815	0.444	-0.892
333.15	0.447	0.382	0.816	0.465	-0.889
338.15	0.443	0.383	0.813	0.484	-0.897
343.15	0.431	0.390	0.804	0.502	-0.906
348.15	0.425	0.405	0.798	0.526	-0.903
353.15	0.412	0.439	0.789	0.556	-0.903

Table 7.11 – Excess Molar Volumes, V^E ($cm^3 \cdot mol^{-1}$), of the ionic liquids mixtures studied in this work.

	V^E ($cm^3 \cdot mol^{-1}$)				
***T*(K)**	**$[C_2mim][C(CN)_3]_{0.75}$ $[C_2mim][Gly]_{0.25}$**	**$[C_2mim][C(CN)_3]_{0.75}$ $[C_2mim][L\text{-}Ala]_{0.25}$**	**$[C_2mim][C(CN)_3]_{0.75}$ $[C_2mim][Tau]_{0.25}$**	**$[C_2mim][C(CN)_3]_{0.75}$ $[C_2mim][L\text{-}Ser]_{0.25}$**	**$[C_2mim][C(CN)_3]_{0.75}$ $[C_2mim][L\text{-}Pro]_{0.25}$**
293.15	0.178	0.289	0.571	0.226	-0.518
298.15	0.161	0.299	0.554	0.234	-0.532
303.15	0.164	0.295	0.542	0.245	-0.551
308.15	0.155	0.283	0.528	0.251	-0.579
313.15	0.132	0.284	0.518	0.248	-0.596
318.15	0.144	0.280	0.515	0.248	-0.603
323.15	0.148	0.269	0.516	0.253	-0.613
328.15	0.145	0.265	0.511	0.254	-0.626
333.15	0.140	0.257	0.514	0.262	-0.635
338.15	0.134	0.257	0.512	0.276	-0.644
343.15	0.127	0.255	0.510	0.279	-0.653
348.15	0.110	0.251	0.518	0.273	-0.659
353.15	0.091	0.259	0.528	0.288	-0.657

7.5 Appendix 5

Table 7.12 - Measured viscosities, η (mPa·s), of the pure ionic liquids studied in this work.

T(K)	η (mPa·s)					
	$[C_2mim][C(CN)_3]$	$[C_2mim][Gly]$	$[C_2mim][L\text{-}Ala]$	$[C_2mim][Tau]$	$[C_2mim][L\text{-}Ser]$	$[C_2mim][L\text{-}Pro]$
293.15	16.624	240.183	382.060	760.887	3630.267	2134.400
298.15	14.187	171.967	263.983	514.667	2142.100	1304.800
303.15	12.177	126.193	187.793	359.357	1318.767	834.360
308.15	10.578	95.040	137.467	258.037	846.613	554.815
313.15	9.024	73.496	103.537	190.440	564.400	382.355
318.15	8.202	57.661	79.337	143.313	389.003	271.195
323.15	7.314	46.214	62.207	110.353	276.377	197.995
328.15	6.563	37.657	49.686	86.591	201.877	147.955
333.15	5.719	31.241	40.499	69.359	151.430	113.380
338.15	5.379	26.078	33.223	56.045	115.477	88.134
343.15	4.910	22.108	27.717	46.098	90.011	69.799
348.15	4.501	18.946	23.380	38.400	71.431	56.241
353.15	3.980	16.454	20.034	32.531	57.841	46.170

Table 7.13 - Measured viscosities, η (mPa·s), of the ionic liquid mixtures studied in this work.

T(K)	η (mPa·s)				
	$[C_2mim][C(CN)_3]_{0.25}$ $[C_2mim][Gly]_{0.75}$	$[C_2mim][C(CN)_3]_{0.25}$ $[C_2mim][L\text{-}Ala]_{0.75}$	$[C_2mim][C(CN)_3]_{0.25}$ $[C_2mim][Tau]_{0.75}$	$[C_2mim][C(CN)_3]_{0.25}$ $[C_2mim][L\text{-}Ser]_{0.75}$	$[C_2mim][C(CN)_3]_{0.25}$ $[C_2mim][L\text{-}Pro]_{0.75}$
293.15	94.033	146.567	242.413	586.840	551.760
298.15	70.853	107.203	176.640	384.165	366.287
303.15	54.704	80.465	131.510	261.065	245.533
308.15	43.186	61.832	100.213	183.685	175.647
313.15	34.805	49.162	78.029	133.405	130.353
318.15	28.425	38.955	61.397	98.943	98.339
323.15	23.591	31.747	49.465	75.387	75.906
328.15	19.865	26.274	40.431	58.746	59.705
333.15	16.916	22.293	33.606	46.898	48.020
338.15	14.577	18.699	28.096	37.791	38.916
343.15	12.670	16.040	23.825	31.009	32.137
348.15	11.101	13.894	20.435	25.751	26.892
353.15	9.773	12.278	17.769	21.139	22.882

Table 7.14 - Measured viscosities, η (mPa·s), of the ionic liquid mixtures studied in this work.

	η (mPa·s)				
***T*(K)**	**$[C_2mim][C(CN)_3]_{0.5}$ $[C_2mim][Gly]_{0.5}$**	**$[C_2mim][C(CN)_3]_{0.5}$ $[C_2mim][L\text{-}Ala]_{0.5}$**	**$[C_2mim][C(CN)_3]_{0.5}$ $[C_2mim][Tau]_{0.5}$**	**$[C_2mim][C(CN)_3]_{0.5}$ $[C_2mim][L\text{-}Ser]_{0.5}$**	**$[C_2mim][C(CN)_3]_{0.5}$ $[C_2mim][L\text{-}Pro]_{0.5}$**
293.15	55.692	78.604	84.495	168.520	224.150
298.15	43.395	60.263	64.767	120.683	157.567
303.15	34.456	46.888	50.773	88.952	114.143
308.15	27.612	37.285	40.590	67.282	85.152
313.15	22.597	30.224	33.044	52.277	65.358
318.15	18.972	24.899	27.272	41.254	50.983
323.15	16.083	20.832	22.831	33.282	40.724
328.15	13.918	17.639	19.373	27.294	33.105
333.15	12.140	15.082	16.601	22.782	27.408
338.15	10.443	13.089	14.399	19.183	22.870
343.15	9.041	11.453	12.594	16.370	19.391
348.15	8.133	10.095	11.102	14.117	16.612
353.15	7.189	8.929	9.834	12.307	14.429

Table 7.15 - Measured viscosities, η (mPa·s), of the ionic liquid mixtures studied in this work.

	η (mPa·s)				
***T*(K)**	**$[C_2mim][C(CN)_3]_{0.75}$ $[C_2mim][Gly]_{0.25}$**	**$[C_2mim][C(CN)_3]_{0.75}$ $[C_2mim][L\text{-}Ala]_{0.25}$**	**$[C_2mim][C(CN)_3]_{0.75}$ $[C_2mim][Tau]_{0.25}$**	**$[C_2mim][C(CN)_3]_{0.75}$ $[C_2mim][L\text{-}Ser]_{0.25}$**	**$[C_2mim][C(CN)_3]_{0.75}$ $[C_2mim][L\text{-}Pro]_{0.25}$**
293.15	29.045	31.551	35.420	42.012	57.468
298.15	23.445	25.677	28.767	33.366	44.687
303.15	19.432	21.184	23.706	26.975	35.494
308.15	16.351	17.742	19.843	22.200	28.759
313.15	13.901	14.827	16.611	18.362	23.582
318.15	12.022	12.935	14.441	15.719	19.816
323.15	10.471	11.229	12.511	13.477	16.808
328.15	9.209	9.841	10.936	11.676	14.426
333.15	8.116	8.513	9.521	10.068	12.432
338.15	7.293	7.740	8.618	9.027	10.953
343.15	6.554	6.933	7.715	8.033	9.656
348.15	5.922	6.257	6.964	7.189	8.593
353.15	5.346	5.451	6.191	6.363	7.626

7.6 Appendix 6

Table 7.16 – Correlation coefficients, R^2, obtained for the pure ionic liquids and their mixtures using the logarithmic equation based on Arrhenius model (equation 3.8).

Ionic Liquids	R^2
$[C_2mim][Gly]$	0.9941
$[C_2mim][L\text{-}Ala]$	0.9939
$[C_2mim][Tau]$	0.9945
$[C_2mim][L\text{-}Ser]$	0.9927
$[C_2mim][L\text{-}Pro]$	0.993
$[C_2mim][C(CN)_3]_{0.25}[Gly]_{0.75}$	0.9946
$[C_2mim][C(CN)_3]_{0.25}[L\text{-}Ala]_{0.75}$	0.994
$[C_2mim][C(CN)_3]_{0.25}[Tau]_{0.75}$	0.9953
$[C_2mim][C(CN)_3]_{0.25}[L\text{-}Ser]_{0.75}$	0.9932
$[C_2mim][C(CN)_3]_{0.25}[L\text{-}Pro]_{0.75}$	0.9921
$[C_2mim][C(CN)_3]_{0.5}[Gly]_{0.5}$	0.9951
$[C_2mim][C(CN)_3]_{0.5}[L\text{-}Ala]_{0.5}$	0.9945
$[C_2mim][C(CN)_3]_{0.5}[Tau]_{0.5}$	0.995
$[C_2mim][C(CN)_3]_{0.5}[L\text{-}Ser]_{0.5}$	0.9931
$[C_2mim][C(CN)_3]_{0.5}[L\text{-}Pro]_{0.5}$	0.9928
$[C_2mim][C(CN)_3]_{0.75}[Gly]_{0.25}$	0.9956
$[C_2mim][C(CN)_3]_{0.75}[L\text{-}Ala]_{0.25}$	0.9963
$[C_2mim][C(CN)_3]_{0.75}[Tau]_{0.25}$	0.9953
$[C_2mim][C(CN)_3]_{0.75}[L\text{-}Ser]_{0.25}$	0.9961
$[C_2mim][C(CN)_3]_{0.75}[L\text{-}Pro]_{0.25}$	0.9946
$[C_2mim][C(CN)_3]$	0.9967

7.7 Appendix 7

Table 7.17 – Viscosity deviations, $\Delta \ln \eta$, of the ionic liquids mixtures studied in this work.

	$\Delta \ln \eta$				
***T*(K)**	**$[C_2mim][C(CN)_3]_{0.25}$ $[C_2mim][Gly]_{0.75}$**	**$[C_2mim][C(CN)_3]_{0.25}$ $[C_2mim][L\text{-}Ala]_{0.75}$**	**$[C_2mim][C(CN)_3]_{0.25}$ $[C_2mim][Tau]_{0.75}$**	**$[C_2mim][C(CN)_3]_{0.25}$ $[C_2mim][L\text{-}Ser]_{0.75}$**	**$[C_2mim][C(CN)_3]_{0.25}$ $[C_2mim][L\text{-}Pro]_{0.75}$**
293.15	-0.270	-0.174	-0.188	-0.476	-0.139
298.15	-0.263	-0.170	-0.172	-0.464	-0.140
303.15	-0.251	-0.164	-0.159	-0.448	-0.166
308.15	-0.240	-0.158	-0.147	-0.432	-0.160
313.15	-0.223	-0.135	-0.130	-0.408	-0.139
318.15	-0.220	-0.144	-0.133	-0.404	-0.140
323.15	-0.212	-0.137	-0.124	-0.391	-0.134
328.15	-0.203	-0.131	-0.117	-0.378	-0.129
333.15	-0.189	-0.108	-0.101	-0.353	-0.112
338.15	-0.187	-0.120	-0.105	-0.350	-0.118
343.15	-0.181	-0.114	-0.100	-0.338	-0.112
348.15	-0.175	-0.109	-0.095	-0.329	-0.106
353.15	-0.166	-0.086	-0.080	-0.337	-0.089

Table 7.18 - Viscosity deviations, $\Delta \ln \eta$, of the ionic liquids mixtures studied in this work.

	$\Delta \ln \eta$				
***T*(K)**	**$[C_2mim][C(CN)_3]_{0.5}$ $[C_2mim][Gly]_{0.5}$**	**$[C_2mim][C(CN)_3]_{0.5}$ $[C_2mim][L\text{-}Ala]_{0.5}$**	**$[C_2mim][C(CN)_3]_{0.5}$ $[C_2mim][Tau]_{0.5}$**	**$[C_2mim][C(CN)_3]_{0.5}$ $[C_2mim][L\text{-}Ser]_{0.5}$**	**$[C_2mim][C(CN)_3]_{0.5}$ $[C_2mim][L\text{-}Pro]_{0.5}$**
293.15	-0.126	-0.014	-0.286	-0.377	0.174
298.15	-0.129	-0.015	-0.277	-0.368	0.147
303.15	-0.129	-0.020	-0.265	-0.354	0.124
308.15	-0.138	-0.022	-0.252	-0.341	0.106
313.15	-0.131	-0.011	-0.227	-0.311	0.107
318.15	-0.137	-0.024	-0.229	-0.314	0.078
323.15	-0.134	-0.024	-0.219	-0.301	0.068
328.15	-0.122	-0.023	-0.207	-0.288	0.061
333.15	-0.096	-0.009	-0.182	-0.256	0.074
338.15	-0.126	-0.021	-0.187	-0.262	0.049
343.15	-0.142	-0.018	-0.178	-0.250	0.046
348.15	-0.127	-0.016	-0.169	-0.239	0.043
353.15	-0.118	0.000	-0.146	-0.209	0.062

Table 7.19 - Viscosity deviations, $\Delta \ln \eta$, of the ionic liquids mixtures studied in this work.

	$\Delta \ln \eta$				
***T*(K)**	**$[C_2mim][C(CN)_3]_{0.75}$ $[C_2mim][Gly]_{0.25}$**	**$[C_2mim][C(CN)_3]_{0.75}$ $[C_2mim][L\text{-}Ala]_{0.25}$**	**$[C_2mim][C(CN)_3]_{0.75}$ $[C_2mim][Tau]_{0.25}$**	**$[C_2mim][C(CN)_3]_{0.75}$ $[C_2mim][L\text{-}Ser]_{0.25}$**	**$[C_2mim][C(CN)_3]_{0.75}$ $[C_2mim][L\text{-}Pro]_{0.25}$**
293.15	-0.110	-0.143	-0.199	-0.419	0.027
298.15	-0.121	-0.138	-0.191	-0.399	0.017
303.15	-0.117	-0.130	-0.180	-0.376	0.013
308.15	-0.113	-0.124	-0.170	-0.354	0.010
313.15	-0.092	-0.113	-0.152	-0.324	0.024
318.15	-0.105	-0.112	-0.150	-0.314	0.007
323.15	-0.102	-0.106	-0.142	-0.297	0.007
328.15	-0.098	-0.101	-0.134	-0.280	0.009
333.15	-0.075	-0.092	-0.114	-0.254	0.030
338.15	-0.090	-0.091	-0.115	-0.249	0.012
343.15	-0.087	-0.088	-0.108	-0.235	0.013
348.15	-0.085	-0.083	-0.100	-0.223	0.015
353.15	-0.060	-0.090	-0.083	-0.200	0.037

7.8 Appendix 8

Table 7.20 – Refractive indices, n_D, of the pure ionic liquids studied in this work.

T(K)	n_D					
	[C_2mim][C(CN)$_3$]	[C_2mim][Gly]	[C_2mim][L-Ala]	[C_2mim][Tau]	[C_2mim][L-Ser]	[C_2mim][L-Pro]
293.15	1.514540	1.521285	1.513663	1.514885	1.526986	1.522914
298.15	1.512862	1.519923	1.512234	1.513579	1.525650	1.521510
303.15	1.511139	1.518556	1.510808	1.512252	1.524293	1.520093
308.15	1.509381	1.517187	1.509370	1.510932	1.522938	1.518698
313.15	1.507647	1.515800	1.507933	1.509613	1.521594	1.517314
318.15	1.505948	1.514453	1.506513	1.508302	1.520221	1.515906
323.15	1.504195	1.513079	1.505050	1.506981	1.518872	1.514537
328.15	1.502546	1.511732	1.503580	1.505684	1.517548	1.513154
333.15	1.500872	1.510351	1.502174	1.504341	1.516200	1.511770
338.15	1.499212	1.508984	1.500736	1.503061	1.514860	1.510352
343.15	1.497573	1.507634	1.499318	1.501756	1.513526	1.508965
348.15	1.495928	1.506314	1.497949	1.500410	1.512196	1.507568
353.15	1.494286	1.504903	1.496565	1.499081	1.510835	1.506199

Table 7.21 - Refractive indices, n_D, of the ionic liquid mixtures studied in this work.

T(K)	n_D				
	[C_2mim][C(CN)$_3$]$_{0.25}$ [C_2mim][Gly]$_{0.75}$	[C_2mim][C(CN)$_3$]$_{0.25}$ [C_2mim][L-Ala]$_{0.75}$	[C_2mim][C(CN)$_3$]$_{0.25}$ [C_2mim][Tau]$_{0.75}$	[C_2mim][C(CN)$_3$]$_{0.25}$ [C_2mim][L-Ser]$_{0.75}$	[C_2mim][C(CN)$_3$]$_{0.25}$ [C_2mim][L-Pro]$_{0.75}$
293.15	1.516731	1.514764	1.512417	1.520747	1.520568
298.15	1.515289	1.513300	1.511067	1.519291	1.519130
303.15	1.513836	1.511839	1.509696	1.517842	1.517692
308.15	1.512351	1.510378	1.508314	1.516360	1.516223
313.15	1.510903	1.508884	1.506932	1.514891	1.514773
318.15	1.509434	1.507363	1.505569	1.513431	1.513329
323.15	1.507991	1.505896	1.504159	1.511985	1.511907
328.15	1.506577	1.504362	1.502788	1.510508	1.510462
333.15	1.505139	1.502927	1.501390	1.509016	1.508987
338.15	1.503708	1.501480	1.499978	1.507550	1.507523
343.15	1.502339	1.499971	1.498619	1.506113	1.506112
348.15	1.500908	1.498506	1.497277	1.504592	1.504613
353.15	1.499477	1.497044	1.495925	1.503179	1.503192

Table 7.22 - Refractive indices, n_D, of the ionic liquid mixtures studied in this work.

	n_D				
***T*(K)**	**$[C_2mim][C(CN)_3]_{0.5}$ $[C_2mim][Gly]_{0.5}$**	**$[C_2mim][C(CN)_3]_{0.5}$ $[C_2mim][L\text{-}Ala]_{0.5}$**	**$[C_2mim][C(CN)_3]_{0.5}$ $[C_2mim][Tau]_{0.5}$**	**$[C_2mim][C(CN)_3]_{0.5}$ $[C_2mim][L\text{-}Ser]_{0.5}$**	**$[C_2mim][C(CN)_3]_{0.5}$ $[C_2mim][L\text{-}Pro]_{0.5}$**
293.15	1.515947	1.514087	1.511820	1.518648	1.521826
298.15	1.514464	1.512579	1.510388	1.517185	1.520322
303.15	1.512972	1.511068	1.508921	1.515628	1.518834
308.15	1.511458	1.509501	1.507435	1.514089	1.517342
313.15	1.509869	1.507963	1.505969	1.512544	1.515819
318.15	1.508345	1.506428	1.504437	1.510991	1.514322
323.15	1.506833	1.504877	1.502962	1.509427	1.512816
328.15	1.505320	1.503375	1.501492	1.507840	1.511350
333.15	1.503771	1.501908	1.500001	1.506325	1.509829
338.15	1.502313	1.500386	1.498546	1.504747	1.508319
343.15	1.500798	1.498883	1.497108	1.503237	1.506833
348.15	1.499275	1.497393	1.495669	1.501731	1.505333
353.15	1.497794	1.495891	1.494222	1.500180	1.503828

Table 7.23 - Refractive indices, n_D, of the ionic liquid mixtures studied in this work.

	n_D				
***T*(K)**	**$[C_2mim][C(CN)_3]_{0.75}$ $[C_2mim][Gly]_{0.25}$**	**$[C_2mim][C(CN)_3]_{0.75}$ $[C_2mim][L\text{-}Ala]_{0.25}$**	**$[C_2mim][C(CN)_3]_{0.75}$ $[C_2mim][Tau]_{0.25}$**	**$[C_2mim][C(CN)_3]_{0.75}$ $[C_2mim][L\text{-}Ser]_{0.25}$**	**$[C_2mim][C(CN)_3]_{0.75}$ $[C_2mim][L\text{-}Pro]_{0.25}$**
293.15	1.515128	1.513671	1.512463	1.515520	1.518956
298.15	1.513551	1.512101	1.510906	1.513900	1.517408
303.15	1.511945	1.510527	1.509308	1.512281	1.515742
308.15	1.510325	1.508928	1.507691	1.510635	1.514092
313.15	1.508711	1.507305	1.506148	1.508993	1.512438
318.15	1.507125	1.505679	1.504302	1.507356	1.510787
323.15	1.505554	1.504005	1.502911	1.505745	1.509136
328.15	1.503937	1.502443	1.501430	1.504084	1.507485
333.15	1.502412	1.500851	1.499755	1.502527	1.505859
338.15	1.500830	1.499264	1.498354	1.500926	1.504144
343.15	1.499247	1.497710	1.496892	1.499317	1.502532
348.15	1.497698	1.496133	1.495417	1.497743	1.500856
353.15	1.496116	1.494562	1.493870	1.496145	1.499171

7.9 Appendix 9

Table 7.24 – Calculated molar refractions (R_m) and free molar volumes (f_m) for the pure ionic liquids studied in this work.

T(K)	$[C_2mim][C(CN)_3]$		$[C_2mim][Gly]$		$[C_2mim][L\text{-}Ala]$		$[C_2mim][Tau]$		$[C_2mim][L\text{-}Ser]$		$[C_2mim][L\text{-}Pro]$	
	R_m ($cm^3 \cdot mol^{-1}$)	f_m ($cm^3 \cdot mol^{-1}$)	R_m ($cm^3 \cdot mol^{-1}$)	f_m ($cm^3 \cdot mol^{-1}$)	R_m ($cm^3 \cdot mol^{-1}$)	f_m ($cm^3 \cdot mol^{-1}$)	R_m ($cm^3 \cdot mol^{-1}$)	f_m ($cm^3 \cdot mol^{-1}$)	R_m ($cm^3 \cdot mol^{-1}$)	f_m ($cm^3 \cdot mol^{-1}$)	R_m ($cm^3 \cdot mol^{-1}$)	f_m ($cm^3 \cdot mol^{-1}$)
293.15	55.871	129.548	48.461	110.617	53.231	123.681	56.526	130.960	54.833	123.526	60.136	136.750
298.15	55.903	130.134	48.487	111.025	53.261	124.166	56.563	131.447	54.857	123.961	60.167	137.265
303.15	55.926	130.715	48.509	111.430	53.288	124.646	56.593	131.928	54.885	124.411	60.199	137.789
308.15	55.947	131.308	48.529	111.830	53.312	125.126	56.621	132.405	54.914	124.866	60.231	138.309
313.15	55.969	131.899	48.547	112.234	53.333	125.602	56.644	132.870	54.947	125.330	60.262	138.827
318.15	55.987	132.474	48.568	112.638	53.354	126.075	56.658	133.315	54.966	125.774	60.279	139.323
323.15	56.001	133.062	48.586	113.042	53.368	126.547	56.675	133.774	54.991	126.226	60.305	139.829
328.15	56.025	133.644	48.606	113.446	53.386	127.034	56.695	134.233	55.015	126.671	60.325	140.331
333.15	56.045	134.228	48.624	113.859	53.407	127.510	56.713	134.707	55.036	127.117	60.346	140.836
338.15	56.065	134.811	48.644	114.273	53.426	127.996	56.735	135.169	55.054	127.557	60.361	141.343
343.15	56.088	135.399	48.667	114.695	53.445	128.479	56.755	135.641	55.074	128.003	60.381	141.854
348.15	56.112	135.997	48.692	115.113	53.473	128.969	56.769	136.111	55.093	128.448	60.399	142.364
353.15	56.137	136.598	48.720	115.565	53.505	129.478	56.788	136.593	55.112	128.904	60.424	142.888

Table 7.25 - Calculated molar refractions (R_m) and free molar volumes (f_m) for the ionic liquid mixtures studied in this work.

T(K)	$[C_2mim][C(CN)_3]_{0.25}$ $[C_2mim][Gly]_{0.75}$		$[C_2mim][C(CN)_3]_{0.25}$ $[C_2mim][L\text{-}Ala]_{0.75}$		$[C_2mim][C(CN)_3]_{0.25}$ $[C_2mim][Tau]_{0.75}$		$[C_2mim][C(CN)_3]_{0.25}$ $[C_2mim][L\text{-}Ser]_{0.75}$		$[C_2mim][C(CN)_3]_{0.25}$ $[C_2mim][L\text{-}Pro]_{0.75}$	
	R_m	f_m	R_m	f_m	R_m	f_m	R_m	f_m	R_m	f_m
	($cm^3 \cdot mol^{-1}$)		($cm^3 \cdot mol^{-1}$)		($cm^3 \cdot mol^{-1}$)		($cm^3 \cdot mol^{-1}$)		($cm^3 \cdot mol^{-1}$)	
293.15	50.185	115.770	54.063	125.290	56.384	131.391	54.749	125.123	58.650	134.096
298.15	50.211	116.221	54.095	125.796	56.413	131.876	54.788	125.636	58.688	134.631
303.15	50.234	116.669	54.123	126.293	56.440	132.367	54.823	126.141	58.719	135.153
308.15	50.256	117.128	54.145	126.778	56.463	132.853	54.845	126.630	58.745	135.677
313.15	50.277	117.577	54.168	127.281	56.485	133.339	54.869	127.120	58.769	136.194
318.15	50.291	118.017	54.180	127.770	56.498	133.804	54.882	127.586	58.793	136.709
323.15	50.311	118.467	54.204	128.272	56.517	134.297	54.903	128.069	58.807	137.201
328.15	50.334	118.922	54.221	128.780	56.539	134.790	54.924	128.564	58.830	137.723
333.15	50.355	119.377	54.244	129.277	56.557	135.285	54.941	129.057	58.849	138.246
338.15	50.376	119.834	54.267	129.779	56.572	135.780	54.960	129.551	58.866	138.768
343.15	50.399	120.282	54.284	130.290	56.592	136.272	54.984	130.051	58.893	139.295
348.15	50.418	120.741	54.304	130.799	56.617	136.774	54.996	130.550	58.905	139.822
353.15	50.438	121.203	54.332	131.328	56.642	137.283	55.023	131.053	58.925	140.344

Table 7.26 - Calculated molar refractions (R_m) and free molar volumes (f_m) for the ionic liquid mixtures studied in this work.

T(K)	$[C_2mim][C(CN)_3]_{0.5}$ $[C_2mim][Gly]_{0.5}$		$[C_2mim][C(CN)_3]_{0.5}$ $[C_2mim][L\text{-}Ala]_{0.5}$		$[C_2mim][C(CN)_3]_{0.5}$ $[C_2mim][Tau]_{0.5}$		$[C_2mim][C(CN)_3]_{0.5}$ $[C_2mim][L\text{-}Ser]_{0.5}$		$[C_2mim][C(CN)_3]_{0.5}$ $[C_2mim][L\text{-}Pro]_{0.5}$	
	R_m	f_m	R_m	f_m	R_m	f_m	R_m	f_m	R_m	f_m
	($cm^3 \cdot mol^{-1}$)		($cm^3 \cdot mol^{-1}$)		($cm^3 \cdot mol^{-1}$)		($cm^3 \cdot mol^{-1}$)		($cm^3 \cdot mol^{-1}$)	
293.15	52.181	120.594	54.704	126.977	56.210	131.169	55.322	127.051	58.071	132.385
298.15	52.213	121.088	54.732	127.492	56.242	131.686	55.356	127.562	58.102	132.917
303.15	52.240	121.575	54.759	128.009	56.270	132.209	55.384	128.093	58.130	133.443
308.15	52.266	122.068	54.781	128.533	56.292	132.726	55.406	128.606	58.157	133.969
313.15	52.281	122.562	54.805	129.059	56.317	133.248	55.428	129.122	58.181	134.501
318.15	52.297	123.043	54.823	129.572	56.329	133.764	55.448	129.643	58.200	135.017
323.15	52.318	123.533	54.843	130.097	56.349	134.281	55.468	130.168	58.225	135.554
328.15	52.337	124.022	54.867	130.621	56.370	134.805	55.485	130.698	58.251	136.081
333.15	52.357	124.529	54.894	131.145	56.390	135.334	55.511	131.229	58.275	136.626
338.15	52.381	125.020	54.916	131.677	56.409	135.855	55.527	131.762	58.294	137.160
343.15	52.400	125.519	54.942	132.216	56.430	136.378	55.552	132.295	58.318	137.699
348.15	52.419	126.025	54.974	132.768	56.451	136.903	55.578	132.835	58.344	138.252
353.15	52.445	126.538	55.014	133.347	56.473	137.437	55.603	133.391	58.371	138.812

Table 7.27 - Calculated molar refractions (R_m) and free molar volumes (f_m) for the ionic liquid mixtures studied in this work.

T(K)	$[C_2mim][C(CN)_3]_{0.75}$ $[C_2mim][Gly]_{0.25}$		$[C_2mim][C(CN)_3]_{0.75}$ $[C_2mim][L\text{-}Ala]_{0.25}$		$[C_2mim][C(CN)_3]_{0.75}$ $[C_2mim][Tau]_{0.25}$		$[C_2mim][C(CN)_3]_{0.75}$ $[C_2mim][L\text{-}Ser]_{0.25}$		$[C_2mim][C(CN)_3]_{0.75}$ $[C_2mim][L\text{-}Pro]_{0.25}$	
	R_m	f_m	R_m	f_m	R_m	f_m	R_m	f_m	R_m	f_m
	($cm^3 \cdot mol^{-1}$)		($cm^3 \cdot mol^{-1}$)		($cm^3 \cdot mol^{-1}$)		($cm^3 \cdot mol^{-1}$)		($cm^3 \cdot mol^{-1}$)	
293.15	54.020	125.083	55.266	128.406	56.035	130.562	55.523	128.447	57.014	130.844
298.15	54.047	125.610	55.304	128.969	56.064	131.110	55.553	129.004	57.049	131.396
303.15	54.074	126.147	55.334	129.517	56.086	131.657	55.581	129.560	57.067	131.950
308.15	54.096	126.681	55.359	130.066	56.107	132.210	55.606	130.122	57.085	132.503
313.15	54.114	127.206	55.384	130.625	56.133	132.755	55.629	130.680	57.105	133.063
318.15	54.139	127.744	55.402	131.173	56.125	133.321	55.645	131.225	57.119	133.615
323.15	54.164	128.280	55.413	131.723	56.163	133.855	55.667	131.780	57.135	134.174
328.15	54.183	128.820	55.438	132.276	56.191	134.396	55.682	132.338	57.149	134.732
333.15	54.208	129.350	55.457	132.826	56.202	134.964	55.707	132.890	57.166	135.292
338.15	54.227	129.886	55.478	133.384	56.236	135.501	55.728	133.450	57.172	135.860
343.15	54.247	130.429	55.503	133.942	56.266	136.051	55.746	134.011	57.190	136.425
348.15	54.269	130.968	55.526	134.510	56.298	136.615	55.766	134.567	57.203	137.005
353.15	54.289	131.518	55.556	135.094	56.325	137.193	55.791	135.146	57.218	137.597